Aus der Abt. Cardiovascular Genomics and Epigenomics
der Medizinischen Fakultät Mannheim
(Direktor: Prof. Dr. Gergana Dobreva)

Metabolic rewiring and HIF1α accumulation upon Rnf20 loss result in lung cancer progression

Inauguraldissertation
zur Erlangung des Doctor scientiarum humanarum (Dr. sc.hum.)
der
Medizinischen Fakultät Mannheim
der Ruprecht-Karls-Universität
zu
Heidelberg

vorgelegt von
Liu, Hao

aus
Chongqing, China
2025

Dekan: Prof. Dr. med. Sergij Goerdt

Referentin: Frau Prof. Dr. Gergana Dobreva

CONTENT

LIST OF ABBREVIATIONS

ACLY	ATP citrate lyase
ACSS2	Acetyl-CoA synthetase 2
AD	Adenocarcinoma
ALK	Anaplastic lymphoma Kinase
AMPK	Adenosine monophosphate-activated protein kinase
AP-2α	Activator protein 2α
AR	Androgen receptor
AT2	Alveolar Type II
ATCC	American Type Culture Collection
B2B	BEAS-2B
BAT	Brown adipose tissue
ccRCC	Clear cell renal cell carcinoma
CGRP	Calcitonin gene-related peptide
CH3	Methyl groups
CEA	Carcinoembryonic Antigen
ChIP	Chromatin immunoprecipitation
CH3	Methyl groups
-COCH3	Acetyl group
COPD	Chronic obstructive pulmonary disease
CPT1	Carnitine Palmitoyl transferase 1
CT	Computed tomography
CTCs	Circulating tumor cells
CTD	Carboxy-terminal Domain
CTLA-4	Cytotoxic c T-lymphocyte associated antigen 4
CYFRA 21-1	Cytokeratin 19 Fragment
DNMTs	DNA methyltransferases
DISC	Death-inducing signaling complex
DLL3	Delta-like ligand 3

DNMTs	DNA methyltransferases
DSBs	Double-strand DNA breaks
DSIF	Positive elongation factor b
ECAR	Extracellular acidification rate
ECM	Extracellular matrix
EGFR	Epidermal Growth Factor Receptor
EMT	Epithelial-mesenchymal transition
EMT-TFs	EMT transcription factors
EUCOMM	European Conditional Mouse Mutagenesis Program
F6P	Fructose-6-phosphate
FA	Fatty acid
FASN	Fatty acid synthase enzyme
FBS	Fetal bovine serum
G6P	Glucose-6-phosphate
GLS	Glutaminase
GLUT1	Glucose transporter 1
GO	Gene Ontology
gRNA	Guide RNA
H&E	Hematoxylin and eosin
H2Bub1	H2B monoubiquitinating
H_2O_2	Hydrogen peroxide
H3K4me	Mono-methylation of histone H3 at lysine 4
H3K4me3	Tri- methylation of histone H3 at lysine 4
HAT	Histone acetyltransferase
HDAC	Histone deacetylases
HGSOC	High-grade ovarian cancer
HIF1α	Hypoxia-inducible transcription factor 1α
HIFs	Hypoxia-inducible factors
HK1	Hexokinase 1
HK2	Hexokinase 2

HMGCR	HMG-CoA reductase
HMTs	Histone methyltransferases
HRR	Homologous recombination repair
IGF-1R	IGF-1 receptor
IGFs	Insulin-like growth factors
IHC	Immunohistochemistry
IL-18	Interleukin-18
iWAT	Inguinal white adipose tissue
KEGG	Kyoto Encyclopedia of Genes and Genomes
KRAS	Kirsten Rat Sarcoma Viral Oncogene Homolog
LAG-3	Lymphocyte activation gene 3
LCC	Large-cell Carcinoma
LC-MS	Liquid chromatography-mass spectrometry
LDCT	Low-dose computed tomography
LDHA	Lactate dehydrogenase
LUAD	Lung Adenocarcinoma
MLL	Mixed-lineage leukemia
MMPs	Matrix metalloproteinase
mRNA	Messenger RNA
NCoR1	Nuclear corepressor 1
NELF	Negative elongation factor
NF-κB	Nuclear factor κB
NHEJ	Error-prone non-homologous end-joining
NK	Natural killer
NSCLC	Non-Small Cell Lung Cancer
NSE	Neuron-Specific Enolase
O_2^-	Superoxide anion
OXPHOS	Oxidative phosphorylation
PD-1	Programmed death-1
PET	Positron emission tomography

PHD	Prolyl hydroxylation
PIC	Preinitiation complex
PIKK	Phosphoinositide three-kinase-related kinas
PKM2	Pyruvate Kinase M2
Pol II	RNA polymerase II
ProGRP	Pro-Gastrin-Releasing Peptide
PSG	Penicillin/streptomycin/glutamine
P-TEFb	Positive elongation factor b
RB	Retinoblastoma protein
RIPA	Radioimmunoprecipitation Assay
Rnf20	Ring finger protein 20
Rnf40	Ring finger protein 40
ROS	Reactive oxygen species
SAC	Spindle assembly checkpoint
SAM	S-adenosylmethionine
SCLC	Small cell lung cancer
SREBP	Sterol regulatory-element binding protein
SREBP1c	Sterol regulatory element binding protein 1c
SYP	Synaptophysin
TCA	Tricarboxylic acid
TCGA	The cancer genome atlas program
TME	Tumor microenvironment
TRAIL	TNF-related apoptosis-inducing ligand
TSS	Transcription start site
TTF1	Thyroid transcription factor-1
VEGF	Vascular endothelial growth factor
VHL	Hippel-Lindau tumor suppressor protein
WB	Western Blot
•OH	Hydroxyl radicals
2-DG	2-deoxyglucose

5hmc	5-hydroxymethylcytosine
5-mc	5-methylcytosnine
µl	Microliter
µm	Micrometer
µM	Micromolar
%	Percent
°C	Celsius degree

1 INTRODUCTION

1.1 Lung cancer types and related markers

1.1.1 Lung cancer types

Lung cancer contributes the most among the cancer related death, and also the leading diagnosed cancer world-wide (Liang, Cai et al. 2019). The number of cases has increased by 51% since 1985, partly due to advancements in new diagnostic technologies. However, the mechanism of carcinogenesis remain unclear and still under investigation, but risk factors like smoking, arsenic, air pollution, radiation exposure are convinced to be involved in raising of lung cancer incidence (Schabath and Cote 2019). These factors influence tumor progression through distinct mechanisms that vary across different types of tumors.

Lung cancer is divided into two main types on the basis of pathologic appearances, small cell lung cancer (SCLC), which accounts for approximately 15% of cases, and non-small cell lung cancer (NSCLC) which represents 80-85% of all lung cancer cases (Schabath and Cote 2019, Rudin, Brambilla et al. 2021). Among NSCLC subtypes, adenocarcinoma is the most common which comprising about 40% of cases, while SCLC is the second most common type (Fig. 1). These different lung cancer types have distinct origins as well as clinical and pathological features (Ferone, Lee et al. 2020). Adenocarcinoma (AD) is thought to originate from alveolar type II (AT2) cells, which play a crucial role in maintaining alveolar function and integrity (Sainz de Aja, Dost et al. 2021). While, squamous cell carcinoma (SCC) can arise from basal epithelial cells, club cells and AT2 cells. Small cell lung cancer (SCLC) typically originates from neuroendocrine cells and is known for its rapid growth and spread (Sutherland and Berns 2010) (Fig. 1). Lung cancer is a heterogeneous disease; however, the most common causes of lung cancers are smoking and exposure to carcinogenic substances, such as radon, asbestos, and air pollution (Nicholson, Tsao et al. 2022). Direct exposure to these chemicals causes DNA damage, which imperatively contributes to cancer development and progression of cancer. In this regard, the E3 ubiquitin ligase RNF20 plays a key role in the repair of double-strand DNA breaks (DSBs) via error-prone non-homologous end-joining (NHEJ) or high-

fidelity homologous recombination repair (HRR), primarily by promoting H2B monoubiquitination (H2Bub1) (Moyal, Lerenthal et al. 2011, Nakamura, Kato et al. 2011).

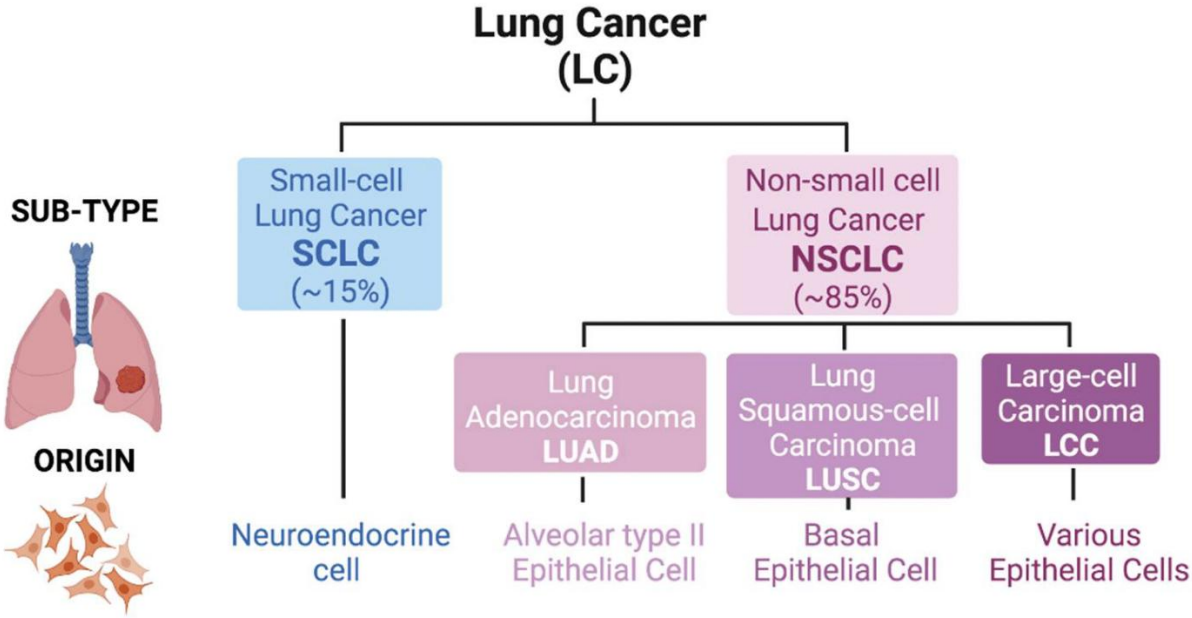

Figure 1. The classification of lung cancer. Lung cancer is divided into two main categories, the SCLC and NSCLC. Among NSCLC, there are 3 subtypes, which are Lung Adenocarcinoma (LUAD), Lung Squamous-cell Carcinoma (LUSC) and Large-cell Carcinoma (LCC). (Miriam Sánchez-Ortega *et al,* 2018). Permission is conveyed through Copyright clearance Center, Inc.

1.1.2 Lung cancer markers

Lung cancer markers are substances that can be detected in blood, tissue, or other body fluids that may indicate the presence of lung cancer or help track its progression (Schneider 2006). Lung cancer patients usually appear to have no obvious symptoms like dyspnea, cough, and thoracic pain at the early stage. Thus, it is valuable markers for diagnosing and managing patients with the disease especially at early stage, these biomarkers offer insight into the origin, relationships, and biological behavior of lung cancers. Among NSCLC, especially squamous cell carcinoma (SCC), elevated expression of Cytokeratin 19 Fragment (CYFRA 21-1) is an indicator that is well studied in cancer and help in monitoring cancer progression and treatment outcomes (Okamura, Takayama et al. 2013). Another example is the Carcinoembryonic Antigen (CEA) which the level is usually elevated in lung cancer, especially LUAD (Grunnet and Sorensen 2012). Thyroid transcription factor-1 (TTF1) with the role as a marker for lung adenocarcinoma also associated with prognosis of lung patients (Kim, Kim et

al. 2018). Additionally, Napsin A was regarded as a new marker for lung adenocarcinoma which is more sensitive in diagnose (Turner, Cagle et al. 2012). Other NSCLC targets include the Epidermal Growth Factor Receptor (EGFR) mutations, which is commonly mutated in adenocarcinoma and can be used to identify new candidates in target therapy (da Cunha Santos, Shepherd et al. 2011). The Anaplastic lymphoma Kinase (ALK) rearrangements are also observed in some NSCLC patients (Shaw and Engelman 2013). The Kirsten Rat Sarcoma Viral Oncogene Homolog (KRAS) mutation are also commonly seen in lung cancer patients, especially in smokers (Riely, Marks et al. 2009). On the other hand, the markers for SCLC include, the specific marker Pro-Gastrin-Releasing Peptide (ProGRP), which can be used for diagnosis and monitoring, and the Neuron-Specific Enolase (NSE), which can assist the tumor's response under therapy (Ferrigno, Buccheri et al. 2003). In addition, because SCLC subtypes belong to the neuroendocrine category, with tumor cells exhibiting typical neuroendocrine features which express neuroendocrine markers such as synaptophysin SYP and Calcitonin gene-related peptide CGRP (Gottschling, Jauch et al. 2012, Lv, Chen et al. 2022), are commonly used in SCLC. To date, these markers are commonly used in combination with imaging tests, biopsies, and clinical evaluations to determine the most accurate diagnosis and help to choose the most appropriate treatment strategy for lung cancer.

1.2 Lung cancer risk factor, diagnosis, treatment and prevention

1.2.1 Lung cancer risk factor

Lung cancer risk is influenced by a combination of lifestyle choices, environmental exposure, genetic factors and pre-existing medical conditions. Tobacco smoking is the leading risk factor of lung cancer; statistics show it responsible for approximately 85-90% of cases and contributes more to SCLC than NSCLC (Walser, Cui et al. 2008). The exposure to asbestos is another strong incentive in lung carcinogenesis (Bade and Cruz 2020). For instance, researchers reported that approximately 12% of individuals diagnosed with asbestosis subsequently developed lung cancer.(Klebe, Leigh et al. 2020). In addition, factors like exposure in radon, arsenic, and ionizing radiation are also factors in lung cancer initiation and development (Tran, Kappelhoff et al. 2022, Yang, Li et al. 2022, Martin-Gisbert, Ruano-Ravina et al. 2023). For

example, study concluded that lung cancer risk is likely dependent on the absorbed dose of inorganic arsenic rather than the route of exposure either through ingestion or inhalation (Smith, Ercumen et al. 2009). These factors cause DNA damage by forming DNA adducts and generating reactive oxygen species (ROS), leading to mutations in critical genes such as *p53* and *kras* or *Egfr*. Recent data supported the idea that p53 mutations in lung cancer result from direct DNA damage caused by cigarette smoke (Hainaut and Pfeifer 2001). Furthermore, reports suggest that diet and obesity are factors influencing lung cancer risk and progression as well. High glycemic diet such as white bread and bagels were linked to increased risk of lung cancer, particularly among non-smokers (Zhu, Shu et al. 2022). Visceral fat promotes inflammation and alteration of hormone which facilitate tumor growth , links obesity with cancer progression. In fact, a case study conducted in Canada, involving 21,022 incident case of different types of cancer and 5,039 control aged 20-76 years, found that obesity was responsible for 7.7% of all cancer (Pan, Johnson et al. 2004). This evidence suggests a role of metabolic changes in lung cancer development.

1.2.2 Diagnosis of lung cancer

Lung cancer is a lethal disease, as lung cancer often has a poor prognosis when diagnosed in advanced stages (Kasper, Fauci et al. 2015). The conventional methods for diagnosing lung cancer involve extracting suspicious tissue samples for histological examination. Additionally, computed tomography (CT) scans are commonly used to support diagnosis. Newer technologies, such as helical (spiral) CT, are increasingly employed for early lung cancer screening (Adams, Stone et al. 2023). Another advanced imaging technique is positron emission tomography (PET), which is highly sensitive and can detect pre-invasive carcinomas as well as metastatic tumors based on the unique metabolic characteristics of cancer cells (Ng, Ng et al. 2023). To date, these technologies have been utilized in early screening and providing suggestions for treatment. However, confirmation of lung cancer, particularly its pathological subtypes, is important for guiding appropriate therapy. Through microscopic examination of the lesion’s location and morphological patterns, pathologists can determine whether it represents a malignant tumor, inflammation, or hyperplasia. Now, by combination of these technologies, lung cancer diagnosis is accurate and efficacy.

1.2.3 Lung cancer therapy

Lung cancer therapies vary based on several factors, including the stage and grade of the tumor, the overall condition of the patient, and the pathological type of the tumor (Cooper and Spiro 2006, Gadgeel, Ramalingam et al. 2012). Treatment approaches can include surgery, chemotherapy, radiation therapy, or a combination of these methods. In addition, numerous targeted therapies have been developed, focusing on specific oncogenic proteins driving cancer. Unlike conventional chemotherapy targeted therapies (Table 1) tend to have fewer side effects and offer better overall survival for patients (Mayekar and Bivona 2017). For example, erlotinib or crizotinib are used in non-small cell lung cancer (NSCLC) patients with EGFR mutation and EML4-ALK translocation, respectively (Wu, House et al. 2012, Aggarwal 2014). Moreover, sotorasib is used in patients with KRAS mutation (Skoulidis, Li et al. 2021).

Additionally, immunotherapy works by stimulating the body's own immune system to recognize and fight cancer cells is particularly effective for advanced lung cancer, especially non-small cell lung cancer (NSCLC) (Lahiri, Maji et al. 2023). Emerging immunotherapies, such as vaccines, immune modulators and monoclonal antibodies targeting checkpoint inhibitors, have demonstrated significant promise in the treatment of cancer. However, most of these approaches have faced challenges in treatment effectiveness, primarily because cancer cells often evade immune detection early on. Recent studies, fortunately, have demonstrated that targeting programmed death-1 (PD-1) and cytotoxic c T-lymphocyte associated antigen 4 (CTLA-4) can lead to more efficient clinical responses (Guo, Liang et al. 2022, Liu, Hu et al. 2022, Zhang, Xie et al. 2022). Besides, recent preclinical studies have demonstrated promising results of Chimeric Antigen Receptor (CAR) T-cell therapy. By which researchers developed CAR T cells engineered to target Delta-like ligand 3 (DLL3), a protein commonly overexpressed in SCLC cells, these CAR T cells were further modified to secrete interleukin-18 (IL-18), enhancing their anti-tumor activity (Jaspers, Khan et al. 2023).

Table 1. Targeted therapies in the treatment of lung cancer. (Manasi K *et al,* 2017).

Targeted oncogenic driver	FDA-approved drugs	Drugs under study	10% NSCLC patients
EGFR	Gefitinib, erlotinib, afatinib, osimertinib	Dacomitinib, olmutinib (HM61713), ASP8273,	10-15%

		nazartinib (EGF816), avitinib, PF-06747775, hs-10296	
ALK	Crizotinib, ceritinib, alectinib, brigatinib	Ensartinib, entrectinib, lorlatinib	3–7%
ROS1	Crizotinib	Ceritinib, cabozantinib, entrectinib, lorlatinib	1–2%
RET		RXDX-105, cabozantinib, vandetanib, sunitinib, sorafenib, alectinib, lenvatinib, nintedanib, ponatinib, regorafenib	1–2%
NTRK		Entrectinib, larotrectinib (LOXO-101), LOXO-195	1–2%
BRAF	Dabrafenib and trametinib combination	Vemurafenib, PLX8394, selumetinib	1–4%
HER2		Afatinib, dacomitinib, trastuzumab	1–2%
MET		Crizotinib, cabozantinib, capmatinib, MGCD265	4–5%
KRAS		Selumetinib, trametinib, ARS853	15–30%

1.3 Cancer growth and metastasis

1.3.1 Uncontrolled cell proliferation

Cancer is primarily understood as a disease characterized by uncontrolled proliferation and survival. Instead of growing and behaving normally, cancer cells divide and proliferate in an uncontrolled manner, leading to abnormal growth that invades surrounding tissues and organs, and potentially spreading throughout the body. As cancer cells grow and divide, they damage the surrounding tissues, depriving them of essential nutrients that support normal growth, while also impairing the physiological function of the affected organs.

1.3.1.1 Gene mutations in cancer proliferation

Cell growth and division are coordinately controlled by genes, cancerous cells appear after mutations accumulated in certain genes (Marte 2004). These genes often control processes such as cell cycle arrest and programmed cell death (apoptosis) and are broadly classified as oncogenes or tumor suppressor genes. There are several types of gene mutations, for example, point mutation represents the simplest type of mutation, which consist of a change in a single nucleotide base pair in the DNA sequence. Other mutations include insertions or deletions, which involves the addition of loss of one or more nucleotides, which leads to a shift in the reading frame and results in change of protein products (Timoféeff-Ressovsky, Zimmer et al. 2011). While different cancers exhibit distinct mutational signatures, certain genes are commonly mutated across various tumor types, especially in lung cancer (Table 2). For instance, mutations in the tumor suppressor gene p53 are found in the majority of cancers, including lung adenocarcinoma and SCLC (Sherr and McCormick 2002, Muller and Vousden 2013). The protein coded by them are both play pivotal role in regulating cell cycle arrest and apoptosis (Engeland 2022). Besides, the prevalent EGFR mutation which involves a deletion in exon 19, results in a truncated EGFR that remains continuously active, driving sustained lung adenocarcinoma cell signaling and promoting uncontrolled cell proliferation (Metro and Crinò 2012). Another mutation often occurs in lung cancer is KRAS, which related to tobacco exposure, particularly at codon 12, impairing its ability to hydrolyze GTP that leads to constitutive activation of RAS signaling in lung adenocarcinoma (Riely, Marks et al. 2009, Ferrer, Zugazagoitia et al. 2018).

Table 2. Organized Gene mutations of lung cancer. (Miranda B. Carper *et al,* 2015; gnacio I *et al,* 2001).

Genetic alterations	Incidence (%)	Downstream effect
Adenocarcinomas		
EGFR	Approximately 15	↑Proliferation, survival, angiogenesis, and metastasis
EML4-ALK	2-7	↑ Proliferation, survival, and migration
KRAS	Approximately 30	↑ Chemoresistance, proliferation, and survival

MET	3-5	↑ Cell survival, proliferation, and survival
ROS1	1-2	↑ Survival
RET	1-2	↑ Proliferation
BRAF	5-10	↑ Resistance to EGFR inhibitors, proliferation, and survival
TP53	46	↑ Growth;↓ apoptosis
Squamous cell carcinomas		
FGFR1	16-25	↑Proliferation, survival, chemoresistance; ↓patient prognosis
PIK3CA	8-18	↑Proliferation and survival
DDR2	4	↑ Cell migration, invasion, proliferation, and survival
MET	3	↑ Cell survival, proliferation, and metastasis
SOX2	21	↑ Proliferation
PTEN	15-29	↑ PI3K signaling, proliferation, and survival
TP53	81	↑ Growth, ↓apoptosis
CDKN2A	51	↑ Growth
Small cell lung cancer (SCLC)		
PTEN	9	↑ Proliferation
MYC*	18-31	↑ Cell migration and invasion
BRCA1	10	↑Proliferation and chemoresistance
TP53	90	↑Proliferation and survival
RB1	90	↑Proliferation and survival

* Amplification

1.3.1.2 DNA damage and cancer growth

DNA is continuously subjected to stress and damage, as a result, the DNA strands is damaged, and DNA double-strand breaks appear to be the most abundant types of

damaged results. To maintain the regular cellular processes, an equilibrium of DNA damage and DNA damage repair must be attained. The damage of DNA comes for a variety of reasons. Chemical carcinogens that I concluded previously like tobacco smoke, asbestos, or UV and ionizing radiation (Sinha and Häder 2002, Santivasi and Xia 2014), and even viral infections such as HPV participate in DNA damage (Zhao, Guo et al. 2019). Besides, endogenous factors like ROS generated during cellular metabolism (Fig. 2) (Srinivas, Tan et al. 2019) and mistakes during DNA replication (Liu, Xue et al. 2016) can introduce DNA damage. In fact, DNA damage occurs during whole processes of cellular cycle including those in DNA replication or mitosis. In addition to repair DNA breaks directly, cells respond to DNA damage by stopping cell cycle progression or initiating programmed cell death.

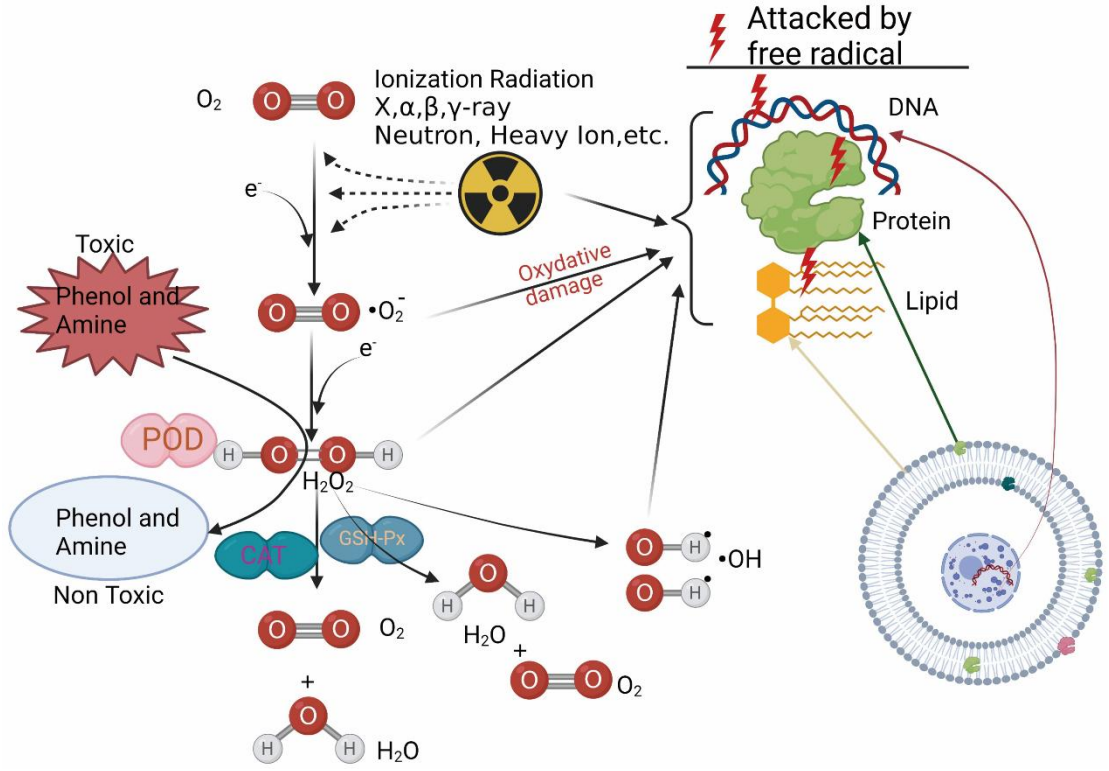

Figure 2. DNA damage by active oxygen metabolism in cells. (Chengyou Jia *et al,* 2021). Permission is conveyed through Copyright Clearance Center, Inc.

Accordingly, cell cycle checkpoints are activated to arrest the cell cycle to eliminate and repair the damaged DNA. These checkpoints serve as critical control stages during the cell cycle, where the cell assesses genomic integrity and decides whether to proceed with division or initiate apoptosis. (Matthews, Bertoli et al. 2022). The DNA damage checkpoint response is regulated by members of the phosphoinositide three-

kinase-related kinases (PIKK) family (Liu, Xue et al. 2016). Upon DNA damage, the PIKK family kinases ATM and ATR phosphorylate target proteins at serine and threonine residues, thereby activating the DNA damage checkpoint (Cimprich and Cortez 2008). ATM phosphorylates and activates CHK2, which then amplifies the checkpoint response by further phosphorylating CDC25 for degradation, preventing CDK2 activation and blocking the G1/S transition (Falck, Mailand et al. 2001). Similarly, ATM phosphorylates p53, enhancing its transcription. The increased p21 protein levels lead to G1 phase arrest by inhibiting cyclin E/CDK2 and cyclin D/CDK4 complexes.

(Weinberg, Veprintsev et al. 2005, Chen 2016) (Fig. 3). In addition, researchers have found that the G2/M phase could also be arrested by p53, which exerts its regulatory function through downstream targets such as 14-3-3 σ, cdc25C, mir34a (Martín-Caballero, Flores et al. 2001, Clair, Giono et al. 2004, Chang, Wentzel et al. 2007). Cycle arrest gives cells time to repair lethal damage such as DSBs. Since the p53 gene is mutated in most cancers, its ability to induce cell cycle arrest is impaired. This disruption compromises DNA repair mechanisms, ultimately leading to genomic instability and contributing to cancer development (Vaddavalli and Schumacher 2022). This is supported by the fact that mice lacking p53 develop normally but have an increased susceptibility to spontaneous tumor formation (Donehower, Harvey et al. 1992).

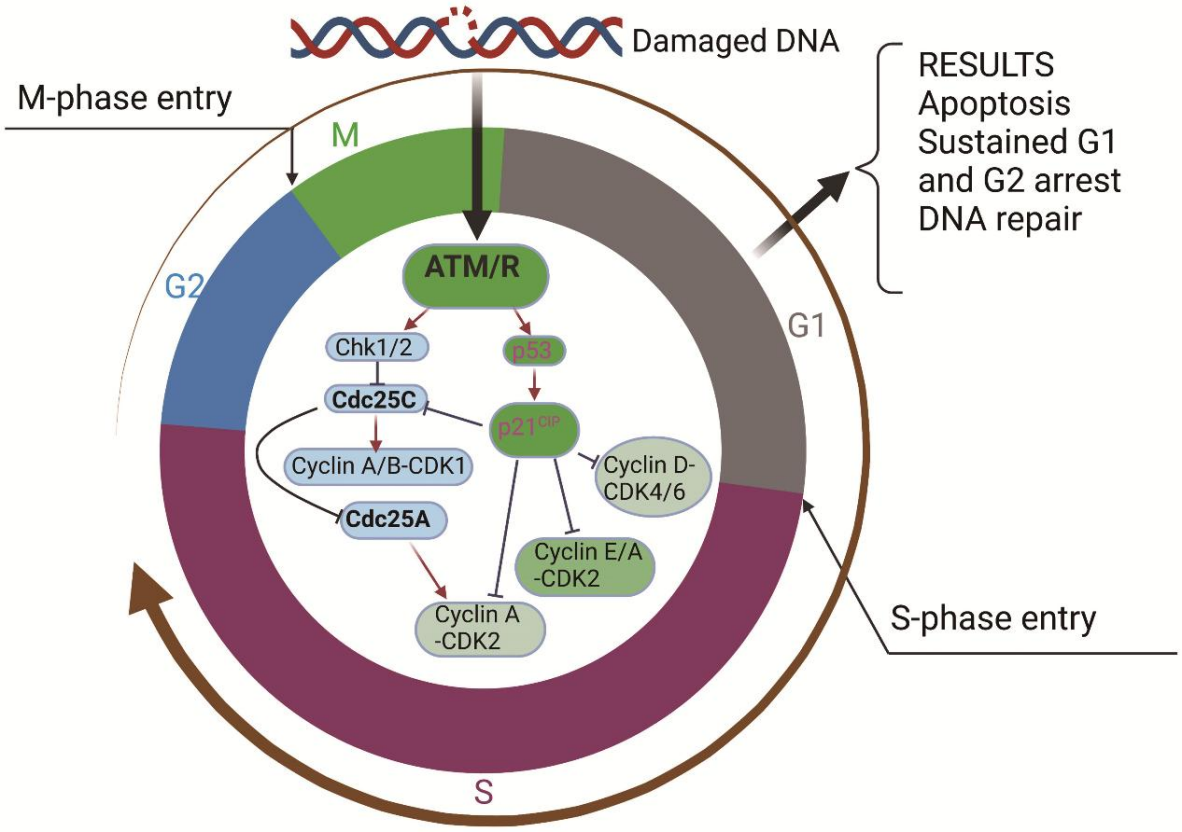

Figure 3. The checkpoint control by ATM of cell cycle. (Chengyou Jia *et al,* 2021). Permission is conveyed through Copyright Clearance Center, Inc.

The tumor suppressor p53 was discovered nearly two decades ago, and extensive research has since established its role as a key regulatory hub within the protein network that governs cellular responses to both endogenous and exogenous stresses (Robles, Linke et al. 2002). The p53 gene is mutated in more than half of all human cancers, including lung cancers (Harris 1996). In healthy tissue, p53 exists at low levels in a latent and post-transcriptionally modified state. However, in response to various stresses, additional post-transcriptional modifications activate p53, resulting in its accumulation in the nucleus (Appella and Anderson 2001). In this role, p53 safeguards efficient DNA repair and maintains chromosomal stability. Rather than causing only random genetic instability, its loss in cancer models is also associated with significant epigenetic alterations. In fact, activated p53 can reduce binding and alleviate transcriptional repression of DNA cytosine methyltransferase 1 (DNMT1) mRNA, thereby influencing DNA methylation pattern and further shaping the epigenetic landscape of the cell (Peterson, Bögler et al. 2003). Further analysis of DNA methylation disturbances in p53-deficient cells has revealed a close relationship between p53 function and the regulation of epigenetic metabolism. The transition of

premalignant to malignant lesions is often associated with *p53* mutations, which is characterized by a reduction in 5-hydroxymethylcytosine (5hmC) levels and accumulation of α-ketoglutarate (Morris IV, Yashinskie et al. 2019). Additionally, *p53* deficient cells showed a low level of S-adenosylmethionine (SAM), which is a major methyl-donor in methylation. SAM is a product of one carbon metabolism, a pathway that is modulated by p53. It has been shown that p53 regulates genes involved in one carbon metabolism, such as *Slc43a2* (Panatta, Butera et al. 2022, Bin, Wang et al. 2024). Furthermore, deregulation of *Slc34a2* among cancer cells leads to epigenetic instability, loss of transcription control, and the emergence of repetitive transcription of sequences in affected genomic regions, all of which contribute to genomic instability (Fig. 4). These findings indicate that the disruption of p53 impairs the epigenetic balance, thereby facilitating the transition from premalignant to malignant state and contributing to cancer growth.

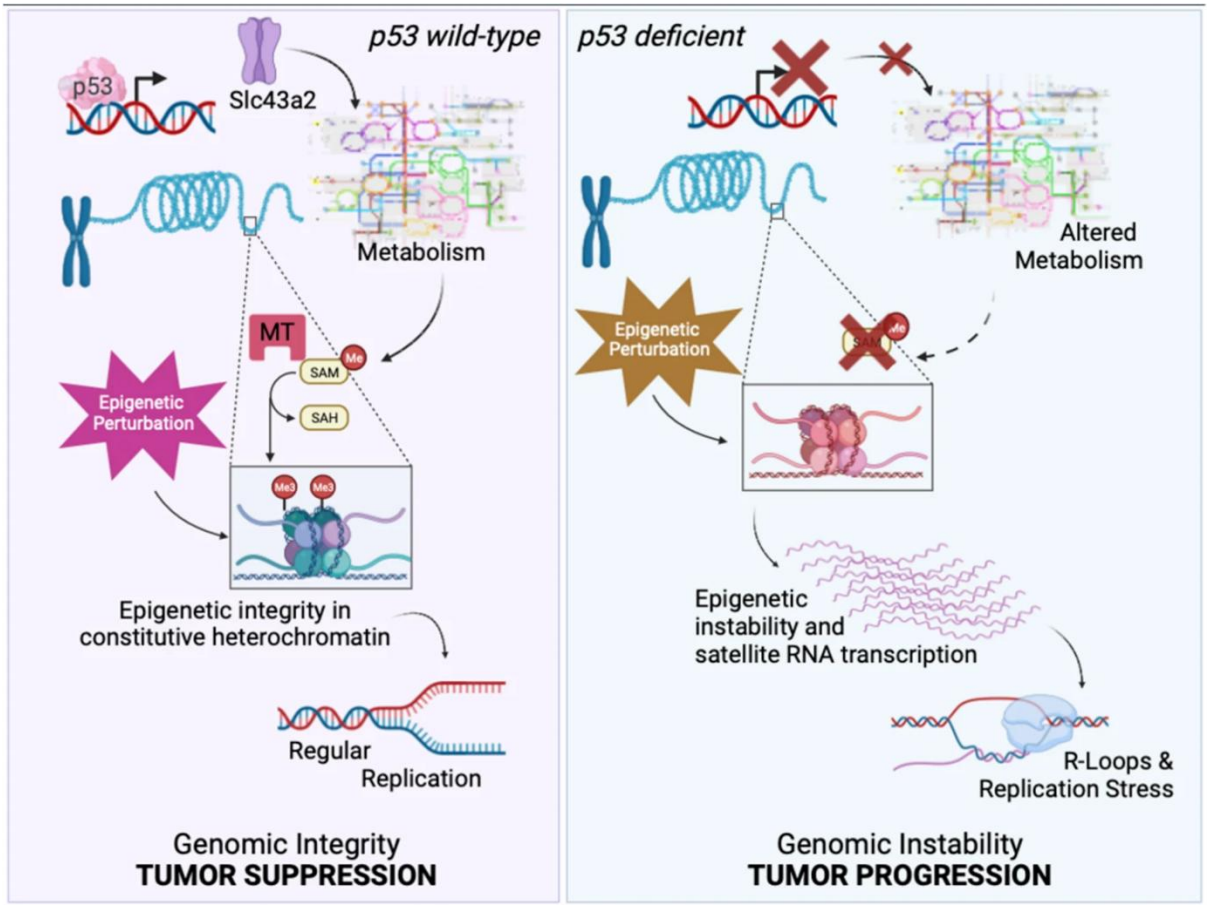

Figure 4. *p53* controls genomic integrity in tumor progression. (Ana Janic *et al,* 2024). Permission is conveyed through Copyright Clearance Center, Inc.

1.3.1.3 Evasion of apoptosis

Apoptosis is a natural mechanism by which damaged or abnormal cells are eliminated. Unlike necrosis, apoptosis is a carefully orchestrated process and cells undergoing apoptosis are efficiently removed by phagocytes, avoiding inflammation and tissue damage. The apoptosis process is mediated by a variety of ways, signals such as DNA damage or dysfunction of mitochondrial, involving the release of cytochrome c from mitochondria and activation of caspases (Clair, Giono et al. 2004, Jeong and Seol 2008). Additionally, signals like binding of death receptor on the cell surface to their ligand also leading to caspase activation. For example, FADD binds to the cross-linked Fas receptors via its C-terminal death domain which induce the binding of FADD and caspase-9, and the complex is called the death-inducing signaling complex (DISC) (Huang, Eberstadt et al. 1996, Lavrik and Krammer 2012). This binding activates caspase-8 triggering a cascade activation of capase-1, caspase-4, caspase-6, and caspase-7 which eventually leads to cell death (Cohen 1997). Excessive apoptosis usually results in neurodegenerative diseases such as Alzheimer disease or Parkinson disease (Mattson 2000, Radi, Formichi et al. 2014). However, in cancer, cells often acquire abilities which allow them to escape from apoptosis, even if they have already accumulated significant damage. This enables them to survive and proliferate (Singh and Lim 2022). Cancer cells often overexpress anti-apoptotic proteins like Bcl2 and Mcl1, which block pro-apoptotic signaling pathways and prevent the permeabilization of the mitochondrial outer membrane, a crucial step in apoptosis (Song, Coppola et al. 2005, Thomadaki and Scorilas 2006). While simultaneous downregulation or mutation of pro-apoptosis proteins such as Bax, Bak, and Puma further prevents the release of cytochrome c and the activation of caspase, thus inhibiting apoptosis (Scorrano, Oakes et al. 2003, Pemberton, Nguyen et al. 2023). In addition to the frequent mutations or loss of function in the tumor suppressor p53, a central regulator of apoptosis that responds to cellular stress by inducing the transcription of pro-apoptotic genes, leading to apoptotic cell death, however, in many cancers, mutations in p53 impair its ability to activate apoptosis, thereby enabling tumor cells to survive despite genomic instability (Vazquez, Bond et al. 2008). On the other hand, the extrinsic apoptosis pathway is also frequently disrupted, as seen in the downregulation or mutation of death receptors like Fas and TNF-related apoptosis-inducing ligand (TRAIL) receptors, which prevent the binding of their respective ligands and subsequent activation of caspase cascades

(Fulda and Debatin 2006). Moreover, inhibitors of apoptosis proteins like XIAP, cIAP1, and cIAP2 directly inhibit caspases that prevent apoptosis and contribute to cancer cell survival (Silke and Meier 2013). Dysregulation of mitochondrial metabolism and ROS production in cancer cells can also promote resistance to apoptosis by altering mitochondrial membrane integrity and reducing sensitivity to apoptotic stimuli (Vyas, Zaganjor et al. 2016). Recent studies also revealed that immune evasion mechanisms, such as the upregulation of PD-L1, enable cancer cells to escape immune-mediated apoptosis by suppressing cytotoxic T-cell activity (Topalian, Taube et al. 2020). Ultimately demonstrating that cancer cells employ a multifaced strategy to escape apoptosis, which not only contributes to tumor growth and survival but also poses significant challenges for treatment.

1.3.2 Cancer metastasis

1.3.2.1 Metastatic cascade

Metastasis is the leading cause of cancer-related deaths, with the spread of primary tumors marking a critical step in malignant transformation (Bogenrieder and Herlyn 2003). This complex process involves multiple biological changes that enable cancer cells to detach from their original site, survive in circulation, and establish secondary tumors in distant organs. To initiate migration, cancer cells must degrade and traverse the extracellular matrix (ECM) and the basement membrane of surrounding tissues near the blood and lymphatic vessels. This process often involved the activation of enzymes such as matrix metalloproteinases (MMPs), which facilitate ECM breakdown and tumor cell invasion (Mook, Frederiks et al. 2004). Once cancer cells reach nearby blood or lymphatic vessels, they interact with endothelial cells to invade vessel walls and enter circulation (Maishi and Hida 2017). Within the bloodstream or lymphatic system, circulating tumor cells (CTCs) encounter immune surveillance and mechanical stress, which eliminate the majority of them. However, a small subset of cancer cells evades immune destruction, survive in circulation, and ultimately invade the microenvironment of distant organ. Once in a foreign tissue, these cancer cells must adapt to new conditions and establish metastatic growth (Fig. 5).

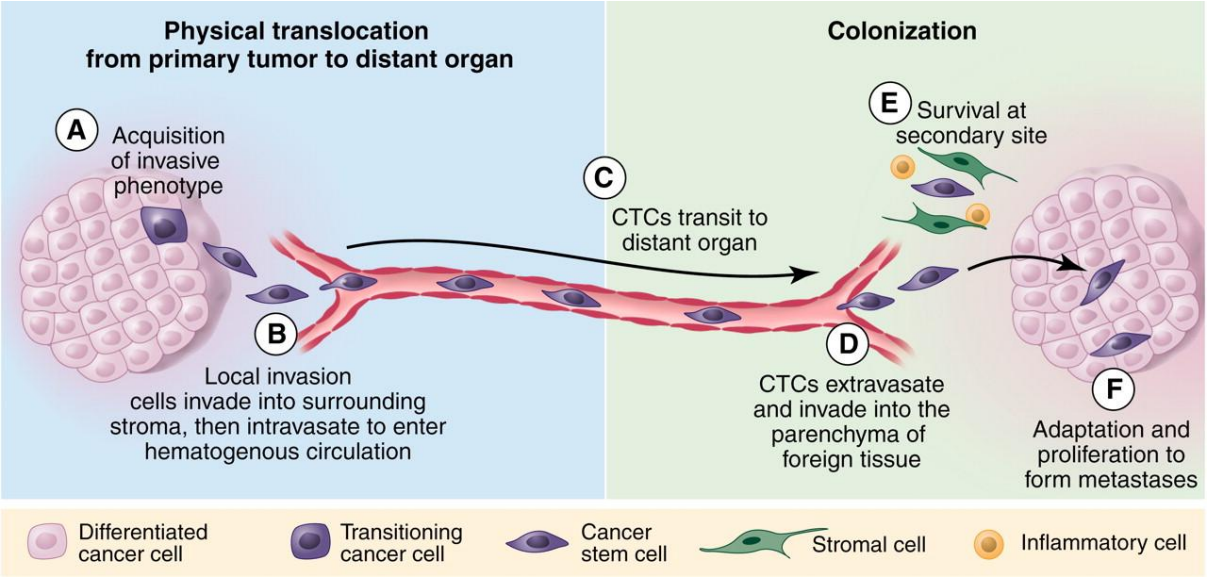

Figure 5. The metastasis cascade of cancer. Cancer migration starts by acquisition of invasive phenotype, and through local invasion, cancer cells invade into circulation system. Cancer cells finally adapt and survival at foreign tissues to form metastasis. (Christine L. Chaffer *et al,* 2011). Permission is conveyed through Copyright clearance Center, Inc.

1.3.2.2 EMT

Epithelial cells are defined by their apical-basal polarity and their connection to adjacent cells through tight junctions and adherent junctions. In contrast, ,mesenchymal cells lack these epithelial characteristics, allowing them to remain detached from neighboring tissues (Brabletz, Kalluri et al. 2018).

To adapt to the demands of the tumor microenvironment and facilitate metastasis, cancer cell undergo significant genetic alterations and epigenetic modifications that drive their progression, and one of the key consequences of these changes is the induction of epithelial-mesenchymal transition (EMT), a process in which epithelial cells lose their characteristic polarity and cell-cell adhesion properties, acquiring mesenchymal-like traits that enhance their motility and invasive capacity (Fig. 6), which is primarily regulated by EMT transcription factors (EMT-TFs) such as Snai1, Twist, Zeb families, and E-cadherin, which play crucial roles in suppressing epithelial markers and activating mesenchymal gene expression (Brabletz, Kalluri et al. 2018). EMT is classically described to participate in three major biological contexts, the first is involved in development processes during embryogenesis to facilitate tissue and organ formation, the second is occurring wound healing and fibrosis, and the third is participate in promoting malignant transformation, enhances metastatic potential, and increases resistance to cell death in which its role in cancer progression has been well

documented across various types of malignancies, including lung (Xiao, Tan et al. 2023), prostate (Byles, Zhu et al. 2012), liver (Lin, Zhou et al. 2020), pancreatic (Aiello, Brabletz et al. 2017), and breast cancer (Ye, Brabletz et al. 2017). Study demonstrates that EMT enables cancer cells to detach from the primary tumor, invade surrounding tissue, enter circulation via the blood or lymphatic system, and eventually colonize distant organs, thereby contributing to the formation of metastasis. As seen in lung cancer, where the decay of Snai1 mRNA, induced by UDP-glucose, has been found to impair metastasis by disrupting the EMT process (Wang, Liu et al. 2019). In breast cancer, where the downregulation of E-cadherin, a critical cell-cell adhesion molecule, has been linked to increased metastatic colonization in the liver (Chao and Wells 2010), suggesting that changes in cadherin expression play an essential role in tumor cell plasticity and metastatic behavior. Yet despite its well documented role in cancer dissemination, EMT is rarely fully executed in most tumors, as cancer often exhibit partial or hybrid EMT states, in which they retain some epithelial features while acquiring certain mesenchymal properties, and rather than undergoing a complete transition, these cells exist in an intermediate state that is sufficient to enhance migration, invasion, and resistance to apoptosis. This phenomenon, known as EMT plasticity, allows cancer cells to revert to an epithelial phenotype upon reaching metastatic sites, facilitating colonization and tumor outgrowth. EMT plasticity has been observed in several cancers and is closely linked to therapeutic resistance and disease progression (Saitoh 2018), highlighting the importance of dynamic EMT regulation.

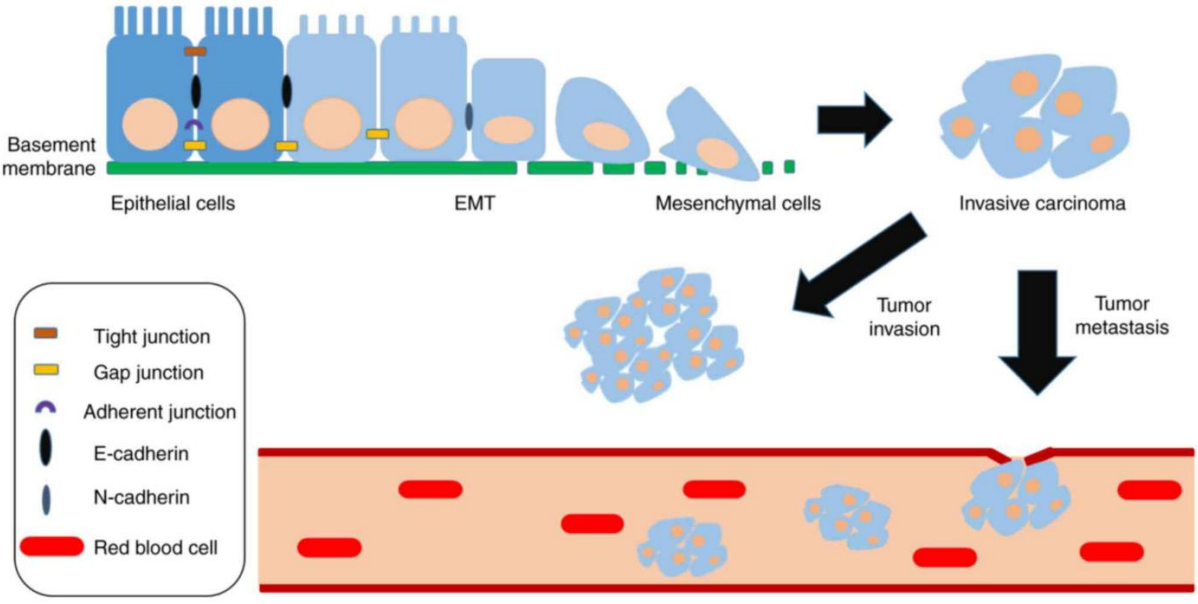

Figure 6. The biological process of EMT. The transition of epithelial cells to a mesenchymal phenotype is characterized by the loss of cell polarity, tight junction, and adherent junctions, by which leads to the transformation of epithelial cells into mesenchymal cells with enhanced migratory and invasive capabilities. (Mingzhe Li *et al,* 2011). Permission is conveyed through Copyright clearance Center, Inc.

1.3.2.3 Cancer metastatic site preference

As proposed by Stephen Paget's "seed and soil" hypothesis, which suggests that circulating tumor cells preferentially colonize organs that provide a favorable niche, with factors such as blood flow patterns, adhesion molecules, immune evasion, and stromal interactions (Fidler and Poste 2008). Evidence showed that, breast cancer commonly migrate to the bone (Chen, Sosnoski et al. 2010), lung (Medeiros and Allan 2019), liver (Selzner, Morse et al. 2000), and brain (Palmieri, Smith et al. 2007) due to the presence of chemokine receptor interactions like CXCR4 and CXCL12 (Luker and Luker 2006). Prostate cancer has a strong predilection for bone metastases, likely mediated by the expression of bone homing factors such as BMPs and RANKL (Wong, Mohamad et al. 2019). Colorectal cancer prefers spreading to the liver due to portal circulation drainage from the primary tumor site (Manfredi, Lepage et al. 2006),while lung cancer frequently spreads to the brain, reflecting its high vascularity and the ability of tumor cells to breach the blood-brain barrier (Yousefi, Bahrami et al. 2017). Recent studies highlight the importance of exosome communication, immune system modulation, and metabolic reprogramming in shaping organ specific metastases, as tumor-derived exosome can prepare pre-metastatic niches by altering local stromal cells, suppressing immune surveillance, and facilitating extracellular matrix remodeling, thereby enhancing the ability of disseminated tumor cells to colonize distant organs (Hoshino, Costa-Silva et al. 2015, Peinado, Zhang et al. 2017). Advances in molecular profiling have identified key genetic and epigenetic changes that influence metastatic preference, such as EMT related transcription factors in promoting invasion and dissemination (Lamouille, Xu et al. 2014), and hypoxia-inducible factors (HIFs) in driving metabolic adaptations that enable cancer cells to survive and thrive in distant sites (Rankin and Giaccia 2016).

1.4 Cancer metabolism

To support growth, division, and metastasis under nutrient-limited conditions, cancer cells exhibit metabolic plasticity, allowing them to adapt and survive. Compared to

normal cells, metabolic rewiring is a hallmark of cancer and serves as a key driving force for tumor progression and metastasis. Nearly all cancer types share distinct metabolic patterns (Krysztofiak, Szymonowicz et al. 2021), influenced by a multitude of genetic alterations and the activation or loss of specific signaling pathways.

1.4.1 Glycolysis and HIF1α in cancer

A hallmark example of metabolic reprogramming in cancer is aerobic glycolysis, commonly known as the Warburg effect (Lunt and Vander Heiden 2011). Under normal physiological conditions, following the initial step of anaerobic glycolysis, cells typically channel metabolites into the Krebs cycle, also known as the tricarboxylic acid (TCA) cycle for oxidative phosphorylation (OXPHOS) when sufficient oxygen is available (Unterlass and Curtin 2019) (Fig. 7). This process efficiently generates ATP by utilizing oxygen to fully oxidize glucose derived pyruvate in the mitochondria. In contrast, under oxygen deprivation, cells shift toward fermentation, converting pyruvate into lactate and producing ATP less efficiently. However, unlike normal cells, cancer cells preferentially undergo aerobic glycolysis even in the presence of oxygen, a phenomenon that distinguishes their metabolic phenotype from non-malignant counterparts (Wang and Patti 2023) (Fig. 7). One of the key reasons cancer cells favor aerobic glycolysis is its ability to provide intermediate metabolites necessary for rapid cell growth and proliferation. Glycolytic intermediates contribute to the biosynthesis of essential macromolecules, including nucleotides, amino acids, and lipids, which are required for sustained tumor expansion. Additionally, rather than directing pyruvate into the mitochondria for oxidative phosphorylation, cancer cells preferentially convert pyruvate into lactate. This results in lactate accumulation in the extracellular space, creating an acidic tumor microenvironment that promotes tumor invasion, angiogenesis, and immune evasion (Hirschhaeuser, Sattler et al. 2011). The acidic conditions help cancer cells outcompete normal cells and suppress immune responses by impairing the activity of cytotoxic T cells and natural killer (NK) cells, which are critical components of anti-tumor immunity.

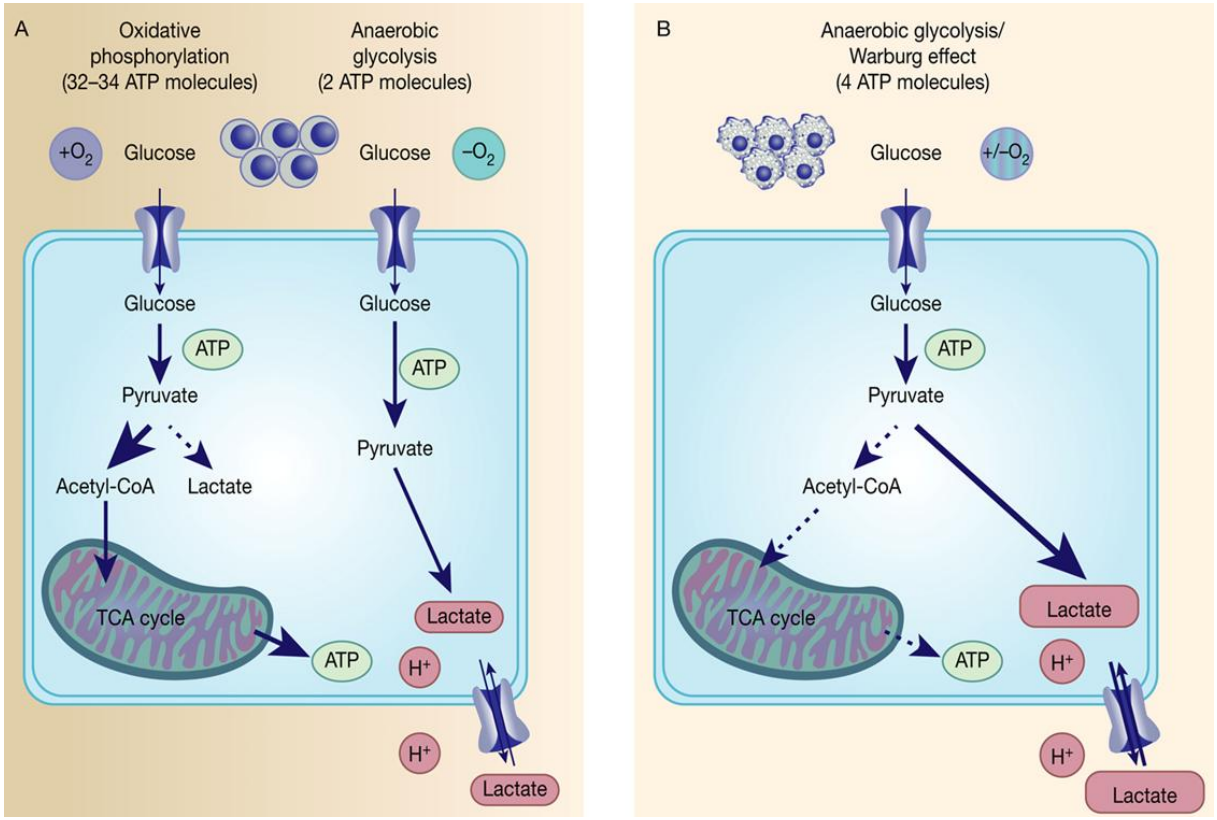

Figure 7. The process of oxidative phosphorylation, anaerobic glycolysis. (Judith E. Unterlass *et al,* 2019). Permission is conveyed through Copyright clearance Center, Inc.

On the other hand, due to the rapid growth of cancer, most tumor cells exist in a hypoxic microenvironment, where oxygen availability is severely limited. A key regulator under hypoxic condition is hypoxia-inducible factor-1 alpha (HIF1α), which accumulates in response to oxygen deprivation. HIF1α is part of the hypoxia-inducible factor (HIF) family of transcription factors, which regulate the expression of genes involved in angiogenesis, metabolism, cell survival, immune evasion, and metastasis. Under hypoxia, HIF1α promotes tumor adaption by upregulating critical genes such as vascular endothelial growth factor (VEGF) for angiogenesis (Rattner, Williams et al. 2019), glucose transporter 1 (GLUT1) for enhanced glucose uptake (Meijer, Kaanders et al. 2012), hexokinase 1 (HK1) for glycolysis (Denko 2008), and lactate dehydrogenase A (LDHA), which facilitates lactate production and acidification of the tumor microenvironment (Ooi and Gomperts 2015). Moreover, HIF1α is a key player in EMT, a process essential for cancer metastasis. HIF1α promotes the upregulation of Snai1, and important EMT marker that facilitates the loss of epithelial character and the acquisition of mesenchymal traits, enabling cancer cells to become more invasive and migratory (Xu, Tan et al. 2015). This shift in cell phenotype allows cancer cells to invade surrounding tissues and spread to distant organs. In contrast, under normal

oxygen conditions, HIF1α is regulated by prolyl hydroxylation (PHD), which facilitates its binding to von Hippel-Lindau tumor suppressor protein (VHL). This interaction allows the E3 ubiquitin ligase complex to recognize and ubiquitinate HIF1α, marking it for proteasomal degradation, thereby preventing its excessive accumulation and transcriptional activity (Fig. 8) (Weidemann and Johnson 2008). However, in many cancers, VHL mutations or hypoxic conditions prevent HIF1α degradation, leading to its sustained activation and promoting tumorigenesis. As a result, cancer cells undergo metabolic reprogramming under hypoxic conditions, allowing them to thrive in oxygen-deprived environments (Cairns 2015).

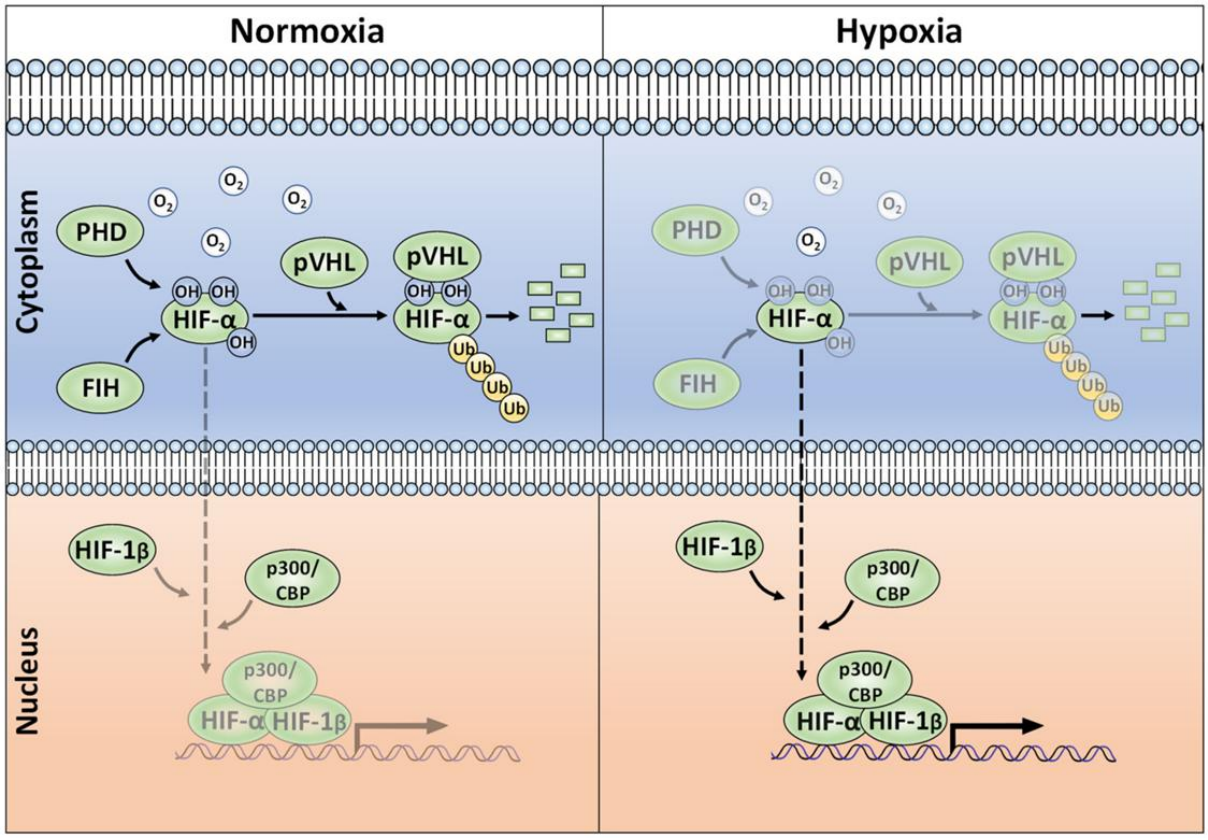

Figure 8. HIF1α was degraded under normoxic condition, while HIF1α was accumulated upon hypoxia. (Adam Albanese *et al,* 2021). Permission is conveyed through Copyright clearance Center, Inc.

A growing body of evidence suggests that HIF1α levels could serve as a prognostic indicator in various types of cancer. For instance, Yoshifumi Baba *et al*. demonstrated that elevated HIF1α expression is associated with a poor prognosis in colorectal cancer, correlating with more aggressive tumor behavior and lower survival rates (Baba, Nosho et al. 2010). Additionally, Richard Y *et al*. found that HIF1α signaling plays a significant role in promoting the proliferation of breast cancer cells in the brain, highlighting its role in enhancing metastatic growth and suggesting its potential as a therapeutic target in

brain metastasis (Ebright, Zachariah et al. 2020). These findings underline the importance of HIF1α as both a biomarker and a therapeutic target in cancer treatment strategies.

1.4.2 Altered mitochondrial function in cancer cells

While cancer cells predominantly rely on glycolysis for energy production, mitochondria still play a crucial role in supporting biosynthesis and providing metabolic intermediates necessary for rapid cell proliferation (Osellame, Blacker et al. 2012). Key mitochondrial byproducts, such as citrate and α-ketoglutarate (α-KG), are utilized in the synthesis of essential molecules, including lipids, amino acids, and nucleotides, all of which are critical for the growth and survival of cancer cells (Wallace 2012). Furthermore, mitochondria are a major source of reactive oxygen species (ROS), byproducts of oxidative metabolism. These include molecules like superoxide anion (O_2^-), hydrogen peroxide (H_2O_2), and hydroxyl radicals (•OH). Under normal conditions, ROS function as signaling molecules involved in immune response, cellular signaling, and metabolic regulation (Sena and Chandel 2012). In cancer cells, elevated ROS levels are often result of mitochondrial dysfunction or increased oxidative stress, which can lead to a cascade of genomic instability. Excessive ROS can contribute to DNA damage, including base modifications, single- and double-strand breaks, and DNA cross-linking, all of which promote mutagenesis and tumorigenesis (Ogrunc, Di Micco et al. 2014, Srinivas, Tan et al. 2019). Notably, p53 mutations, commonly found in various cancers, can be induced by oxidative DNA damage (Shi, Nikulenkov et al. 2014). Elevated ROS levels also activate oncogenes such as Ras and Myc, which drive uncontrolled cell proliferation (Park, Kim et al. 2014, de Sá Junior, Câmara et al. 2017). Additionally, ROS have been reported to promote angiogenesis by activating HIF1α, further enhancing the tumor's ability to grow and metastasis (Belaidi, Morand et al. 2016). Thus, while ROS are essential for normal cellular processes, their dysregulation in cancer cells accelerates tumor progression by enhancing DNA damage, mutation accumulation, and the promotion of angiogenesis.

1.4.3 TCA cycle and cancer progression

In addition to undergoing metabolic reprogramming, glycolysis also impacts tricarboxylic acid (TCA) cycle in cancer cells. The TCA cycle, also known as the Krebs

cycle, is widely recognized as a central hub for cellular energy production and biosynthetic precursor generation, primarily through the oxidation of acetyl-CoA to produce NADH and GTP, which are essential for oxidative phosphorylation (Wallace 2012). In normal cells, the TCA cycle integrates carbon metabolism from glucose, fatty acids, and amino acids, supplying energy and critical intermediates required for cells. However, in cancer, the TCA cycle undergoes metabolic reprogramming to meet the heightened energy and biosynthetic demands of rapidly proliferation tumor cells (Muir, Danai et al. 2018). Many cancer cells display aerobic glycolysis, where pyruvate is converted into lactate even in the presence of oxygen, diverting metabolic intermediates away from the TCA cycle (Warburg 1956). This shift allows for faster ATP production, but also creates a demand for alternative biosynthetic precursors, like citrate and α-KG. These intermediates are utilized in the synthesis of lipid, amino acids, and nucleotide synthesis, critical for cancer cell growth (Anderson, Mucka et al. 2018). Additionally, elevated ROS, produced due to TCA cycle dysregulation, contribute to oxidative stress and genomic instability, promoting tumorigenesis (Nakamura and Takada 2021). Alterations in tumor suppressor genes, such as *p53*, and oncogenes such as *Myc* further disrupt the TCA cycle, enhancing glycolytic flux and promoting tumor progression (Yeung, Pan et al. 2008). Moreover, TCA cycle intermediates themselves can directly influence cancer development, progression, and immune evasion. For example, accumulation of fumarate, caused by loss of fumarate hydratase, promote renal cancer through activating of EMT (Sciacovelli, Frezza et al. 2017). Furthermore, fumarate derived from cancer cells has been shown to impair the anti-tumor function of CD8+ T cells within the tumor microenvironment, contributing to immune escape (Cheng, Yan et al. 2023).

1.4.4 Lipid metabolism and cancer

In cancer, lipid metabolism refers to the altered processes by which cancer cells produce, consume, and use lipids, such as fatty acids (FA), cholesterol, and other lipids. These changes are crucial to support the rapid growth, survival, and invasion of cancer cells as well. The FA synthesis upregulation referred to a classic change in cancer metabolism, which by increasing the de novo synthesis of FA from glucose derived intermediates, contributes to incorporation of cell membrane. This process is achieved through the upregulation of lipogenic enzymes such as ATP citrate lyase (ACLY) and

acetyl-CoA synthetase 2 (ACSS2) (Li, Liu et al. 2024). All of which facilitate rapid cell division. For example, ACLY activity was found to be significantly higher compared with normal lung tissue in human NSCLC samples, suggesting its role in promoting cancer growth (Zhao 2019). ACSS2 is also reported to be upregulated in cancer *in vivo* and *in vitro*, which supplies a key source of acetyl-CoA for FA synthesis (Kargbo 2019).

Some cancer cells also rely on fatty acid oxidation to generate energy, especially when glucose is limited. Fatty acids can be oxidized in the mitochondria to provide ATP. For certain types of cancers, such as breast and prostate cancers, fatty acid oxidation becomes an important metabolic pathway during periods of metabolic stress. In this regard, Carnitine Palmitoyl transferase 1 (CPT1) plays a crucial role in transport of fatty acids into mitochondria for oxidation. Cancers with high CPT1 have been shown to be more aggressive and resistant to therapies. An *in vivo* study reported that, inhibition of CPT1 block the cellular fatty acid oxidation and xenograft tumor growth (Xiong, Wen et al. 2020). Now, fatty acid oxidation enzyme inhibitors such as CPT1 inhibitors, are being explored in clinical trials as a way to disrupt the ability of cancer cells to rely on fatty acid oxidation for energy production (Mallick, Bhowmik et al. 2023).

Cholesterol is another critical lipid for cancer cells. It serves not only as a structural component of membranes but also as a precursor for signaling molecules (Kuzu, Noory et al. 2016). In many types of cancers, cholesterol biosynthesis is upregulated, supporting both membrane stability and cell signaling that contributes to tumor development. A key enzyme involved in this process is HMG-CoA reductase (HMGCR), which catalyzes the rate-limiting step in cholesterol synthesis. For instance, in gastric cancer, the mRNA level of HMGCR is significantly increased compared to that in normal tissues (Chushi, Wei et al. 2016). Furthermore, in lung cancer, inhibition of HMGCR via SIAH1 induced ubiquitination has been shown to suppress tumor development and enhance drug sensitivity by interfering with cholesterol biosynthesis (Yuan, Wu et al. 2023). Additionally, a study indicated that cholesterol can promote tumor cell proliferation by activating the mTORC1 pathway at the lysosomal surface via SLC38A9, a lysosomal transmembrane protein that functions as a sensor for both cholesterol and arginine through distinct, independent motifs (Castellano, Thelen et al. 2017).

1.4.5 Glutamine metabolism and cancer

Glutamine metabolism was initially studied for its role in maintaining cellular homeostasis, as glutamine is considered a non-essential amino acid that can be synthesized de novo from glucose, serving as a key carbon and nitrogen source (Nair and Sarma 2021). In recent years, glutamine has been recognized as a central player in cancer metabolism, particularly due to its involvement in fueling the TCA cycle. The glutamine homeostasis is tightly regulated by the expression of enzymes, and their expression patterns are often altered in cancer. In many tumors, upregulation or hyperactivation of glutamine related enzymes elevates intracellular glutamine levels to meet the increased metabolic demands of proliferating cancer cells. One key enzymes is glutaminase (GLS), which plays a vital role in transporting exogenous glutamine and catalyzing its conversion to glutamate within the mitochondria (Tardito, Oudin et al. 2015). For example, the GLS levels are highly increased in liver cancer compared with the surrounding tissues, and inhibition of the GLS expression impairs tumor development (Xiang, Stine et al. 2015). However, the role of GLS appears to be context dependent. Studies have shown that GLS is not essential for NSCLC growth *in vivo* (Davidson, Papagiannakopoulos et al. 2016). Instead, NSCLC cells directly accumulate glutamine synthesized from glucose (Marin-Valencia, Yang et al. 2012). Beyond energy metabolism, glutamine also supports redox homeostasis by fueling glutathione synthesis, thereby protecting cancer cells from oxidative stress and chemotherapy induced cytotoxicity (Lyssiotis, Son et al. 2013). Interestingly, the tumor microenvironment (TME) has a significant impact on glutamine metabolism. Under hypoxic and nutrient deprived conditions, some tumors adapt by shifting toward reductive carboxylation, a metabolic pathway that generates citrate from glutamine under low oxygen conditions. This allows continued biosynthesis even in metabolically challenging environments (Metallo, Gameiro et al. 2012).

1.4.6 Factors and signal pathways in regulation of cancer metabolism

1.4.6.1 AMP-Activated Protein Kinase (AMPK)

Adenosine monophosphate-activated protein kinase (AMPK) is a highly conserved enzyme composed of a catalytic α-subunit and regulatory β and γ subunits, acting as

a critical metabolic sensor that maintains cellular energy homeostasis, particularly in glucose and lipid metabolism (Luo, Saha et al. 2005). Under conditions of low energy availability, AMPK is activated to restore ATP balance by promoting catabolic pathways that generate ATP while simultaneously inhibiting anabolic pathways that consume it (Keerthana, Rayginia et al. 2023). For example, AMPK enhances glycolysis by activating hexokinase 2 (HK2), the first enzyme in the glycolytic pathway, and by upregulating glucose transporter 1 (GLUT1), thereby facilitating glucose uptake (Hu, Chen et al. 2019). In cancer cells, AMPK also plays a role in regulating vascular endothelial growth factor (VEGF), which promotes angiogenesis to ensure an adequate supply of oxygen and nutrients for tumor proliferation (Keerthana, Rayginia et al. 2023). Notably, studies have shown that AMPK is involved in metal-induced VEGF expression, emphasizing its role in metal-driven carcinogenesis (Lee, Hwang et al. 2006). However, AMPK is not solely an oncogenic factor, it can also function as a tumor suppressor by constraining metabolic reprogramming. For instance, the loss of AMPK signaling has been shown to accelerate MYC-driven tumorigenesis and enhance the Warburg effect in lymphoma development, highlighting its inhibitory role in certain cancer contexts (Faubert, Boily et al. 2013). These findings suggest that AMK plays a dual role in cancer metabolism, acting as both a tumor promoter and suppressor depending on the cellular and metabolic environment.

1.4.6.2 Insulin and Insulin-Like Growth Factors (IGFs)

Insulin, a hormone secreted by the pancreas, primarily regulates glucose metabolism by promoting cellular glucose uptake and facilitating its conversion into energy or storage as glycogen. Beyond its physiological role, insulin significantly influences cancer cell metabolism by enhancing glucose uptake and utilization. For example, insulin has been shown to increase glucose uptake in osteosarcoma cells and tissues by upregulating GLUT1 expression, a key glucose transporter (Cifuentes, García et al. 2011). Additionally, insulin enhances glycolytic enzyme activity, thereby promoting cancer progression. In hepatocellular carcinoma, insulin accelerates glycolysis through the upregulation of pyruvate kinase M2 (PKM2), contributing to tumor development (Liu, Zhi et al. 2021). In addition to its role in glucose metabolism, insulin also modulates lipid metabolism, a process frequently dysregulated in cancer to support membrane biosynthesis, cell signaling, and energy storage. For instance, a study

reported that insulin exposure led to increased fatty acid synthase (FASN) levels in human breast cancer (MCF-7) cells, mediated by transcriptional activation through sterol regulatory-element binding protein (SREBP) (McClellan, Pham et al. 2022). Similarly, insulin-like growth factors (IGFs), particularly IGF-1 and IGF-2, play a crucial role in regulating cancer metabolism, like insulin, IGFs modulate key metabolic pathways that support rapid cell growth and survival. IGFs exert their effects by binding to and activating the IGF-1 receptor (IGF-1R), a receptor tyrosine kinase that triggers downstream signaling cascades such as PI3K/AKT and MAPK. These pathways enhance glycolysis by upregulating glucose transporters and glycolytic enzymes, thereby increasing glucose uptake and utilization to fuel cancer cell proliferation (Ma and Bai 2012, Oda, Inoue et al. 2022). Furthermore, IGF signaling has been implicated in lipid metabolism and anabolic processes, contributing to membrane biosynthesis and energy story, which are also essential for sustaining uncontrolled tumor growth.

1.4.6.3 Oncogenes

The primary drivers of carcinogenesis are oncogenes, which promote cancer development and progression by altering key metabolic pathways essential for meeting the energy and biosynthetic demands of rapidly proliferating tumor cells. One of the most well studied oncogenes, *Kras*, frequently mutated in pancreatic, colorectal, and lung cancer, enhances glucose uptake and glycolysis while also promoting glutamine metabolism to fuel the TCA cycle and support biosynthetic processes (Cenigaonandia-Campillo, Serna-Blasco et al. 2021). Similarly, Myc is commonly deregulated in many cancers, promotes aerobic glycolysis by upregulating glycolytic enzymes, increasing glucose GLUT1, and enhancing glutamine catabolism to provide carbon and nitrogen for nucleotide and amino acids biosynthesis (Dang, Le et al. 2009). Similarly, in a study of colon cancer, researchers illustrated that glucose deprivation accelerated the emergence of activating mutations in the Ras oncogene. The surviving clones exhibited enhanced adaptation to glucose limitation primarily through upregulation of the GLUT1. Notably, some of these clones acquired *kras* mutations, and further analysis confirmed that mutant *kras* directly upregulates GLUTA expression, thereby increasing glucose uptake and conferring heightened sensitivity to glycolytic inhibition (Yun, Rago et al. 2009). In addition to oncogenes, mutations in tumor suppressor genes also alter cancer cell metabolism. For instance, p53 mutations are associated

with mitochondrial dysfunction and impaired oxidative phosphorylation, leading to a metabolic shift toward glycolysis (Harami-Papp, Pongor et al. 2016). Furthermore, oncogenes influence nucleotide metabolism, a pathway essential for DNA replication and repair, which are highly active in rapidly dividing cancer cells (Aird and Zhang 2015). These metabolic adaptations collectively support tumor growth and survival under various physiological and environmental stresses.

1.5 Epigenetic modification and cancer

1.5.1 DNA methylation in the development of cancer

Epigenetic modifications can reversibly and heritably regulate gene expression without altering the underlying DNA sequence (Davalos and Esteller 2023), these modifications include DNA methylation and histone modification. CpG island refers to a genomic region with a higher frequency of CpG dinucleotides compared to the rest of the genome. These islands are commonly located at gene promoters (Fazzari and Greally 2004). DNA methylation typically occurs in these islands, where it suppresses gene transcription either by preventing transcription factors from binding to the promoter region of target genes or by recruiting gene repression associated proteins (Moore, Le et al. 2013). DNA methylation is essential for various processes, including genomic stability and regulation of gene expression. Also, DNA methylation is a central mechanism in the development and progression of cancer. Aberrant methylation patterns lead to the silencing of tumor suppressor genes and the activation of oncogenes, contributing to tumorigenesis, metastasis, and therapeutic resistance. Among which, hypermethylation of the promoter regions of tumor suppressor gene represents the most studied mechanism in cancer. Methylation of these promoter regions leads to the silencing of tumor suppressor genes, resulting in uncontrolled cell proliferation and compromised genomic stability (Fig. 9). For instance, BRCA1, which is involved in DNA repair and maintenance of genomic integrity, is silenced by promoter methylation in both breast and ovarian cancers (Magdinier, Ribieras et al. 1998, Ruscito, Dimitrova et al. 2014, Wong, Southey et al. 2020). In study of renal cell carcinoma, hypermethylation of VHL gene promoter occurs exclusively, leading to the accumulation of HIF1α and HIF2α, drives angiogenesis, cell proliferation, as well as tumor progression (Herman, Latif et al. 1994). Similarly, TIMP-3, a gene encoding a

tissue inhibitor of metalloproteinases, is frequently silenced through promoter hypermethylation in renal cancer, which impairs its role in inhibiting ECM degradation and tissue invasion (Bachman, Herman et al. 1999). The candidate tumor suppressor RASSF1A gene that associated with RAS, is hypermethylated in various types of tumors, which results in its transcriptional silencing and contribute to tumorigenesis (Grote, Schmiemann et al. 2006).

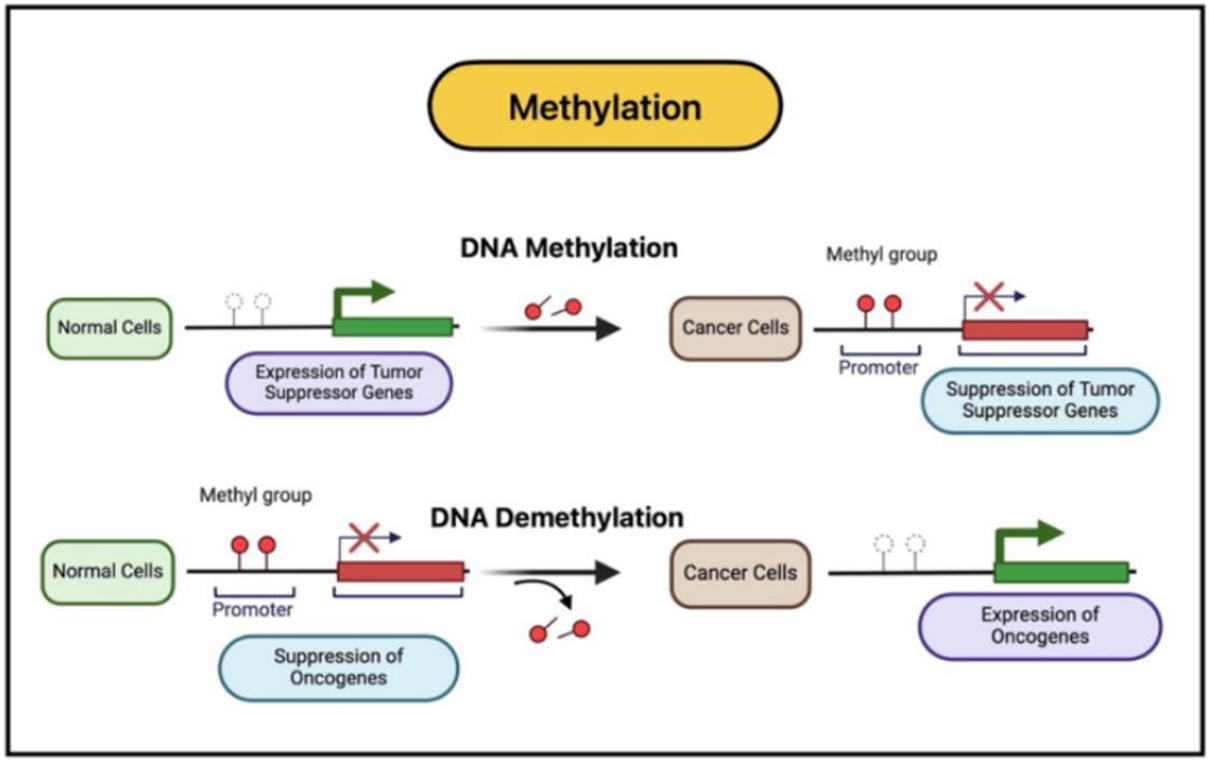

Figure 9. DNA methylation in the regulation of tumor suppressor genes and oncogenes. (Sher Zaman Safi, 2024). Permission is conveyed through Copyright clearance Center, Inc.

In contrast to the hypermethylation of tumor suppressor genes, which leads to gene silencing, hypomethylation of oncogenes can result in their aberrant activation, promoting cancer cell growth and correlates with tumor progressions. Loss of DNA methylation at CpG island can occur due to dysregulation of DNA methyltransferase (DNMTs) or enzymes such as Ten-Eleven-Translocation (TET) enzymes, which produces 5-hydroxymethylcytosine (5hmc) by oxidating 5-methylcytosnie (5-mC), leading to DNA demethylation (de Souza, Leal et al. 2013, Fatma, Maurya et al. 2022). Indeed, studies have demonstrated that hypomethylation of specific repetitive DNA elements is significantly correlated with tumor recurrence and aggressiveness. For example, in hepatocellular carcinoma (HCC), a high degree of hypomethylation in repetitive sequences has been strongly associated with postoperative recurrence

(Shen, Fang et al. 1998). Similarly, in ovarian cancer, hypomethylation of centromeric and pericentromeric satellite DNAs has been linked to higher tumor grade (Widschwendter, Jiang et al. 2004). Furthermore, oncogenes such as *KRAS* have been shown to undergo promoter hypomethylation in several types of cancer, including urothelial carcinoma and colorectal cancer. This epigenetic alteration leads to increased *KRAS* expression, which drives cancer cell proliferation and contributes to tumor progression (Nishigaki, Aoyagi et al. 2005, Wu and Brenner 2014, Debernardi, Libera et al. 2021, Tripathi, Goel et al. 2021).

Both gene mutations and DNA methylation can suppress gene expression, but a key distinction lies in their reversibility. Gene mutations are permanent alterations in the DNA sequence, whereas epigenetic modifications such as DNA methylation are potentially reversible. The reversibility of epigenetic silencing presents opportunities for the development of targeted therapies aimed at reactivating silenced tumor suppressor genes. Moreover, aberrant methylation patterns have emerged as valuable biomarkers for cancer risk assessment, early detection, prognosis prediction, and treatment monitoring. These insights provide a foundation for personalized medicine approaches, enabling clinicians to tailor treatments based on individual epigenetic profiles and ultimately improve patient outcomes.

1.5.2 Histone modifications in the regulation of cancer

1.5.2.1 Histone acetylation

Histone modification refers to chemical changes made to histone proteins, which help package DNA into the fundamental units of chromatin called nucleosomes. These modifications involve the addition or removal of various chemical groups, such as acetyl, methyl, phosphoryl, or ubiquitin groups. Depending on the type and location of the modification, these changes can either activate or repress gene transcription by altering the accessibility of DNA to transcriptional machinery. Among these, histone acetylation is one of the most well-studied modifications. It involves the addition of an acetyl group (-COCH3), primarily to lysine residues on histone tails. This process neutralizes the positive charge of lysine, reducing the electrostatic interaction between histones and negatively charged DNA. As a results, chromatin becomes less compact, allowing transcription factors easier access to DNA and facilitating gene activation

(Yen, Huang et al. 2016). The level of histone acetylation is regulated by the dynamic balance between histone acetyltransferases (HATs) and histone deacetylase (HDACs) (Ropero and Esteller 2007). Dysregulation of this balance can disrupt normal gene expression patterns and has been implicated in the development of various diseases, particularly cancer (Yasui, Oue et al. 2003). Recent studies have shown that alterations in histone acetylation, especially on histone H3, are closely associated with cancer aggressiveness. For instance, changes in H3K4 acetylation (H3K4ac) correlate with the degree of tumor invasiveness (Miziak, Baran et al. 2024). Elevated levels of H3K4ac have been observed near the promoter regions of estrogen receptor (ER) signaling -responsive genes in both ER-positive MCF7 cells and triple-negative MD-MB-231 breast cancer cells (Messier, Gordon et al. 2016). Additionally, H3K4ac has been detected at the promoters of epithelial-mesenchymal transition (EMT) markers genes such as GLI1(GLI1) (Liu, Liu et al. 2020) and CDH1 (E-cadherin) (Markouli, Strepkos et al. 2021).

The link between H3K4ac and EMT, a key process in cancer metastasis, is also influenced by HDAC activity. Inhibition of HDACs enhances H3K4ac levels, promoting the expression of EMT related genes. Furthermore, HDACs have been shown to remove H3K4ac and suppress EMT gene expression under hypoxic conditions, suggesting a crucial role in hypoxia-induced EMT and metastasis (Lin and Wu 2020, Wang, Yan et al. 2020). Beyond H3K4ac, other acetylation markers such as H3K9ac and H3K27 ac also contribute to oncogenic processes. Aberrant acetylation at these sites can activate genes involved in uncontrolled cell growth, migration, and invasion. For example, pan-HDAC inhibitors increase H3K9 acetylation at the promoter of the nedd9 gene, which enhances breast cancer metastasis (Hu, Wei et al. 2023). Similarly, H3K27 acetylation has been shown to activate COL6A1, thereby promoting cell migration and invasion in osteosarcoma (Zhang, Liu et al. 2021).

1.5.2.2 Histone methylation

Methylation of histones involves the addition of methyl groups (CH3) from S-adenosylmethionine (SAM) to specific amino acids of the histone proteins, most commonly to lysine or arginine residues, and typically catalyzed by histone methyltransferases (HMTs). In contrast, histone demethylases (HDMs) remove these methyl groups, reversing the methylation marks (Greer and Shi 2012). This

modification can either activate or repress gene expression, depending on the specific histone and the amino acid position (Kouzarides 2002). There are 3 types of histone methylation depending on the number of methyl, mono-methylation has one methyl group added, Di-methylation has 2, and Tri-methylation has 3 methyl groups added which represents the most common histone methylation (Cheung and Lau 2005). Mono-methylation of histone H3 at lysine 4 (H3K4me) is usually associated with active gene transcription (Benayoun, Pollina et al. 2014), while methylation at H3K27me3 (Hansen, Bracken et al. 2008, Igolkina, Zinkevich et al. 2019) and H3K9me3 is associated with gene silencing and the formation of repressive chromatin structure. In cancer, aberrant histone methylation patterns are commonly observed (Song, Wu et al. 2016), leading to the activation of oncogenes or silencing of tumor suppressor genes. For example, H3K9me3 are often found at the promoters of tumor suppressor genes like p16INK4a, which result in the silencing of the genes and thus facilitate cancer cell proliferation and metastasis (Kostaki, Manona et al. 2014). Conversely, the activation of oncogenes can be facilitated by aberrant methylation patterns, such as H3K4me3, which is often found at the promoters of genes that drive cancer cell proliferation. For example, H3K4me3 activates RAS transcription by NSD2 drives lung cancer proliferation (García-Carpizo, Sarmentero et al. 2016). Besides, the dysregulation of histone methylation is frequently associated with the loss of normal cell cycle control and metastasis, and as such, HMTs and demethylases are being explored as potential therapeutic targets in cancer treatment. Besides, histone methylation can regulate genes involved in cancer immune response, for example, low enrichment of repressive histone marks, such as H3K27me3 and H3K9me3 are associated with the expression of lymphocyte activation gene 3 (LAG-3), immune checkpoint gene like programmed death receptor 1 (PD-1), and Cytotoxic T-lymphocyte associated protein 4 (CTL-4) in human colorectal and primary breast cancer (Sasidharan Nair, El Salhat et al. 2018, Sasidharan Nair, Toor et al. 2018). This reduction in repressive histone marks can decrease immune inhibitory signals, thereby promoting immune evasion of tumor cells. Thus, understanding and targeting these epigenetic mechanisms offers promising avenues for more precise and effective cancer therapies.

1.6 The role of RNA polymerase II (Pol II) in cancer

1.6.1 The regulation of Pol II pause and release

RNA transcription is a fundamental process in which RNA is synthesized from a DNA template. Among eukaryotic cells, RNA polymerase II (Pol II) is primarily responsible for transcribing protein-coding genes into messenger RNA (mRNA). Transcription initiation begins with the recognition of core promoter elements, such as the TATA box, by a set of general transcription factors (TFIIA, TFIIB, TFIID, TFIIE, TFIIF, TFIIH), These factors coordinate with Pol II and additional cofactors to assemble the preinitiation complex (PIC).

A critical step in the transition from initiation to elongation involves the phosphorylation of the C-terminal domain (CTD) of Pol II by TFIIH. This modification facilitates the recruitment of elongation factors, including positive transcription elongation factor b (P-TEFb), which releases Pol II from transcriptional pausing, stabilizes the nascent RNA, and ensures efficient transcriptional elongation. Once Pol II reaches a termination signal, and RNA cleavage complex processes the nascent transcript, and the resulting pre-mRNA undergoes key modifications, which are 5’ capping, intron splicing, and 3’ polyadenylation, to become mature mRNA.

Pol II frequently undergoes promoter-proximal pausing shortly after initiating transcription. This regulated pause enables precise control over gene expression and is tightly linked to CTD phosphorylation. The paused Pol II is typically enriched with serine 5 phosphorylation (ser5) and is stabilized at the promoter region by the DRB sensitivity-inducing factor (DSIF) and negative elongation factor (NELF). The release from this paused state is mediated by P-TEFb, a complex composed of cyclin T and CDK9, which phosphorylates serine 2 (ser2) on the CTD (Liu, Kraus et al. 2015). In addition, P-TEFb phosphorylates DSIF and NELF, leading to the dissociation of NELF and the conversion of DSIF into a positive elongation factor (Fujinaga, Irwin et al. 2004) (Fig. 10). As such, the release of paused Pol II to active elongation is tightly regulated, influenced by multiple signals including extracellular stress, transcription factors, and intracellular signaling pathways. For example, heat-induced transcriptional memory has been shown to accelerate Pol II pause release (Vihervaara, Mahat et al. 2021). Under hypoxic conditions, HIF1α interacts with the CDK8 mediator complex to recruit

P-TEFb and promote transcriptional elongation (Galbraith, Allen et al. 2013). Moreover, Rnf20, as reported by Shema *et al*, can inhibit transcriptional elongation by modulating TFIIS activity, thereby suppressing the expression of oncogenes (Shema, Kim et al. 2011).

Conclusively, transcription by Pol II is a complex and tightly regulated process. The controlled pausing and release of Pol II serve as critical regulatory checkpoints, allowing cells to integrate environmental cues and signaling pathways to fine-tune gene expression, particularly in response to stress and in disease contexts such as cancer.

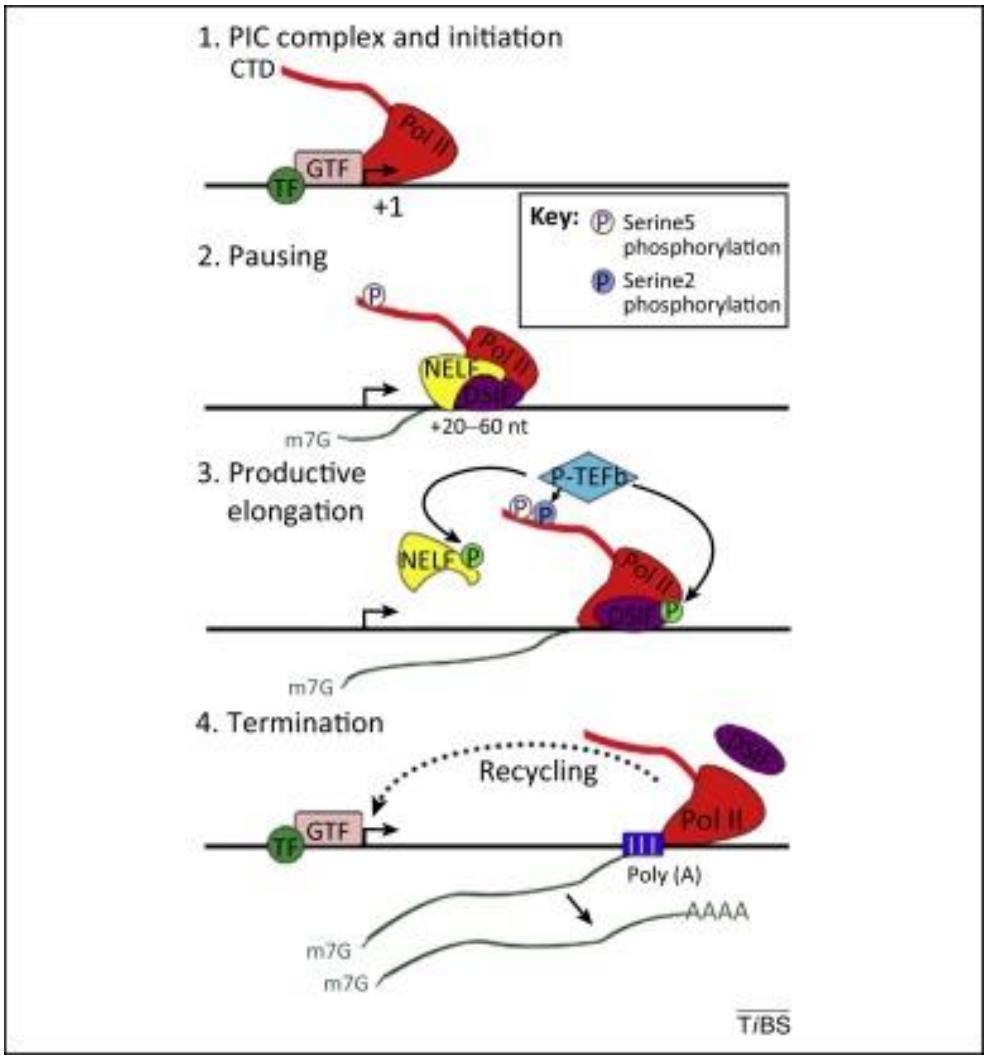

Figure 10. Gene transcription mediated by RNA polymerase II (Pol II) occurs through a series of distinct steps. (Xiuli Liu *et al,* 2024). Permission is conveyed through Copyright clearance Center, Inc.

1.6.2 Pol II pause and release in the development of cancer

As Pol II pause and release represents an important checkpoint in transcription regulation, it was believed to be involved in maintaining cellular homeostasis by ensuring precise control over gene expression. While direct links between Pol II pausing dysregulation and oncogenesis have historically been limited, emerging evidence suggests that aberrant regulation of Pol II pause-release mechanisms is closely associated with cancer progression.

For example, a study in neuroblastoma cells revealed that Aurora-A impairs competes with TFIIC for chromatin binding, disrupting the recruitment of RAD21 to N-MYC target sites. This interference suppresses N-MYC driven promoter escape and Pol II pause release, suggesting that MYC-driven tumors are especially dependent on Aurora-A to avoid transcription replication conflicts. This dependency highlighting a potential vulnerability that could be exploited for the rational development of targeted therapies against these tumors (Büchel, Carstensen et al. 2017). This is further supported by the role of super enhancer, which recruits BRD4, a key coactivator and regulator of P-TEFb activity (Jang, Mochizuki et al. 2005), to drive the high expression of oncogenes. Thus, creating a transcriptional addiction in cancer cells, making them particularly sensitive to BRD4 inhibitors, which can effectively disrupt the transcriptional machinery essential for tumor cell survival (Donato, Croci et al. 2017). Additionally, mutation of BRCA2 impairs the recruitment of PAF1, a transcription elongation factor, leading to Pol II stalling at promoter-proximal pause (PPP) sites. This stalling causes DNA damage and contributes to genomic instability, a hallmark of cancer (Shivji, Renaudin et al. 2018). In breast cancer, treatment with DNA demethylation agents was shown to promote release of Pol II at genes with hypermethylated upstream regions, further supporting the role of chromatin context in regulating transcription dynamics (Tao, Liu et al. 2011). Moreover, recent research in colon cancer cells revealed that selective inhibiting CDK12 activates P-TEFb, thereby enhancing Pol II pause release and promoting transcriptional elongation of genes within key oncogenic pathways, including p53 and NF-κB (Wang, Himanen et al. 2023). These findings underscore the importance of Pol II pausing and release in cancer biology and suggest that targeting transcriptional dependencies, particularly at the level of pause-release regulation,

could offer novel and selective therapeutic strategies for treating aggressive and treatment-resistant cancers.

1.7 RNF20

1.7.1 RNF20, H2Bub1, and DNA damage

Ring finger protein 20 (RNF20), also known as BRE1A, is a member of the RING finger protein family and functions as a ubiquitin ligase (Nakamura, Kato et al. 2011). It forms a heterodimeric complex with RNF40 and specifically mono-ubiquitinates histone H2B at lysine 120 (H2Bub1) (Fig. 11), a modification crucial for various cellular processes such as DNA repair, transcription elongation, cell cycle regulation, and tumor progression (Shiloh, Shema et al. 2011, Tarcic, Granit et al. 2017, Wang, Xu et al. 2021). One of the key functions of RNF20 mediated H2Bub1 is in homologous recombination repair (HRR). H2Bub1 enhances chromatin accessibility at sites of DNA double-strand breaks, facilitating the recruitment of DNA repair proteins such as the RAD6 complex. This modification supports the efficient assembly of the repair machinery, thereby promoting accurate and timely DNA repair (Nakamura, Kato et al. 2011, So, Ramachandran et al. 2019, Deng, Ai et al. 2023).By modulating chromatin structure, RNF20 makes DNA damage sites more accessible to repair enzymes, supporting accurate DNA repair. The importance of RNF20 in maintaining genome integrity is further highlighted by studies demonstrating that loss of RNF20 results in genomic instability, impaired DNA repair, increased mutation rates, and chromosomal abnormalities, all of which contribute to tumorigenesis (Sethi, Shanmugam et al. 2018). Moreover, suppression of RNF20 and the subsequent loss of H2Bub1 have been shown to reduce the expression of the tumor suppressor p53 and its downstream target p21, linking RNF20 activity to cell cycle regulation and tumor suppression (Wu, Cui et al. 2020).

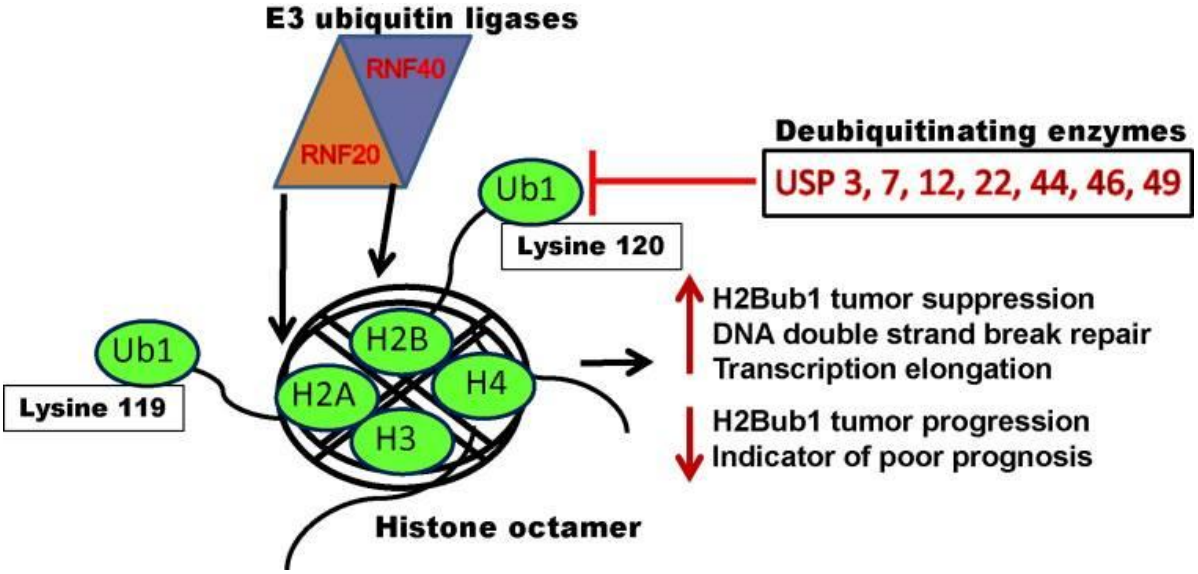

Figure 11. The post translational modification (PTM) of H2B on specific amino acid residues on histone. And the regulation of various processes like DNA DSB repair, transcription elongation, role of tumor suppressor and onco-protein. (Gautam Sethi *et al,* 2018). Permission is conveyed through Copyright clearance Center, Inc.

1.7.2 Emerging role of RNF20 in metabolic regulation

While the role of RNF20 in the DNA damage response and transcriptional regulation is well established, recent studies suggest that RNF20 also plays an important role in metabolic processes, particularly those related to energy production, nutrient sensing, and lipid storage. One study reported that RNF20 facilitates the degradation of nuclear corepressor 1 (NCoR1), thereby activating PPARγ mediated transcription and promoting adipogenesis (Jeon, Lee et al. 2020). Besides, RNF20 has been shown to regulate adipose thermogenesis in response to cold exposure by interacting with substrates specific to brown adipose tissue (BAT) and inguinal white adipose tissue (iWAT), supporting its role in temperature responsive metabolic adaptation (Jeon, Nahmgoong et al. 2024). Beyond adipogenesis, RNF20, together with RNF40, also contributes to glucose -stimulated insulin secretion by modulating histone modifications in pancreatic β-cells, thereby influencing the transcription of genes essential for insulin release (Pierre, Liu et al. 2024). In line with these findings, an *in vivo* study showed that *Rnf20* knockout in mice leads to progressive fat loss, organomegaly, and hyperinsulinemia, indicating that RNF20 is essential for adipose tissue development and metabolic homeostasis (Liang, Tao et al. 2021). This is also evidenced by the role of RNF20 in the polyubiquitination of the transcription factor activator protein 2α (AP-2α), which induces the degradation of the protein, and impairs

the adipocyte differentiation(Wu and Brenner 2014). Although much of the current research has focused on the role of RNF20 in adipose tissue metabolism, its potential functions in other metabolic pathways remain largely unexplored. Interestingly, a recent study in breast cancer identified a cooperative interaction between HIF1α, RNF20, and RNF40, suggesting that RNF20 may also contribute to the regulation of glycolysis in cancer cells (Lyu, Yang et al. 2024).This finding opens new avenues for investigating RNF20's broader role in cellular metabolism beyond adipose biology.

1.7.3 Dual role of RNF20 in cancer: tumor suppressor and context-dependent oncogenic functions

Extensive studies have established a strong link between chromatin modifications and cancer development. As a key regulator of histone ubiquitination, RNF20 plays a critical role in maintaining cellular homeostasis, and its dysregulation has been implicated in the initiation and progression of multiple cancers. Somatic alterations in RNF20 have been identified across various malignancies, including breast cancer, prostate cancer, lung cancer, clear cell renal cell carcinoma (ccRCC), and pancreatic cancer (Sethi, Shanmugam et al. 2018) (Table 3).

RNF20 helps maintain the ubiquitination levels of H2B, which is essential for normal cellular function, and disruptions at H2Bub1 level often leads to malignant transformation. For example, malignant breast cancer samples exhibit significantly reduced H2Bub1 levels compared to benign tissues (Prenzel, Begus-Nahrmann et al. 2011). This decrease has been linked to elevated expression of USP22, a deubiquitinating enzyme highly expressed in aggressive breast cancers. USP22 overexpression reduces H2Bub1 levels, enhances tumor aggressiveness, and is associated with lymph node metastasis and disease recurrence (Liu, Yang et al. 2010, Zhang, Yao et al. 2011). In clear cell renal cell cancer, RNF20 overexpression suppresses lipogenesis and cell proliferation by downregulating sterol regulatory element-binding protein 1c (SREBP1c), resulting in reduced tumor growth and lipid accumulation in xenograft mouse models. Moreover, low RNF20 expression correlates with poor prognosis in ccRCC patients (Sethi, Shanmugam et al. 2017). Indicating that RNF20 functions as a tumor suppressor in this context.

Cancer cells are characterized by chronic inflammation(Coussens and Werb 2002). Inflammation becomes chronic when the body's immune system remains activated for extended periods of time, which is often observed in tumor microenvironments and has been linked to the development of cancer like colorectal cancer, gastric cancer, and liver cancer(Berasain, Castillo et al. 2009, Schmitt and Greten 2021, Jaroenlapnopparat, Bhatia et al. 2022). Thus, factors connecting inflammation and cancer are of significant interest. Notably, *Rnf20+/-* mice are more susceptible to both acute and chronic colonic inflammation and the subsequent development of colorectal cancer (Tarcic, Pateras et al. 2016, Kosinsky, Chua et al. 2019, Kosinsky, Zerche et al. 2021). Mechanistically, downregulation of RNF20 and H2Bub1 favors the binding of p65-containing nuclear factor κB (NF-κB) dimers over repressive p50 homodimers, promoting pro-inflammatory gene transcription and contributing to inflammation-associated tumorigenesis (Tarcic, Pateras et al. 2016, Zhou, Cai et al. 2021, Kumar, Basu et al. 2024). Moreover, the downregulation of RNF20 is associated with chromosomal instability, further facilitating colorectal carcinogenesis (Barber, McManus et al. 2008). On the other hand, depletion of RNF20 and the consequent loss of H2Bub1 in fallopian tube epithelial cells which is the presumed site origin for many high grade serous ovarian cancers (HGSOCs), lead to an elevated expression of IL6 and enhanced cell migration(Hooda, Novak et al. 2019), suggesting that RNF20 loss may contribute to a pro-tumorigenic inflammatory environment and increased metastatic potential in HGSOC development.

Despite its tumor suppressive roles, RNF20 can also function as tumor promoter in certain malignancies. In primary glioma, RNF20 promotes tumorigenesis by inducing polyubiquitination and degradation of the tumor suppressor Ebp1 (Liu, Oh et al. 2009). Similarly, findings presented at the AACR annual meeting (2018) highlighted RNF20's role in ovarian cancer, showing that it is highly expressed in 87% of high grade serous ovarian cancer (HGSOC) cases. Notably, downregulation of RNF20 impaired cisplatin sensitivity, suggesting that RNF20 acts as a tumor promoter and a potential therapeutic target for enhancing ovarian cancer treatment efficacy (Cole, Dickson et al. 2018). Additionally, a study identified RNF20 as a crucial chromatin regulator in mixed-lineage leukemia (MLL) rearranged leukemogenesis. Suppression of RNF20 in leukemia cells inhibited proliferation *in vitro* and slowed disease progression *in vivo*, underscoring its role in promoting leukemia development (Blank, Tang et al. 2012). Moreover, in

prostate cancer, RNF20 has been found to interact with the androgen receptor (AR), and its depletion was associated with reduced prostate cancer cell proliferation, indicating that RNF20 may drive tumor growth by modulating AR signaling pathways(Sethi, Shanmugam et al. 2018). These findings collectively suggest that RNF20 functions as a context dependent regulator of cancer progression, acting as either a tumor suppressor or a tumor promoter depending on the tumor type.

Table 3. RNF20 mutations in different cancer types. (Gautam Sethi *et al,* 2018).

Cancer type	Number of new cases diagnosed in U.S and Canada	Overall alterations (%) (deletions, mutations, amplification, multiple)
Breast	276,989	1.1
Lung	252,826	1.6
Prostate	202,499	3.3
Colorectal	160,640	3.3
Uterine	79,607	5.8
Pancreatic	58,230	3.7

1.8 Objective:

Evolving cancer treatment strategies focus on identifying novel therapeutic targets that exploit genetic aberrations driving oncogenesis to counter cancer growth and metastasis. In recent years, chromatin-binding enzymes have been identified as key regulators of post-transcriptional modifications, wither their dysregulated expression closely linked to tumorigenesis. The E3 ubiquitin ligase RNF20, which catalyzes the ubiquitination of histone H2B, has been increasingly recognized for its role in cancer. Emerging studies have demonstrated that RNF20 and H2Bub expression are significantly reduced across various tumor types, suggesting their potential involvement in cancer development and progression. However, there is limited evidence discussing the role of RNF20 in lung cancer, and its mechanisms involvement across different cancer types remain unclear. Thus, this study aims to address the following questions:

(1) Does the loss of *Rnf20* contribute to lung cancer progression?
(2) What are the underlying mechanisms by which RNF20 loss drives lung cancer cell growth and migration?
(3) What is the relationship between *RNF20* expression levels and lung cancer in patients?

2 MATERIALS AND METHODS

2.1 Materials

2.1.1 Equipment

Equipment	Source of supply
Agilent 2100 Bioanalyzer System	Agilent
Agilent Seahorse Xfe24 Analyzer	Agilent
Bacterial incubator 37 °C	Thermo Scientific
Balance LC 4800 P	Sartorius
Binocular microscope M165FC	Leica
Binocular microscope MZ16FA	Leica
Cell culture incubator	Thermo Scientific
Cell culture safety cabinet	Thermo Scientific
Centrifuge HERAEUS Fresco 17	Thermo Electron Corporation
Centrifuge HERAEUS Multifuge 1S-R	Thermo Electron Corporation
Centrifuge HERAEUS Pico 17	Thermo Electron Corporation
Confocal microscope LSM 700	Zeiss
Covaris M220 Focused Ultrasonicator	PerkinElmer Company
Fluorescence microscope DM6000B	Leica
Leica Biosystems RM2245	Leica
Thermo Scientific HistoStar	Thermo Scientific
PH meter	Millipore
Hypoxia chamber	Coylab
Heating block TH 21	HLC BioTech
Light microscope Wilovert S	Hund Wetzlar
Qubit™ Fluorometer	Thermo Scientific
Real-Time StepOne Plus Real-Time PCR System	Applied Biosystems
Rocking platform 444-0142	VWR
Rotator SB3	Stuart
SDS-PAGE apparatus	Bio-Rad
Sonifier Sonopuls GM 2070	Bandelin electronic
Thermal cycler C1000 Touch	BIO-RAD
Thermo block 5436	Eppendorf
Thermo block MHR 23	HLC BioTech
Vortexer VF2	IKA®-Labortechnik Staufen
Water bath cell culture WMB 22	Memmert
Water bath Julabo U3	Julabo Labortechnik GMBH
Western Blotting Transfer apparatus	Bio-Rad

2.1.2 Chemicals

Chemicals	Source of supply	Reference number
1 kb Plus DNA ladder (0.1-10.0 kb)	NEB	N3200L
Agarose NEEO Ultra	Roth	2267.3
Albumin fraction V (BSA)	Roth	8076.2
Ammonium persulfate (APS)	Sigma	A3678-25G
Ampicillin sodium salt	Sigma	A99518-25G
Aqueous 30 % acrylamide and bisacrylamide stock solution (37.5:1)	Carl Roth	3029.1
Bromophenol Blue	Sigma	B0126
BSA (for ChIP)	NEB	B9000s
Chloroform ($CHCl_3$)	Roth	3313.4
Dimethyl sulfoxide (DMSO)	Sigma	D2438
Dithiothreitol (DTT)	Roth	6908.3
Dry milk, nonfat milk	Cell Signaling	9999
dNTP (Nucleoside triphosphate) Set 1	Roth	178.1
Ethanol	Roth	K928.3
Ethanol	Sigma	459844
Ethidium bromide solution	Sigma	E1510-10ML
Ethylene glycol tetraacetic acid (EGTA)	Roth	3054.2
Ethylenediaminetetraacetic acid (EDTA)	Sigma	E5134-250G
Formaldehyde	Sigma	F8775
FuGENE® HD Transfection Reagent	Roche	4709705/100
Glycerol	Roth	3783,1
Glycine	Sigma	15527
Halt Protease Inhibitor Cocktail (100X) 5 mL	Thermo Fischer	78429
Hexadimethrine bromide (polybrene)	Sigma-Aldrich	H9268
Isopropanol (C_3H_8O)	Roth	6752,4
LB-agar	Roth	X965,2
LB-medium	Roth	X964,2
Low-melt agar	Roth	
Magnesium chloride ($MgCl_2$)	Sigma	M2393-500G
Methanol (CH_3OH)	Roth	4627.5
Nonidet P-40 (NP-40)	Fluka	74385
PageRuler Plus Prestained Protein Ladder, 10 to 250 kDA	Thermo Fischer	26619
Paraformaldehyde (PFA)	Thermo Fischer	12587010
Phosphatase inhibitor cocktail set	Millipore	524632-1SET

Potassium chloride (KCl)	Roth	6781.3
Puromycin Dihydrochloride 10x1 mL	Thermo Fischer	A1113803
Sodium dodecyl sulfate (SDS)	Sigma	L4390-100G
Sodium phosphate monobasic monohydrate (NaH2PO4 · H2O)	Sigma-Aldrich	53522-1KG
Tetramethylethylenediamine (TEMED)	Roth	2367,1
Tris(hydroxymethyl)aminomethane (TRIS)	Roth	4855.2
Triton X-100	Sigma	X100-500ML
TRIzol LS Reagent 200 mL	Thermo	10296028
TRIzol® reagent	Invitrogen	15596026
Tween 20	Sigma	T2700-500ML
β-mercaptoethanol (C_2H_6SO)	Sigma	60-24-2
Xylol	Carl Roth	2662.5

2.1.3 Cell culture medium and supplements

Medium/supplements	**Source**	**Catalogue number**
DMEM (1x) high glucose. no glutamine	Gibco	10938-025
RPMI 1640	Gibco	11875093
DMEM/F-12 Medium no glutamine	Gibco	21331020
Ham's F 12 Nutrient Mix	Gibco	11765054
Opti-MEM	Gibico	31985062
Polybrene	Sigma-Aldrich	H9268
L-Glutamine	Gibco	25030-024
Penicillin-Streptomycin	Gibco	15140-122
DMSO	Sigma	D2650
FBS	Gibco	10270-106
Lipofectamine 2000	Invitrogen	11668019
Lipofectamine 3000	Invitrogen	L3000008
Lipofectamine™ RNAiMAX Transfection Reagent	Invitrogen	13778075
Puromycin	Gibco	A11138-03
X-tremeGENE HP DNA Transfection Reagent	Roche	6366236001

2.1.4 Buffer and solutions

buffer	Recipe	Usage
RIPA	50mM Tris-HCl, pH 8.0	Extract Proteins

	150mM NaCl 1% NP-40 0.5% sodium deoxycholate 0.1% SDS	
Sodium citrate buffer (pH6.0)	10 mM Sodium Citrate 0.05% Tween 20	Antigen Retrieval for IHC
Lysis Buffer	10mM Tris-HCl pH 8.0 10mM NaCl 0.5% NP-40	Lysis of Chromatins for ChIP
Nuclear Lysis Buffer	50mM Tris-HCl pH 7.5 10mM EDTA 0.5% SDS	Lysis of Chromatins for ChIP
Nuclear Lysis Buffer without SDS	50mM Tris-HCl pH 7.5 10mM EDTA	Lysis of Chromatins for ChIP
2xIP buffer	0.2% SDS 2% Triton X-100 2mM EDTA	Ip buffer for ChIP

	100mM Tris-HCl pH7.5 600mM NaCl 0.2% Na-Doc	
Low salt buffer	0.1% SDS 1% Triton X-100 2mM EDTA 20mM Tris-HCl pH7.5 150Mm NaCl	Wash buffer for ChIP
High salt buffer	0.1% SDS 1% Triton X-100 2mM EDTA 20mM Tris-HCl pH7.5 500Mm NaCl	Wash buffer for ChIP
LiCl buffer	10mM Tris-HCl pH7.5 250mM LiCl 1% NP-40 1% Na-Doc 1mM EDTA	Wash buffer for ChIP
TE buffer	1M Tris-HCl pH8.0 500mM EDTA	DNA dilution
DNA elution buffer	10mM Tris-HCl pH7.5 0.6% SDS 300mM NaCl 0.5mM EDTA	DNA elution
Sodium citrate buffer	10mM Sodium citrate (dihydrate) 0.05% Tween 20	Antigen retrieval

2.1.5 Kits

Kit	Source of supply	Reference number
2x SYBR Green master mix	Applied Biosystems	4367659
Amersham ECL Prime Western Blotting Detection Reagent	GE Healthcare	RPN2232
Bioanalyzer High Sensitivity DNA Analysis	Agilent	5067-4626
Chip DNAb Clean&Concentrator	Zymo	D5205
GenEluteTM gel extraction kit	Sigma	NA1111
GenEluteTM HP plasmid midiprep kit	Sigma	NA0200
GenEluteTM HP plasmid miniprep kit	Sigma	NA0160

GenEluteTM PCR clean-up kit	Sigma	NA1020
High-Capacity cDNA Reverse Transcription Kit	Applied Biosystems	4368813
NEBNext High-Fidelity 2X PCR Master Mix	NEB	M0541S
NEBNext Ultra II DNA Library Prep Kit with Purification Beads 96 reactions	NEB	E7103L
NEBNext® Multiplex Oligos for Illumina® (96 Index Primers)	NEB	E6609S
NEBNext® Multiplex Oligos for Illumina® (Index Primers Set 1)	NEB	E7335S
Pierce™ BCA Protein Assay Kit	Thermo Scientific	23225
Qubit dsDNA HS Assay Kit-100 assays	Thermo Fisher S	Q32851
RNeasy Plus Universal Mini Kit 50	Qiagen	73404
SuperSignal™ West Femto Maximum Sensitivity Substrate	Thermo Fisher	34094
Crystal Violet	Sigma Aldrich	HT901
HEMATOXYLIN	Sigma Aldrich	GHS116
EASIN	Sigma Aldrich	HT-110216
VECTASTAIN Universal Quick HRP Kit	VECTASTAIN	VEC-PK-7800

2.1.6 Consumables

Cell culture materials	Source of supply	Reference number
15ml Centrifuge Tubes	Greiner Bio-One	188271
50ml Centrifuge Tubes	Greiner Bio-One	227261
5ml Plastic pipet	Greiner Bio-One	606180
10ml Plastic pipet	Greiner Bio-One	607180
25ml Plastic pipet	Greiner Bio-One	760180
6-cm dish (cell culture)	Greiner Bio-One	628160
10-cm dish (cell culture)	Greiner Bio-One	664160
15-cm dish (cell culture)	Greiner Bio-One	639160
6-well plates (cell culture)	Greiner Bio-One	657160

12-well plates (cell culture)	Greiner Bio-One	665180
24-well plates (cell culture)	Greiner Bio-One	662160
48-well plates (cell culture)	Greiner Bio-One	677180
96-well plates (cell culture)	Greiner Bio-One	655180
Reservior	VWR	89094-664
Ultra filter 10KD	AMICON	UFC501024
U-40 insulin syringe	Omnican	24D01C8
Object superFrost	Carl Roth	AAAA00008232E01MNZ 10MH
Transwell insert	Greiner bio-one	662638
Tissue-Tek Cryomold	SAKURA	4565

2.1.7 Antibodies

Antibody	Source	Catalogue number
TTF1	Abcam	ab76013
CD45	Abcam	ab10558
CGRP	Sigma-Aldrich	c8198
Synaptophysin	Cell Signaling	36406S
Napsin A	Abcam	ab73021
Ki67	Abcam	ab15580
P63	Cell Signaling	4981S
RNF20	Novus	NB100-2243
RNF20	Cell Signaling	11974S
RNF40	Novus	NBP1-53086
α-tubulin	Sigma-Aldrich	T5168
α-tubulin	Cell Signaling	2144S
TP53	Cell Signaling	2524S
Rb	Cell Signaling	9309
γH2Ax	Cell Signaling	9718

E-cadherin	Abcam	ab11512
Snai1	Cell Signaling	3879
N-cadherin	Sigma-Aldrich	C3865
Fibronectin	Abcam	ab2413
Vimentin	Cell Signaling	5741
Glut1	Alpha Diagnostic	Gt 11-A
LDHA	Cell Signaling	2012S
HIF1α	Cayman Chemical	10006421
HIF1α	Cell Signaling	14179S
PDK1	Cell Signaling	3062s
H2b	Abcam	1790
H2bub1	Cell Signaling	5546S
Rpb1 NTD	Cell Signaling	14958
H3K4me3	Cell Signaling	9751S
Eno1	Proteintech	11204-1-AP
Pol II p-ser2	Cell Signaling	13499s
Pol II p-ser5	Abcam	ab5131
HPR-Anti-Mouse secondary antibody	Jackson ImmunoR	115-035-003
HRP-Anti-Rabbit secondary antibody	Jackson ImmunoR	111-035-045
HRP-Anti-Rat secondary antibody	Invitrogen	31470
Donkey anti-Mouse IgG (H+L) ReadyProbes™ Secondary Antibody, Alexa Fluor 488	Thermo Fisher Scientific	R37114
Donkey anti-Mouse IgG (H+L) Highly Cross-Adsorbed Secondary Antibody, Alexa Fluor 555	Thermo Fisher Scientific	A-31570
Donkey anti-Rabbit IgG (H+L) Highly Cross-Adsorbed Secondary Antibody, Alexa Fluor 488	Thermo Fisher Scientific	A-21206
DAPI	Cell Signaling	4083S

2.1.8 Primers and oligonucleotides

Primer	Sequence (5'-3')
q-PCR TP53 forward M.musculus	GTGTGGTGCAGATCGCAGT
q-PCR TP53 reverse M.musculus	ATCATGCCTTCGGACTTGATG
q-PCR Rb forward M.musculus	CAAACGGAGGAAATGACTTTGGG
q-PCR Rb reverse M.musculus	GTGTCAGGGTGAGTTGGGTTC
q-PCR RNF20 forward M.musculus	CGACATTGTGAGCTGGAGAA
q-PCR RNF20 reverse M.musculus	GGGCTTTCAACTGCAGACTC
q-PCR RNF20 forward Human	GGAGCTCTTATCCCGGAAGC
q-PCR RNF20 reverse Human	AACTCCTGAGACATGGTGCG
q-PCR RNF40 forward M.musculus	CACGACCACTCTAATCGAACC
q-PCR RNF40 reverse M.musculus	TCCAATTTCTCAATTCTCTCCCG
q-PCR RBX1 forward M.musculus	CCATCTGCAGGAACCACATT
q-PCR RBX1 reverse M.musculus	CTCCCACTCTCTCTGTTGTCCA
q-PCR Actb forward M.musculus	CAGATGCCACTACAGCACG
q-PCR Actb reverse M.musculus	CCTGCCGCTGCCATAGAAG
q-PCR Actb forward Human	ACAGAGCCTCGCCTTTGCC
q-PCR Actb reverse Human	GATATCATCATCCATGGTGAGCTGG
q-PCR Slc2a1 forward M.musculus	ATAGTTACAGCGCGTCCGTT
q-PCR Slc2a1 reverse M.musculus	TAGCCGAACTGCAGTGATCC
q-PCR Hif1α forward M.musculus	GCGGCGAGAACGAGAAGAAA
q-PCR Hif1α reverse M.musculus	GGGGAAGTGGCAACTGATGA
q-PCR Ldha forward M.musculus	AACTTGGCGCTCTACTTGCT
q-PCR Ldha reverse M.musculus	TAGCCGCCTGAGGACTTACT
q-PCR HK1 forward M.musculus	TCCATCCACACTTCTCCAGAATC
q-PCR HK1 reverse M.musculus	AGGAAACACCACTCCGACTT
q-PCR PDK1 forward M.musculus	GGACTTCGGGTCAGTGAATGC
q-PCR PDK1 reverse M.musculus	TCCTGAGAAGATTGTCGGGGA
q-PCR Eno1 forward M.musculus	TGCGTCCACTGGCATCTAC
q-PCR Eno1 reverse M.musculus	CAGAGCAGGCGCAATAGTTTTA

q-PCR Vegfa forward M.musculus	CTCCACCATGCCAAGTGGTC
q-PCR Vegfa reverse M.musculus	GTCCACCAGGGTCTCAATCG
q-PCR Snai1 forward M.musculus	CACACGCTGCCTTGTGTCT
q-PCR Snai1 reverse M.musculus	GGTCAGCAAAAGCACGGTT
q-PCR Cdh1 forward M.musculus	AGCTCTAAGGACAGTGGTCAT
q-PCR Cdh1 reverse M.musculus	CAGTGCTTTACATTCCTCGGT
q-PCR GAPDH forward M.musculus	AACTTTGGCATTGTGGAAGG
q-PCR GAPDH reverse M.musculus	GGATGCAGGGATGATGTTCT
q-PCR Fn1 forward M.musculus	ATGTGGACCCCTCCTGATAGT
q-PCR Fn1 reverse M.musculus	GCCCAGTGATTTCAGCAAAGG
ChIP q-PCR SLC2a1-5utr forward	AGTGACGATCTGAGCTACGG
ChIP q-PCR SLC2a1-5utr reverse	GTTACTCACCTTGCTGCTGG
ChIP q-PCR SLC2a1-gene-body forward	AACGTCAGCAACCTTCAACC
ChIP q-PCR SLC2a1-gene-body reverse	TGCCCATCCCTCAATGTTCT
ChIP q-PCR SLC2a1-3utr forward	CCTCTTGCCTTGGAGCCTT
ChIP q-PCR SLC2a1-3utr reverse	CGCTCTAATTGGTGACGACG
ChIP q-PCR SLC2a1-gene-body forward	AACGTCAGCAACCTTCAACC
ChIP q-PCR VEGFa-5utr forward	GGTAACAGCGGTGGAAGAAA
ChIP q-PCR VEGFa-5utr reverse	ACTCTCCTGTCTCCCCTGAT
ChIP q-PCR VEGFa -gene-body forward	GATGGGGAGGTTCTAAGGCA
ChIP q-PCR VEGFa -gene-body reverse	CAGAAGGAAGGAGAAGGGCA
ChIP q-PCR Ldha-5utr forward	GAGCTTCCATTTAAGGCCCC
ChIP q-PCR Ldha-5utr reverse	CCCAAATCTGAACACCCTGC
ChIP q-PCR Ldha -gene-body forward	GAAAGTCTGACCTCCTGCCT
ChIP q-PCR Ldha -gene-body forward	GTCTTCTCTTCCCTCACCCC
ChIP q-PCR Ldha-3utr forward	TTGCAGCTCAGGTTTTGTCC
ChIP q-PCR Ldha-3utr reverse	CTTAGGGAGTGGCAGTAGGG
ChIP q-PCR Eno1-5utr forward	AAGGTCATCAGCAAGGTCGT
ChIP q-PCR Eno1-5utr reverse	CTTGGGGCATAGCTGGAATG
ChIP q-PCR Eno1-3utr forward	GGTCAGAAAGGGGCATTTGG
ChIP q-PCR Eno1-3utr reverse	AAAATGGATCACGACGCAGC

ChIP q-PCR Pdk1-5utr forward	TGCTAAGGTTCCATCTGCGA
ChIP q-PCR Pdk1-5utr reverse	GCAACAGAAGGCAAAGACCA
ChIP q-PCR Pdk1-3utr forward	AAGTCTCACTGTGTAGCCCC
ChIP q-PCR Pdk1-3utr reverse	CGCTCATCCTCAGATCACCT
gRNA1-RNF20 forward M.musculus	CACCGTGAAAAGCTGGAGCGACGCC
gRNA1-RNF20 reverse M.musculus	AAACGGCGTCGCTCCAGCTTTTCAC
gRNA2-RNF20 forward M.musculus	CACCGGATTTCCATCGCATCTACAT
gRNA2-RNF20 reverse M.musculus	AAACATGTAGATGCGATGGAAATCC
Genotyping for cells forward M.musculus	GCTGTGTCCTTAGTCTCGGT
Genotyping for cells reverse-1 M.musculus	CAAAATCCACTGTCCCGCTC
Genotyping for cells reverse-2 M.musculus	ATTCCCTTCTCAGTGCCCAA
Genotyping for mice forward-1	TCTTTTGAGACAGGGAGCCC
Genotyping for mice forward-2	GAAGACGCGCTATGACACTC
Genotyping for mice reverse	AAGTCTGGGGAACAAGGGAG
Genotyping for cells forward Human	CAGGCCAAGTGATTCTAATGTG
Genotyping for cells reverse-1 Human	GCCCTAAGCGTGATCTAACCTA
Genotyping for cells reverse-2 Human	GAAAGCCAGCCAGCTGATCTTAACAA

2.1.9 Programs and algorithms

Programs and	Source	Website
IGV2.8.13	Integrative Genomics Viewer	https://software.broadinstitute.org/software/igv/download
Image J 1.47v	Image J	https://imagej.nih.gov/ij/download.html
Zen 2.3	ZEISS	https://www.zeiss.de/mikroskopie/produkte/mikroskopsoftware/zen-lite/zen-lite-download.html
DAVID 6.8	(Huang da, Sherman et al. 2009)	https://david.ncifcrf.gov/summary.jsp

Heatmapper	(Babicki, Arndt et al. 2016)	http://www.heatmapper.ca/expression/
GraphPad Prism 8.0.2	GraphPad	https://www.graphpad.com/
Calculate and draw custom Venn diagrams	Bioinformatics & Evolutionary Genomics	http://bioinformatics.psb.ugent.be/webtools/Venn/
STAR version 2.7.3a	(Dobin, Davis et al. 2013)	https://github.com/alexdobin/STAR/blob/master/doc/STARmanual.pdf
Trimmomatic version 0.39	(Bolger, Lohse et al. 2014)	http://www.usadellab.org/cms/?page=trimmomatic
BamTools version 2.5.1	(Barnett, Garrison et al. 2011)	https://github.com/pezmaster31/bamtools
MultiQC version 1.6	(Ewels, Magnusson et al. 2016)	https://multiqc.info/
DESeq2 version 1.28.0	(Love, Huber et al. 2014)	http://bioconductor.org/packages/release/bioc/vignettes/DESeq2/inst/doc/DESeq2.html
Ngsplot version 2.41.4	(Shen, Shao et al. 2014)	https://github.com/shenlab-sinai/ngsplot
Homer version 4.11	(Heinz, Benner et al. 2010)	http://homer.ucsd.edu/homer/motif/
Bowtie2 version 2.3.4.1	(Langmead and Salzberg 2012)	https://github.com/BenLangmead/bowtie2
SAMtools version 1.7	(Li, Handsaker et al. 2009)	http://www.htslib.org/

Picard-tools version 1.119	Broad Institute, 2019b	https://github.com/broadinstitute/picard
deepTools version 3.3.0	(Ramirez, Ryan et al. 2016)	https://deeptools.readthedocs.io/en/develop/
MACS2 version 2.1.1.20160309	Gaspar, 2018	https://pypi.org/project/MACS2/
Metascape version v3.5.20250101	(Zhou, Zhou et al. 2019)	http://metascape.org
Bedtools version 2.28.0	(Quinlan and Hall 2010)	https://bedtools.readthedocs.io/en/latest/
R package DiffBind version 2.16.0	(Ross-Innes, Stark et al. 2012)	http://bioconductor.org/packages/release/bioc/vignettes/DiffBind/inst/doc/DiffBind.pdf
R package ChIPseeker version 1.24.0	(Yu, Wang et al. 2015)	https://guangchuangyu.github.io/software/ChIPseeker/
R package rtracklayer version 1.48.0	(Lawrence, Gentleman et al. 2009)	https://bioconductor.org/packages/release/bioc/html/rtracklayer.html
R package EnhancedVolcano version 1.6.0	(Blighe K et al, 2020)	https://github.com/kevinblighe/EnhancedVolcano
ngs.plot	(Li Shen et al, 2014)	https://github.com/shenlab-sinai/ngsplot
Pausing_Index.py	(Daniel S. Day et al, 2016)	https://github.com/MiMiroot/PIC

2.2 Methods

2.2.1 Mouse line and animal experiment

The Rnf20tm1a (EUCOMM)Wtsi mouse line was generated through micro-injection of Rnf20tm1a (EUCOMM)Wtsi ES cells into blastocysts. The line was obtained from European Conditional Mouse Mutagenesis Program (EUCOMM). All animal experiments were performed according to the institutional guidelines and under an animal experimental protocol approved by the Committee for Animal Rights Protection of the State of Baden-Württemberg (Regierungspraesidium Karlsruhe, Experimental protocol Az.: 35-9185.81/G-260/17). Mice were sacrificed at 6 months and 1 year old. Lungs were isolated, fixed with 3.7% formaldehyde, and embedded in the paraffin. 7 µm thick paraffin sections were used for hematoxylin and eosin staining and IHC staining.

The C57BL/6J and the BALB/cAnN-*Foxn1nu*/Rj mice line were purchased from Janvier Labs and were kept and maintained at the Core Facility Preclinical Models of the Medical Faculty Mannheim. All animal experiments were conducted according to institutional guidelines and approved by the Committee for Animal Rights Protection of the State of Baden-Württemberg (Regierungspraesidium Karlsruhe, Experimental protocol Az.: 35-9185.81/G-119/23). Mice were euthanized at the end of the experiment in accordance with the proposed protocol.

Specifically, for subcutaneous tumor growth assay with A549 cells, A549 (control and RNF20+/-) were cultured in RPMI 1640 medium supplemented with 10% FBS and 1% penicillin-streptomycin (PS). Prior to injection, cells were harvested by trypsinization, washed with PBS, and resuspended in sterile 0.9% NaCl solution at a concentration of $5x10^7$ cells/ml, BALB/cAnN-Foxn1nu/Rj mice (6-8 weeks, Female) received subcutaneous injections of $5x10^6$ cells in 100µl of 0.9% NaCl solution into the right flank. Due to the rapid nature of the procedure and use of a fine needle (27-gauge needle), anesthesia was not required. This procedure was performed in accordance with the approved guidelines of the institutional animal ethics committee, and tumor growth occurs in the subcutaneous elastic adipose and connective tissue, which does not cause pain from tissue displacement. Tumor size was measured every 3 days. Tumor volume was calculated using the formula: volume=(L×(W ^{2})/ 2)(L length; W

width). Mice were euthanized 27 days post injection or when tumors reached a maximum diameter of 1.5cm, which came first. Tumors were excised, fixed in 3.7% formaldehyde, and embedded in paraffin for subsequent analysis.

For tail vein injections and lung metastasis assay with A549 cells, cells (control and RNF20+/- and control and RNF20+/- cells expression control shRNA or shRNA against Hif1α) were cultured as described above, harvested by trypsinization, washed with PBS, and resuspended in sterile 0.9% NaCl solution at a concentration of $1x10^8$ cells/ml, BALB/cAnN-Foxn1nu/Rj mice (6-8 weeks, Female) were briefly anesthetized with 3% isoflurane by inhalation. Using a 27-gauge needle, $1x10^7$ cells in 100µl of 0.9% NaCl solution were injected into the lateral tail vein. After injection, the needle was withdrawn and gentle pressure was applied to the injection site until hemostasis was achieved. Mice recovered from anesthesia within minutes and were monitored for 24 hours post-injection. Mice were euthanized 2-4 weeks post-injection or when human endpoints were reached (based on body condition scoring). Lungs were isolated, fixed in 3.7% formaldehyde, and embedded in paraffin. Sections of 7µm thickness were prepared for H&E staining and quantification of metastatic nodules and metastatic area.

For WZB117 treatment, the treatment was initiated three days after cancer cell injection. Mice injected with control A549 or RNF20+/- A549 cells were randomly assigned to two groups: the control group received PBS/DMSO (1:1, v/v; 100µl), and the WZB117-treated group received WZB117 (10mg/kg body weight) dissolved in PBS/DMSO (1:1, v/v; 100µl). Prior to the end of the experiment, mice were administered daily intraperitoneal injections (ranging from 11 to a maximum of 25 injections) of either the PBS/DMSO vehicle or WZB117. Mice were euthanized and lungs were isolated, fixed in 3.7% formaldehyde, and embedded in paraffin for subsequent experiments.

For tail vein injection and lung metastasis assay with LLC1 cells, cells (control and Rnf20+/-) were cultured as described above, harvested by trypsinization, washed with PBS, and resuspended in sterile 0.9% NaCl solution at a concentration of $1x10^7$ cells/ml, C57BL/6J mice (6-8 weeks, Female) underwent tail vein injection following the same procedure described with $1x10^6$ cells in 100µl of 0.9% NaCl solution. Mice were euthanized 2-4 weeks post injection or when human endpoints were reached. Lungs were processed as described for A549 tail vein injections.

Animals were randomly assigned to groups, and exact group sizes are provided in the corresponding figure legends.

For intratracheal injection and lung metastasis relapse models, paraffin sections from intratracheal (i.t) injection and lung metastasis relapse tumor models. We thank Prof. Dr Rajkumar Savai (Max Planck Institute for Heart and Lung Research, Justus Liebig University, Giessen, Germany) for providing these sections(Schmall et al., 2015). These sections were used for immunohistochemical analysis of RNF20 expression. No animal surgeries or *in vivo* experiments were performed in our laboratory for these models.

2.2.2 Cell culture and generating of cell line

The following cell lines were obtained from the American Type Culture Collection (ATCC): MLE12, LL1, H82, BEAS-2B (B2B), A549, H69, A427, and HEK293T. The culture conditions for each cell line were as follows: MLE12 cells were cultured in DMEM/F12K medium supplemented with 10% fetal bovine serum (FBS) and 1% penicillin/streptomycin/glutamine (PSG). LLC1, B2B, and HEK293T cells were cultured in DMED medium, supplemented with 10% FBS and 1% PSG. H82, H69, and A549 cells were cultured in RPMI 1640 medium, supplemented with 10% FBS and 1% PSG.

Generation of Rnf20+/- MLE12 and LLC1 cells by CRISPR/Cas9 system, 2 guide RNAs (gRNA) were used: gRNA1-RNF20: Forward: M.musculus (5'- CACCGTGAAAAGCTGGAGCGACGCC -3'); Reverse: M.musculus (5'- AAACGGCGTCGCTCCAGCTTTTCAC -3'), gRNA2-RNF20: Forward: M.musculus (5'- CACCGGATTTCCATCGCATCTACAT -3'); Reverse: M.musculus (5'- AAACATGTAGATGCGATGGAAATCC -3'). The gRNAs were ligated into PX459 V2.0 plasmid vectors. Both plasmids were then transfected into MLE12 cells using Lipofectamine 2000, following the manufacturer's instructions. After transfection, the cells were selected with puromycin (2 µg/ml) for 48 hours. Surviving cells were then expanded and single clones were selected for further analysis.

To generate Rnf20+/- SA549 cells, the CRISPR/Cas9 system was utilized with 2 gRNAs: gRNA1-RNF20: Forward: H.homosapien (5'- CACCGTCAGACGGCCGATTGGCTGACGG -3'); Reverse: H.homosapien (5'- AAACTCAGCCAATCGGCCGTCTGAC -3'), gRNA2-RNF20: Forward: H.homosapien

(5’- CACCGGGAGGGCACTACCACTACGCAGG -3’); Reverse: H.homosapien (5’-AAACGCGTAGTGGTAGTGCCCTCCC -3’).

The gRNA was ligated into the LentiCRISPR v2 plasmids. Both plasmids were transfected into A549 cells using Lipofectamine 2000, according to the manufacturer’s instructions. After transfection, the cells were selected with puromycin (4 µg/ml) for 48 hours. Surviving cells were then expanded, and single clones were selected for further analysis.

To generate a stable knockdown cell line, $0.5x10^6$ HEK293T cells were seeded onto a 6 well plate and transfected with 1.5 µg plasmids containing shRNA for *Hif1α* (TRCN0000054448), Rnf40 (TRCN0000004780) and control shRNA obtained from the RNAi consortium (TRC) shRNA library. Packaging plasmids were co-transfected using the X-tremeGENE DNA transfection reagent (Roche, 6366236001). Viral supernatants were then collected 48 hours after transfection and used to transduce control and Rnf20+/- MLE12 cells in the presence of 0.1% polybrene. 48 hours post-transduction, the cells were selected with 5 µg/ml puromycin for 2 passages and were maintained in normal medium containing 2 µg/ml puromycin.

For generating a stable overexpression cell line, $0.5x10^6$ HEK293T cells were seeded on a 6-well plate and transfected with 1.5 µg plasmids containing *Hif1α* OE (TRCN0000475140), RBX1 OE (TRCN0000467366) and control from (TRC) OE-plasmid library. Packaging was done using the same strategy as described for knockdown, and the viral supernatants were collected. The supernatants were then used to transduce MLE12 cells in the presence of 0.1% polybrene. 48 hours post-transduction, the cells were selected with 5 µg/ml puromycin for 2 passages and maintained in normal medium containing 2 µg/ml puromycin.

2.2.3 siRNA transfection and cell treatment

The human Rnf20 siRNA and control siRNA were purchased from Horizon (ON-TARGET plus siRNA, SMART Pool, L-007027-00-0005). $1×10^5$ H82 cells were seeded in a 6-well plate 24 hours before transfection, and the following day, the cells were transfected with 25 nM siRNA using Lipofectamine RNAiMax (Thermo Fisher Scientific, 13778-075) overnight. Fresh medium was added, and cells were harvested for RNA and protein extraction 72 hours after transfection.

To induce DNA damage, H_2O_2 was added to the cells at a final concentration of 0.5mM for 1 hour. Cells were harvest 4 hours after treatment for total protein isolation. For immunofluorescence staining of γH2AX, cells were washed with PBS and fixed with 4% paraformaldehyde (PFA) at 4 hours, 8 hours, 16 hours, and 24 hours post-treatment.

For hypoxia treatment, cells were cultured under 1% O_2, 94% N_2, and 5% CO_2 at 37 °C for 12 hours.

WZB117, a glucose transporter 1 (GLUT1) inhibitor, was purchased from Selleck Chemicals (S7927). WZB117 was added to the cells at a final concentration of 10 μM for 24 hours, followed by Boyden chamber migration assays and Seahorse assays in fresh medium. For colony formation assays, cells were cultured in the continuous presence of WZB117.

2.2.4 Histology, immunohistochemistry (IHC), immunofluorescence (IF) staining

For the H&E (hematoxylin and eosin) staining, heat tissue slides at 55 °C for 10 minutes to soften the paraffin wax and dewax slides by incubating in xylene for 3x5 minutes, followed by rehydration of sections through a graded ethanol series: 100% ethanol for 5 minutes, 75% ethanol for 5 minutes, 50% ethanol for 5 minutes and rinse in PBS for another 5 minutes. Sections were stained either with H&E or using antibodies.

Hematoxylin staining was performed following the manufacturer's instructions (GHS116, Sigma-Aldrich), after washed with tape water, sections were proceeded with Eosin following the manufacturer's guidelines (HT-110216, Sigma-Aldrich).

For immunohistochemistry staining, the rehydrated sections were gone through antigen retrieval by incubate in 10 mM citrate buffer (pH 6.0) for 10 minutes in a microwave and allow them to cool at room temperature. Then proceed with IHC staining using the VECTASTAIN Universal Quick HRP Kit (PK-7800; Vector Laboratories) as per the manufacturer's instruction. The DAB Peroxidase (HRP) Substrate Kit (SK-4100; Vector Laboratories) according to the manufacturer's instructions. Image acquired by Axio Scan. Z1 slide scanner (ZEISS).

For immunofluorescence staining, cells were seeded at 100,000 cells per well on coverslips in 24-well plates, fixed with 4% paraformaldehyde for 10 minutes, blocked

with 5% BSA, permeabilized with 0.2% Triton X-100 for 1 hour, followed by incubated with primary antibody overnight at 4 °C, and secondary antibody for 2 hours at room temperature, DAPI staining for 20 minutes, and mounted with ProLong Gold antifade mountant, with fluorescence images acquired using the Zeiss LSM 700 confocal microscope and analyzed with ImageJ software.

2.2.5 Human tissue microarray quantification of immunoreactivity

The human lung cancer tissue microarray (LC2085c) was purchased from US Biomax Inc. The array consisted of 168 lung cancer samples with multiple types. For immunoreactivity quantification, H-score analysis was performed by randomly selecting ten fields with at least 100 cells each, where the H-score was calculated by adding the percentages of weakly (1x), moderately (2x), and strongly (3x) stained cells, giving a range of 0-300, with the scoring conducted independently by two authors.

2.2.6 MitoSOX Red staining and total ROS assay

Mitochondrial ROS was measured using the MitoSOX™ Red Mitochondrial Superoxide Indicator (Thermo Fisher; CAT# M36008) accoding to the manufacturer's instructions. Briefly, 100,000 cells were seeded on coverslips in a 24-well plate, followd by a wash with PBS, and then incubated with 5 μM MitoSOX reagent for 10 minutes at 37 °C. After three PBS washes, the cells were stained with DAPI for 20 minutes, mounted with Mowiol, and imaged. Cells treated with 200 μM H_2O_2 served as a positive control.

For total cellular ROS measurement, the Total Reactive Oxygen Species (ROS) Assay Kit (Thermo Fisher; CAT# 88-5930) was used following the manufacturer's instructions, with cells mounted with Mowiol for imaging. Cells treated with 200 μM H_2O_2 were also used as a positive control.

2.2.7 LC-MS/MS data acquisition and analysis

Metabolites from the glycolysis, pentose phosphate pathway, and TCA cycle were analyzed as described previously (https://doi.org/10.1161/CIRCRESAHA.123.323084). Briefly, 1 million cells were harvested, and metabolites were extracted using ice-cold methanol/water (85/15, v/v). Isotope-labeled internal standards were added, and

samples were evaporated in a vacuum concentrator (Eppendorf, Hamburg, Germany) at 30 °C. The dried samples were reconstituted in 50 µL methanol/water (50/50, v/v) and transferred to the LC-MS/MS system for analysis. Liquid chromatography was performed using an Agilent 1290 Infinity pump system (Agilent, Waldbronn, Germany) coupled with a Phenomenex Luna Amino-column (100 mm x 2.0 mm, 3 µm). Ammonium acetate (10 mmol/L, pH 9.0) was used as mobile phase A, and 100% acetonitrile as mobile phase B. 5 µL of each sample were injected, and the column temperature was set at 30 °C. The gradient was as follows with a flow rate of 700 µL/min: 0-1 minutes, 5% A; 1-3 minutes, 5-60% A; 3-15 minutes, 60-95% A; 15-18 minutes, 95% A; 18-18.1 minutes, 95-5% A, 18.1-24-1 minutes. 5% A. Mass spectrometry was conducted on a QTrap 5500 mass spectrometer (Sciex, Darmstadt, Germany) using electrospray ionization in negative mode. The ESI parameters were set as follows: TEM 400 °C, IS -4500 V, CUR 25 psi, GS1 40 psi, and GS2 60 psi. Data acquisition and instrument control were performed using MultiQuant 3.0 (Sciex, Darmstadt, Germany). Quantification of metabolites was based on the area under the peak, and the specific MRM transitions were normalized to the appropriate isotope-labeled internal standards and to the protein content of the sample.

2.2.8 Western Blotting, RNA isolation and qPCR

Cultured cells were washed and lysed in Radioimmunoprecipitation Assay (RIPA) buffer containing proteinase and phosphatase inhibitors. The lysate was collected by scraping the cells, with all steps performed on ice. Protein concentrations were determined using the Pierce BCA Protein Assay Kit (Thermo Fisher). The protein samples were mixed with 5x Laemmli sample buffer and boiled for 10 minutes at 95 °C. Protein extracts were loaded onto SDS-PAGE gels, separated by electrophoresis, and transferred to nitrocellulose membranes (Sartorius, 11306-41BL). Membranes were stained with ponceau for 1 minute, followed by blocking with blocking buffer (PBS + 0.1% Tween-20 + 5% BSA) at room temperature for 1 hour. The membranes were then incubated with primary antibodies at 4 °C overnight, followed by incubation with the appropriate secondary antibodies at room temperature for 2hours. Immunoreactive bands were detected using chemiluminescence. Three independent experiments were performed.

For RNA isolation, TRIzol RNA isolation reagent (Invitrogen, 15596018) was used. For quantitative PCR (qPCR), cDNA was synthesized using the High-Capacity cDNA Reverse Transcription Kit (Cat # 4368813, Applied Biosystems), and qPCR was performed with SYBR Green PCR Master Mix (a25742, Applied Biosystems) or qPCRBIO SyGreen Blue Hi-ROX (Nippon Genetics). Cycle numbers were normalized to β-actin levels. A list of primers used in this study is provided in Primers and oligonucleotides.

For RNA sequencing, RNA was isolated using the RNeasy Microarray Kit (Qiagen, 73304).

2.2.9 Scratch wound and Boyden chamber migration assays

Control and Rnf20+/- MLE12, LLC1, and A549 cells were seeded into 6-well plates. When the cells reached 100% confluence, scratches were made using 10 µl pipette tips. The cells were then cultured in medium without FBS for 24 hours and 48 hours. For the Boyden chamber assay, inserts (Corning, 353097) were placed in 24-well plates containing normal culture medium. MLE12 cells ($1x10^5$), LLC1 cells ($5x10^4$), and A549 cells ($5x10^4$) were seeded onto the top of the inserts in medium without FBS. After 6 hours, the insert membranes were fixed with 4% PFA for 10 minutes, followed by three washes with PBS. The upper surface of the membranes was cleaned using a cotton swab then stained with crystal violet for 10 minutes. After three additional washes with PBS, the membranes were cut and mounted onto slides. Images of random areas of the membrane were taken with a 20x objective, and the number of cells that migrated to the lower surface of the membrane was quantified using ImageJ. A minimum of three independent experiments were conducted for each migration assay.

2.2.10 Soft agar and plate colony formation assay

For plate colony formation assays, 3,000 MLE12 cells and 1,000 LLC1 and A549 cells were seeded in 6-well plates. After 10 days, the colonies were stained with Crystal Violet (Thermo Fisher). For soft agar assays, 5000 cells were suspended in complete medium containing 0.3% low-melting agarose (Roth) and plated on a layer of solidified

0.6% agarose in complete normal medium in 6-well plates. The colonies were stained with 0.005% Crystal Violet after 14 days.

2.2.11 Measurement of glucose uptake, lactate secretion and Seahorse assays

The Glucose Uptake Colorimetric Assay Kit and Lactate Assay Kit were used to measure glucose uptake and lactate secretion according to the manufacturer's instructions (MAK083-1KT and MAK065-1KT). The Glucose-6-phosphate Assay Kit was utilized to measure the generation of Glucose-6-phosphate following the manufacturer's guidelines (MAK014-1KT). The extracellular acidification rate (ECAR) was measured using the Seahorse XFe 24 Extracellular Flux Analyzer with the Seahorse XFe Glycolysis Stress Test Kit. Briefly, 5×10^4 MLE12 cells were seeded into a Seahorse XFe 24 cell culture microplate. After calibration and baseline measurements, glucose (10 mM), the oxidative phosphorylation inhibitor oligomycin (1 μM), and the glycolytic inhibitor 2-DG (50 mM) were sequentially injected into each well. The data was analyzed using Seahorse XFe 24 Wave software. Four technical replicates were measured for each biological replicate, and three independent experiments were performed.

2.2.12 ChIP-sequencing and ChIP-qPCR analysis

MLE12 cells, including control, Rnf20+/-, and RNF20+/-*Hif1α* KD, were fixed with 1% methanol-free formaldehyde for 10 min at room temperature, followed by quench with 125 mM glycine. After three washes with PBS, cells were resuspended in cold PBS at 5×10^6/ml. An equal volume of 2x lysis buffer (100 mM Tris-HCl ph 8, 300 mM NaCl, 2% Triton X-100, 10 mM $CaCl_2$) was added, and samples were incubated on ice for 10 min with gentle shaking. Nuclei were washed with cold PBS, centrifuged at 2500 g, 4 °C for 5min, and chromatin was sheared using a Covaris Ultra-sonicator (10% duty factor, 200 cycles, 75 A) for 6 min. The lysates were clarified by centrifugation at 16,000 g for 15min. The chromatin extracts were precleared with 75 μl protein G beads for 2 hours at 4 °C, then incubated with 0.5 μg Pol II antibody (14958S, Cell Signaling Technology), 1 μg H3K4me3 antibody (ab8580, Abcam), 1 μg Pol II p-ser2 (13499s, Cell Signaling Technology), 1 μg Pol II pser5 (ab5131, Abcam), or 1 μg H2Bub1 (5546s, Cell Signaling Technology) overnight at 4 °C, followed by binding 75 μl BSA-coated protein G beads. Then twice washes with low salt buffer (0.1% SDS, 1% Triton X-100, 2 mM

EDTA, 20 mM Tris-HCl pH7.5, 150 mM NaCl), Three washes with high salt buffer (0.1% SDS, 1% Triton X-100, 2 mM EDTA, 20 mM Tris-HCl pH7.5, 500 mM NaCl), twice washes with LiCl buffer (10 mM Tris-HCl pH7.5, 250 mM LiCl, 1% NP-40, 1% sodium deoxycholate, 20 mM EDTA). DNA was eluted using elution buffer (10 mM Tris-HCl pH7.5, 250 mM LiCl, 1% NP-40, 1% sodium deoxycholate, 20 mM EDTA), treated with Rnase A for 1 hour at 37 °C, followed by Proteinase K digestion for 2 hours at 37 °C. Crosslink were reversed by overnight incubation at 65 °C, and DNA was purified using the Qiagen MiniElute PCR purification Kit (Qiagen, 28004).

Libraries were prepared using the NEBNext Ultra II DNA Library Prep Kit for Illumina (NEB, E7103S/L) following the manufacturer's instructions.

ChIP-Seq reads were trimmed using Trimmomatic with a minimum length of 60 bp and a quality score threshold of 15. Trimmed reads were aligned to the mouse genome (mm10, UCSC assembly) using the MarkDuplicates.jar function from Picard 1.136. Peak calling was performed with MACS1.4.53 using default settings, and peaks overlapping the ENCODE-defined blacklist were excluded. The genome-wide distribution of reads was analyzed using lotProfile from the deepTools suit. Bam-mapped files were merged using bamtools merge with default settings, and the merged BAM files were converted to BigWig format using BamCoverage from deepTools with the following parameters: -b 20 -smooth 40 --normalizeUsing RPKM -e 150. The pausing index (PI) was calculated as the ration of normalized counts per million reads (CPM) at the transcription start site (TSS, -50 to +300 bp) to the CPM in the gene body plus 3kb downstream of the transcription termination site (TSS). The calculation was performed using the GitHub repository PIC (https://github.com/MiMiroot/PIC) with the following settings: mm10.gtf --TSSup 50 --TSSdown 300 --GBdown 3000, based on ENSEMBL mm10, version 108.

Differential PI values between control and Rnf20+/- samples were analyzed using the t-test from the rstatix package. Genes were classified as: upregulated: log2FC≥0.58 and p<0.05, downregulated: $\log_2 FC \leq -0.58$ and $p < 0.05$, and genes with decreased PI: $\log_2 FC \leq -0.58$ and $p < 0.05$.

For ChIP-qPCR, 0.1 ng of purified DNA per sample was used. qPCR was performed using SYBR Green PCR Master Mix (A25742, Applied Biosystems) or Qpcrbio SyGreen Blue Hi-ROX (Nippon Genetics).

2.2.13 RNA-Seq data analysis

Raw reads were trimmed using Trimmomatic v0.36, and the trimmed reads were aligned to the mm10 reference genome using STAR. Differential expression analysis was performed and normalized using DESeq2, while reads per kilobase per million mapped reads (RPKM) were calculated using the rpkm. default function from edgeR. Differentially regulated genes were filtered based on the following criteria: fold change ≥1.5; log2 fold change ≤-0.58, ≥0.58; p-value < 0.05. Gene Ontology (GO) analysis was conducted using Metascape, and KEGG pathway analysis was performed using DAVID Bioinformatics.

2.2.14 RNA isolation and quantitative PCR (qPCR) analysis

Total RNA was isolated using TRIzol RNA Isolating Reagent (Invitrogen, Cat # 15596018). For quantitative PCR (qPCR) analysis, cDNA was synthesized using the Hight-Capacity cDNA Reverse Transcription Kit (Applied Biosystems, Cat # 4368813). qPCR was performed using either the SYBR Green PCR Master Mix (A25742, Applied Biosystems) or Qpcrbio SyGreen Blue Hi-ROX (Nippon Genetics). The cycle numbers were normalized to β-actin expression. A list of primers used in this study is provided in Primers and oligonucleotides.

2.2.15 Quantification and Statistical Analysis

All experiments were conducted independently at least three times, and the resulting data were used for statistical analysis. For cell culture studies involving genetically modified cell lines, “n” represents biologically independent clones. Differences between groups were evaluated using an unpaired two-tailed Student’s t-test or ANOVA with multiple comparisons. Bar plots and boxplots were generated using GraphPad Prism v8.0.2 and R v4.4.2.

3 RESULTS

3.1 RNF20 decreased in human lung cancer cells

3.1.1 Level of RNF20 decreased in human lung cancer cells

Since RNF20 expression was previously found to be downregulated in LLC1 cells compared to MLE12 cells, I next investigated RNF20 levels in human lung cancer cell lines. Consistent with earlier observations, RNF20 expression was markedly reduced in human lung adenocarcinoma (AD) cell lines (A549, A472, and H322) relative to the B2B human lung epithelial cell line. Similarly, decreased RNF20 levels were also observed in small cell lung cancer (SCLC) cell lines (H82 and H69) (Fig. 12).

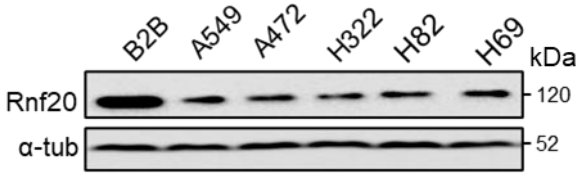

Figure 12. **Decreased level of RNF20 in human lung cancer cells.** RNF20 Western Blot analysis of lysates from human normal lung epithelial cell (B2B), human AD cell lines (A549, A472, H322), and human SCLC lines (H82, H69). α-Tub serve as the control.

3.2 Rnf20 haploinsufficiency leads to decreased DNA damage repair, increased cell growth and cell migration.

3.2.1 Loss of *Rnf20* impairs DNA damage repair

Previously, we found out that the *Rnf20* deficient MLE12 cells showed an impaired DNA damage repair. To investigate further, I checked the γH2AX levels in control, *Rnf20+/-, Rnf20+/-* with RNF20 overexpression MLE12 cells. Interestingly, the increased γH2AX levels upon *Rnf20* loss were significantly rescued by RNF20 overexpression (Fig. 13).

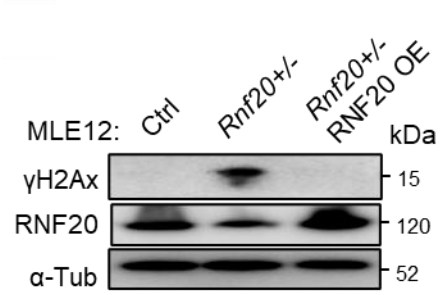

Figure 13. **Loss of *Rnf20* impairs DNA damage repair.** Western Blot analysis of lysates from control, *Rnf20+/-, and Rnf20+/-* with RNF20 OE MLE12 cells.

3.2.2 Loss of *Rnf20* promotes cell growth and migration.

Meanwhile, we also observed loss of *Rnf20* in MLE12 cells markedly increased colony formation in both monolayer and soft agar assays. To determine whether these phenotypes were directly due to *Rnf20* loss, I next checked the phenotypes in RNF20 overexpressed (OE) *Rnf20+/-* MLE12 cells. This overexpression reversed the elevated colony formation and migration capacity of *Rnf20+/-* MLE12 cells to levels similar to those of control cells (Fig. 14a, 14b).

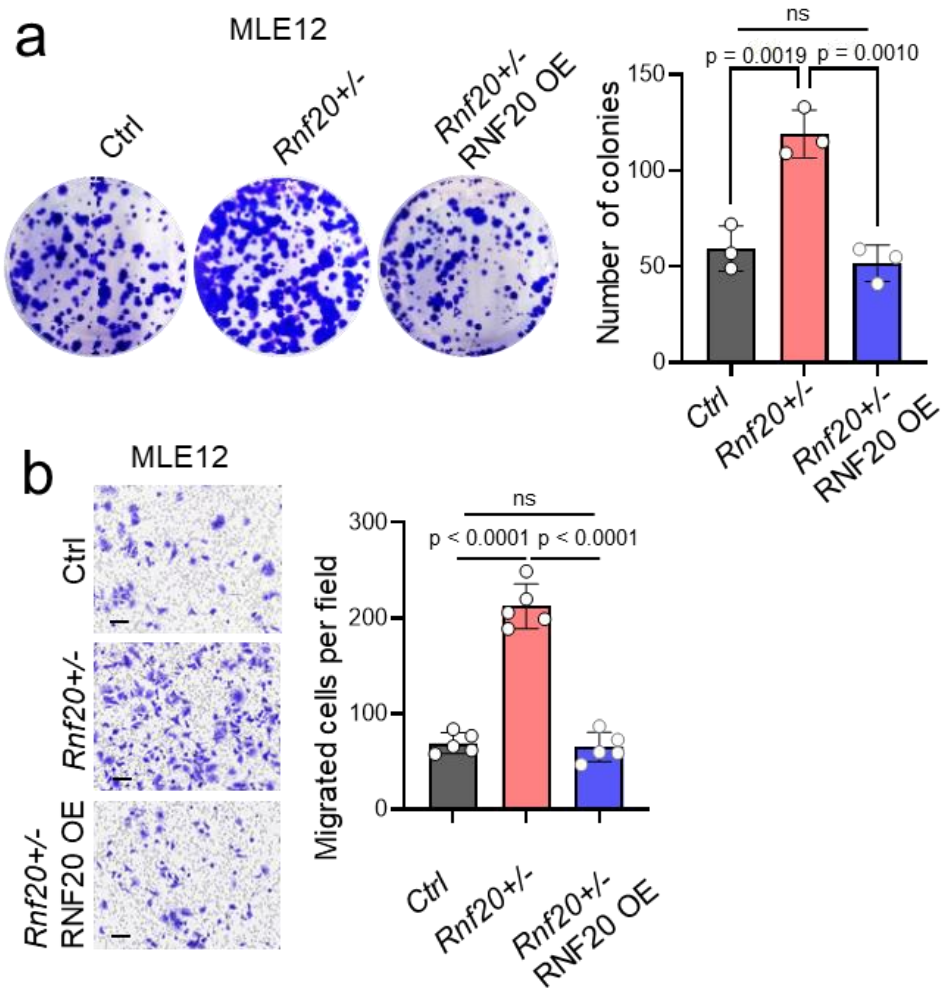

Figure 14. **Loss of *Rnf20* enhances cell growth and migration.** (a) Clonogenic assay in control, *Rnf20+/-*, and RNF20-overexpression (OE) *Rnf20+/-* MLE12 cells. representative images (left panel), and quantification of colony numbers (right panel) (n=3). (b) Boyden chamber migration assay in control, *Rnf20+/-*, and RNF20-overexpression (OE) *Rnf20+/-* MLE12 cells. representative images (left panel), and quantification of colony numbers (right panel) (n=5). Multiple comparisons in (a, b) were performed using one-way ANOVA with Tukey's multiple comparisons test. Data are shown as mean ± SEM. ns, no significance.

3.2.3 Loss of *Rnf20* leads to EMT

To uncover the molecular mechanism underlying the phenotypic change associated with *Rnf20* loss, I performed RNA sequencing on control and *Rnf20+/-* MLE12 cells. Differential expression analysis revealed 1,083 genes significantly upregulated, and 837 genes downregulated following *Rnf20* depletion (n=3; Log2(FC) ≤-0.58, ≥0.58; p-value < 0.05). Notably, Gene Ontology (GO) enrichment analysis of the upregulated genes highlighted biological processes such as regulation of tube morphogenesis, HIF-1 signaling pathway, insulin resistance, extracellular matrix (ECM) organization,

mesenchymal differentiation, and the positive regulation of cell migration (Fig. 15a, 16b). In contrast, the downregulated genes were predominantly associated with TNF signaling pathway and drug metabolism (Figure 15b).

The activation of the epithelial-mesenchymal transition (EMT) program, which is often involved in tumor invasion and metastasis, plays a critical role in cancer progression and malignant transformation (Hanahan and Weinberg 2011, Lambert and Weinberg 2021). Interestingly, the mesenchymal marker Fn1 and Snai1 were significantly upregulated upon *Rnf20* loss. Suggestive of EMT activation. To investigate the EMT phenotype further, I analyzed epithelial and mesenchymal markers in *Rnf20+/-* mice. Notably, *Rnf20+/-* tumors showed a marked reduction in E-cadherin protein levels (Fig. 15d), accompanied by increased expression of the mesenchymal markers SNAI1 and FN1. At the transcript level, *Rnf20+/-* mice exhibited downregulation of *Cdh1* and upregulation of *Snai1* and *Fn1* mRNA compared to control littermates (Fig.15c). These data consistent with our previously results of *Rnf20+/-* MLE12 cells, which exhibited spindle-shaped morphology and altered expression of EMT markers.

These findings indicate that loss of *Rnf20* promotes EMT *in vivo* and may contribute to enhanced metastatic potential.

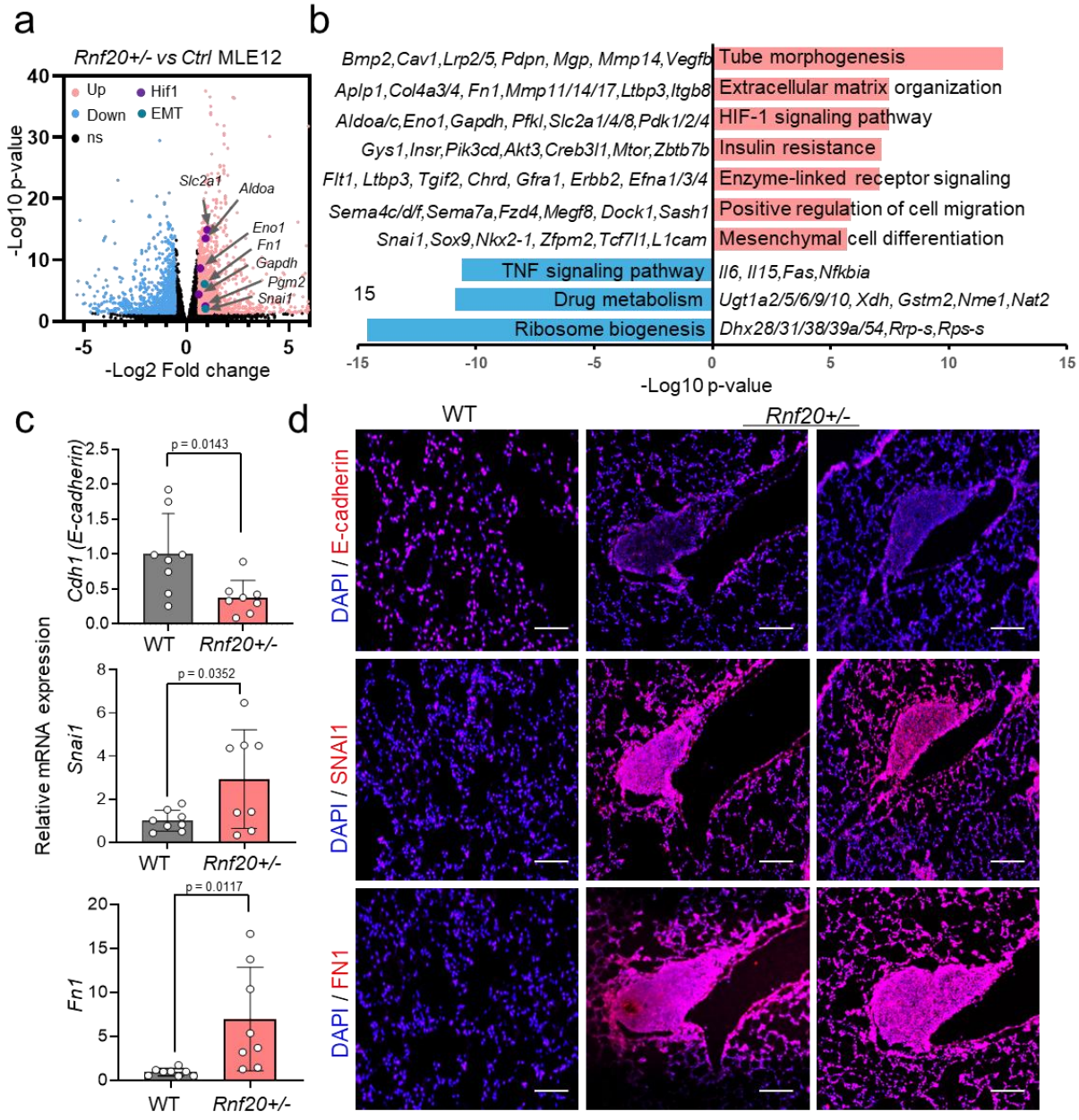

Figure 15. ***Rnf20*** **haploinsufficiency results in epithelial-mesenchymal transition (EMT).** (a) A volcano plot displaying the distribution of differentially expressed gene between *Rnf20*+/- and control MLE12 cells (n=3). Criteria for differential expression include Log2 fold change (FC) ⩽-0.58 or ⩾0.58 with a p-value < 0.05. (b) Top Gene Ontology (GO) terms associated with genes that are upregulated and downregulated in response to *Rnf20* haploinsufficiency, with representative genes highlighted next to their respective GO terms. (c) RT-qPCR validation of EMT genes in RNA isolated from control and *Rnf20*+/- mouse lungs. mRNA expression is presented relative to control wild-type littermates (n=8). (d) Immunostaining for E-cadherin, SNAI1 and FN1 in lung tissues sections of control and *Rnf20*+/- mice. Scale bars, 200 µm. Statistical analysis between two groups in (c) was performed using an unpaired two-tailed Student's t-test. Data are shown as means ± SEM.

3.3 *Rnf20* loss leads to metabolism rewiring

3.3.1 *Rnf20* loss leads to increase of HIF1α signaling

Further complementary Kyoto Encyclopedia of Genes and Genomes (KEGG) pathway analysis identified the HIF-1 signaling pathway as the most significantly upregulated pathway in *Rnf20+/-* cells (Fig. 16a), suggesting that *Rnf20* loss may promote metabolic rewiring via activation of HIF1α. Under normoxic conditions, HIF1α is typically degraded; however, in hypoxia, it accumulates and supports tumor cell survival (Kim and Simon 2022). To validate this, I assessed HIF1α protein levels in control and *Rnf20+/-* MLE12 cells. Remarkably, HIF1α accumulation was observed in *Rnf20+/-* cells under both normoxic and hypoxic conditions (Fig. 16b, 16c). Consistent with these *in vitro* results, elevated HIF1α levels were also detected in lung tissues of *Rnf20+/-* mice compared to wild-type (WT) littermates (Fig. 16d). Together, these findings indicate that loss of RNF20 enhances HIF1α signaling, potentially contributing to a pro-tumorigenic metabolic state.

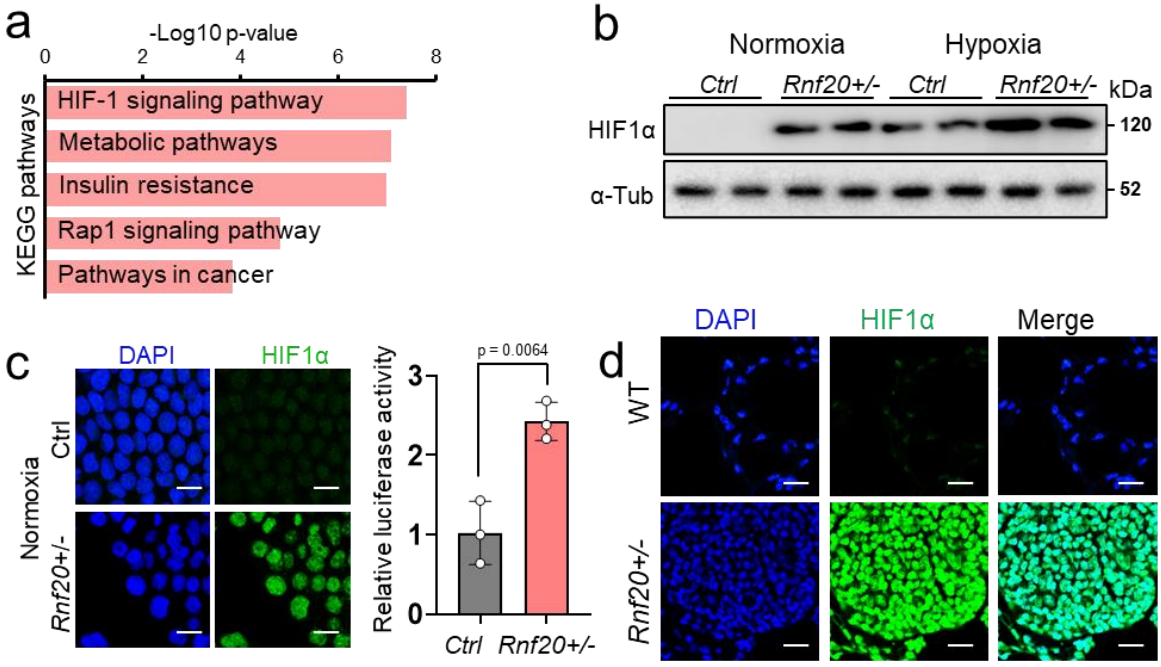

Figure 16. ***Rnf20* haploinsufficiency results in activation of HIF1α.** (a) KEGG pathway analysis of genes upregulated in *Rnf20+/-* MLE12 cells compared to control cells reveals the enriched biological pathways associated with these differentially expressed genes. (b) Western Blot analysis of HIF1α expression in control and *Rnf20+/-* MLE12 cells under both normoxic and hypoxic conditions. (c) Immunostaining for HIF1α (left panel) and HIF1α luciferase reporter activity (right panel) in control and

Rnf20+/- MLE12 cells under normoxic condition (n=3). Scale bars, 20 µm. (d) Immunostaining for HIF1α in lung sections of WT and *Rnf20+/-* mice. Scale bars, 100 µm. Statistical analysis of (c) was performed by an unpaired two-tailed Student's t-test. Data are shown as mean ± SEM.

3.3.2 Total reactive oxygen species (ROS) and mitochondrial ROS were not changed upon loss of *Rnf20*

Reactive oxygen species (ROS) are known to modulate the activity of prolyl hydroxylase domain-containing enzymes (PHDs), which hydroxylate HIF1α and target it for degradation via the von Hippel-Lindau (VHL) pathway (Schofield and Ratcliffe 2004). Inhibition of PHDs by ROS prevents HIF1α hydroxylation, leading to its stabilization and accumulation. In my study, I observed that *Rnf20* loss led to increased HIF1α protein levels, while *Hif1α* mRNA levels remained unchanged (Fig. 17a, 16b), suggesting post-transcriptional regulation.

To investigate whether ROS contributes to HIF1α stabilization in *Rnf20+/-* cells, I measured both total and mitochondrial ROS levels. Notably, there was no significant increase in mitochondrial ROS (Fig. 17b) or total cellular ROS (Fig. 17c, 17d) upon Rnf20 loss. These results indicate that stabilization of HIF1α in *Rnf20+/-* cells occurs independently of elevated mitochondrial or total levels, indicating the involvement of alternative regulatory mechanism.

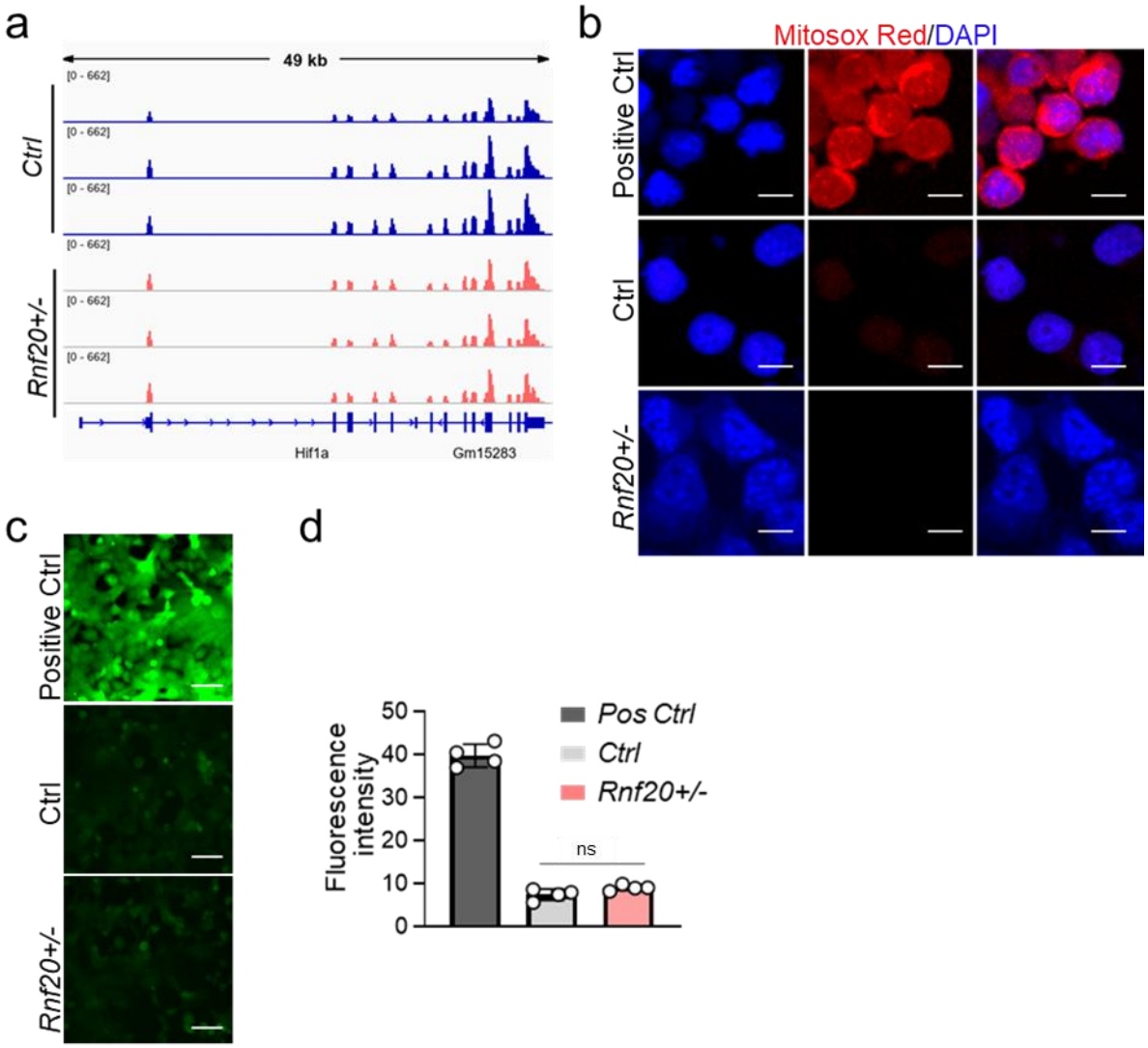

Figure 17. **Functional and molecular changes upon *Rnf20* loss.** (a) Genome tracks of RNA-seq reads of control and *Rnf20+/-* MLE12 cells at *Hif1α*. (b) Mitochondrial superoxide production in control and *Rnf20+/-* MLE12 cells was assessed using the mitochondrial superoxide indicator MitoSOX. Scale bars, 20 μm. Total Reactive Oxygen Species (ROS) levels in control and *Rnf20+/-* MLE12 cells were measured. Images of cells stained with the Total Reactive Oxygen Species (ROS) Assay 488 nm kit (c) and corresponding fluorescence intensity measurements (d) are shown (n=4). Scale bars, 100 μm. Statistical analysis in (d) was performed using two-tailed Student's t-test. Data are shown as means ± SEM. ns, no significance.

3.3.3 *Rnf20* loss promotes glycolysis and TCA cycle

Given that HIF1α serve as a central regulator of cellular metabolism and that cancer cells exhibit metabolic changes, I next performed a comprehensive metabolomic analysis to investigate metabolic alterations induced by *Rnf20* loss. Using Liquid Chromatography-Mass Spectrometry (LC-MS/MS), I profiled metabolites in control and *Rnf20+/-* MLE12 cells. This analysis revealed a concomitant increase in glycolytic

intermediate metabolites, including fructose-6-phosphate (F6P), glyceraldehyde-3-phosphate (G3P), fructose-1,6-bisphosphate (F16B), and pyruvate (Fig. 18a). Additionally, intermediate metabolites of the TCA cycle, such as malic acid, alpha-ketoglutarate (α-KG), succinate, fumarate, and cis-aconitate, were also elevated (Fig. 18a). Importantly, these metabolic changes were consistent with the upregulation of genes encoding key enzymes in these pathways, as identified in our RNA-seq data (Fig. 18a).

To functionally validate enhanced glycolytic activity, I performed Seahorse extracellular flux analysis to measure the extracellular acidification rate (ECAR), a proxy for glycolysis. *Rnf20+/-* MLE12 cells displayed significantly increased glycolytic flux and maximal glycolytic capacity compared to control cells (Fig. 18b). Supporting these findings, *Slc2a21* (GLUT1), a glucose transporter involved in glucose uptake, was upregulated upon RNF20 loss. Correspondingly, glucose uptake assays using 2-deoxyglucose (2-DG) showed significantly higher glucose uptake in *Rnf20+/-* MLE12 cells (Fig. 18c). In addition, lactate dehydrogenase A (*Ldha*), which catalyzes the conversion of pyruvate to lactate during anaerobic glycolysis was also upregulated, as reported in our previous study. In line with this, a lactate secretion assay confirmed significantly elevated lactate production in Rnf20+/- MLE12 cells compared to controls (Fig. 18d). Collectively, these data indicate that RNF20 loss enhances glycolytic and TCA cycle, supporting a shift toward a hypermetabolic and tumor promoting phenotype.

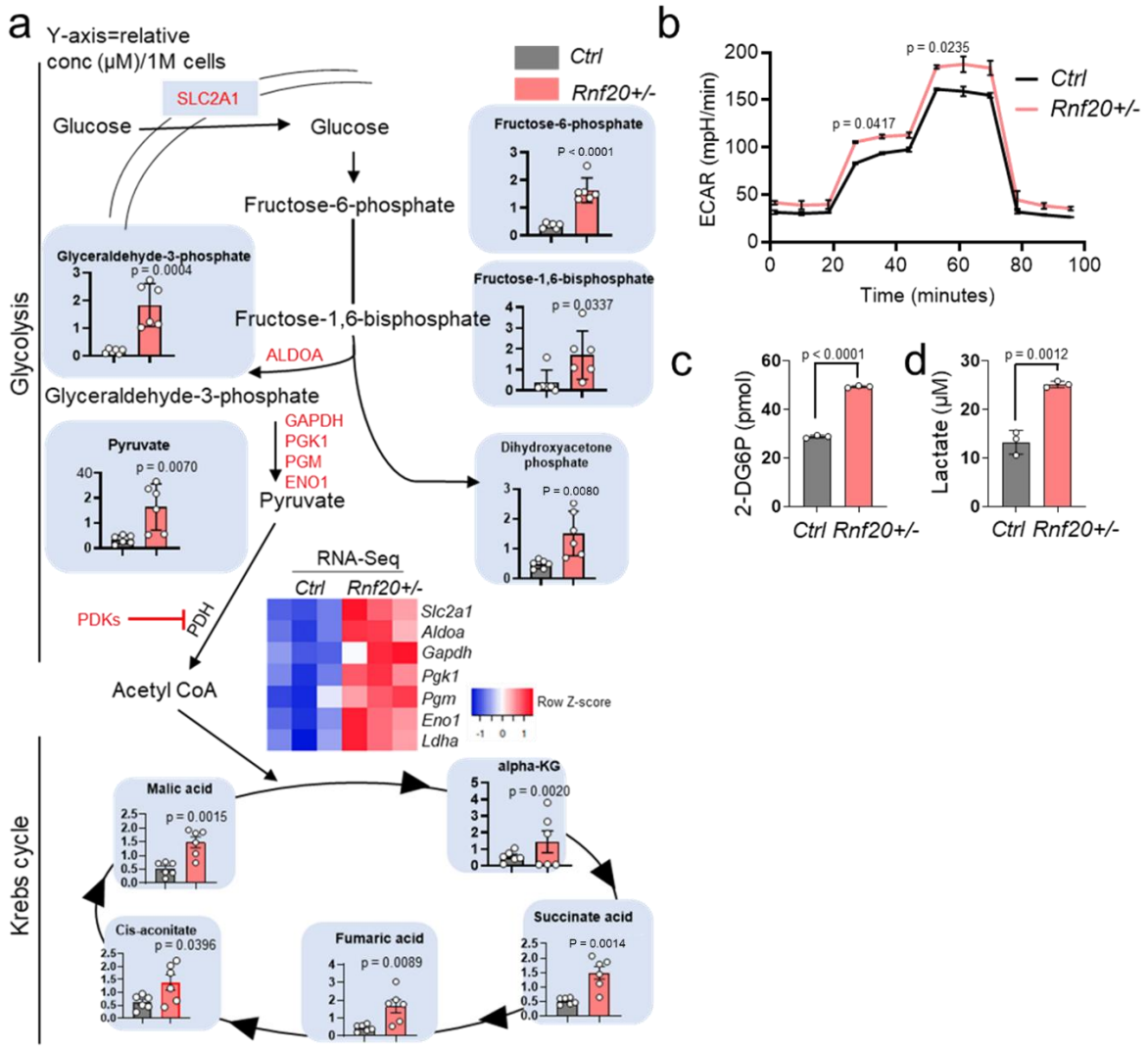

Figure 18. ***Rnf20* haploinsufficiency drives glycolysis and TCA cycle.** (a) Targeted LC-MS/MS-based metabolomic analysis of control and *Rnf20+/-* MLE12 cells (n=6). Metabolic enzymes with altered expression in *Rnf20+/-* MLE12 cells are highlighted in red. The heatmap in the center illustrates the gene expression changes between control and *Rnf20+/-* MLE12 cells, reflecting the metabolic shifts associated with *Rnf20* haploinsufficiency. (b) Extracellular acidification rate (ECAR) of control and *Rnf20+/-* MLE12 cells (n=3) was measured following the sequential addition of glucose, oligomycin, and 2-deoxyglucose (2-DG). 2-DG uptake (n=3) (c) and lactate concentration (n=3) in the supernatant (d) of control and *Rnf20+/-* MLE12 cells were measured to assess cellular glucose metabolism and glycolysis. Statistical analysis between two groups in (a, b, c, d) was performed using an unpaired two-tailed Student's t-test. Data are shown as means ± SEM.

3.3.4 *Rnf20* loss promotes the expression of enzymes involved in glycolysis and HIF1α signaling

Based on the findings above, which revealed upregulation of glycolysis and HIF1α related genes alongside enhanced glycolytic activity following *Rnf20* loss, I further examined the expression of key genes involved in these pathways. RT-qPCR analysis

of lung extracts from WT and *Rnf20+/-* mice revealed significantly increased expression of *Slc2a1*, *Ldha*, *Pdk1*, and *Eno1* in the *Rnf20+/-* group (Fig. 19a). Western blot analysis corroborated these results, showing increased protein levels of PDK1 and LDHA in *Rnf20+/-* MLE12 cells compared to control cells (Fig. 19b). Similarly, immunohistochemical staining of lung sections demonstrated that GLUT1 and LDHA were upregulated in *Rnf20+/-* mouse lungs compared to WT lungs (Fig. 19c). These findings suggest that the loss of *Rnf20* enhances the expression of glycolytic enzymes and hypoxia related targets both *in vitro* and *in vivo*.

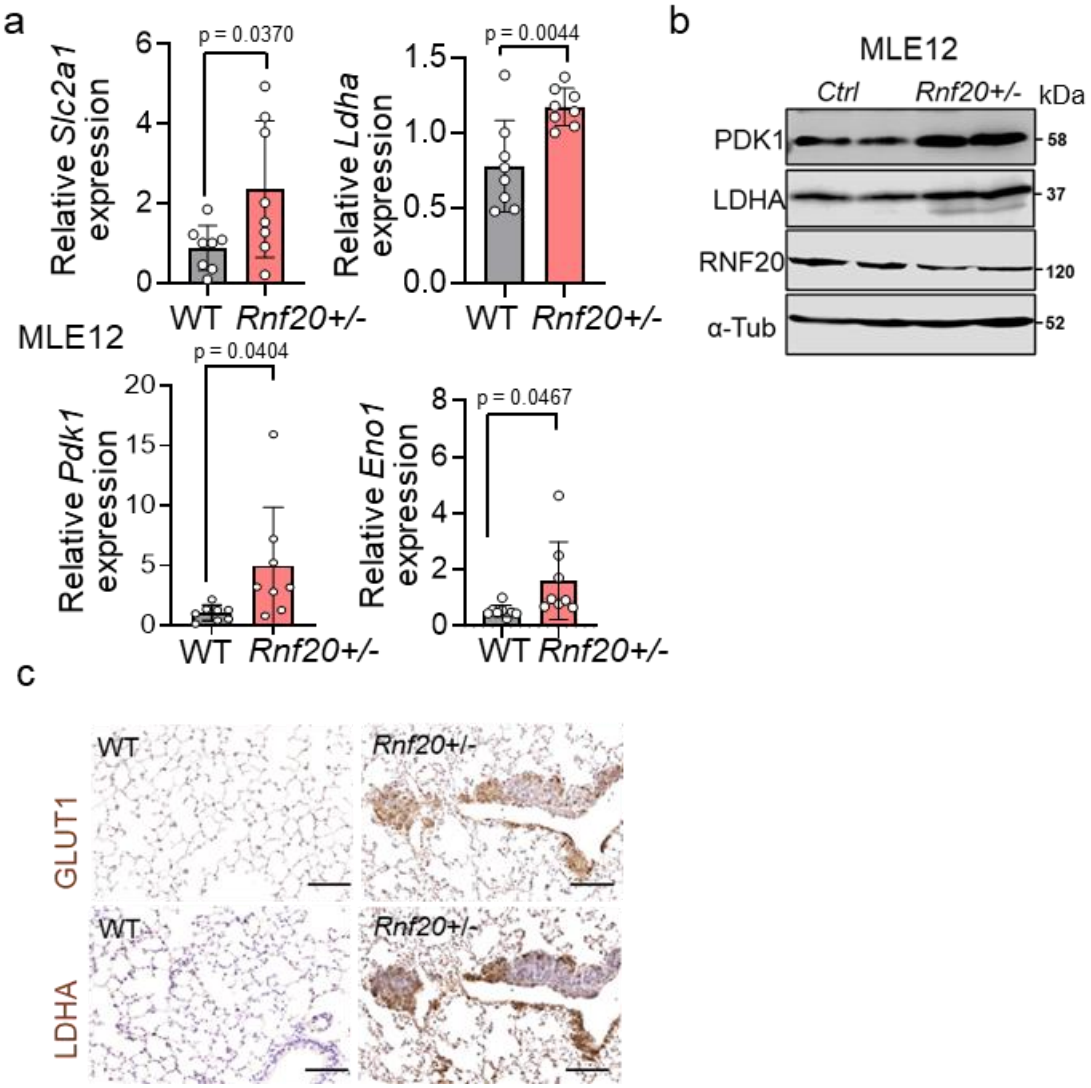

Figure 19. **Loss of *Rnf20* upregulates targets involved in glycolysis and HIF1α.** (a) RT-qPCR analysis of key glycolytic enzymes and hypoxia-regulated genes in WT and *Rnf20+/-* mice lungs (n=8). (b) Western Blot analysis of total protein extracts from control and *Rnf20+/-* MLE12 cells using antibodies against PDK1, LDHA, and RNF20. (c) Immunohistochemical staining for GLUT1 and LDHA in lung tissue sections to visualize the expression and localization of key Glycolytic markers in lung tissue. Scale bars 200 μm. Statistical analysis between two groups in (a) was performed using an unpaired two-tailed Student's t-test. Data are shown as means ± SEM.

3.4 HIF1α activation upon *Rnf20* loss leads to metabolic rewiring

3.4.1 Knockdown of *Hif1α* in *Rnf20+/-* cells rescues the glycolysis and glycolytic enzyme expression

Given the observed nuclear accumulation of HIF1α and enhanced glycolytic activity, our findings suggest that HIF1α activation may drive tumor progression in *Rnf20+/-* mice. To test whether silencing *Hif1α* could reverse the metabolic and phenotype changes induced by *Rnf20* loss, I performed shRNA-mediate knockdown of *Hif1α* in both control and *Rnf20+/-* MLE12 cells. Efficient silencing of *Hif1α* resulted in a significant reduction in the expression of HIF1α target genes (Fig. 20a).

To assess the functional consequences, I evaluated glycolytic activity using the Seahorse glycolysis assay. Notably, *Hif1α* knockdown restored glycolytic flux in *Rnf20+/-* cells to levels comparable to control cells (Fig. 20b). Furthermore, both glucose uptake and lactate secretion, which were elevated in *Rnf20+/-* cells, were significantly reduced upon *Hif1α* knockdown, returning to control levels (Fig. 20c, 20d). These results indicate that HIF1α is a critical mediator of the glycolytic phenotype induced by *Rnf20* loss.

To further validate the role of glucose metabolism in this phenotype, I investigated the effect of pharmacological inhibition of GLUT1, a major glucose transporter upregulated in *Rnf20+/-* cells. Treatment with WZB117, a small molecule inhibitor of GLUT1 (Ojelabi, Lloyd et al. 2016), significantly reduced glycolytic capacity (Fig. 20e), glucose uptake (Fig. 20f) and lactate secretion (Fig. 20g) in both control and *Rnf20+/-* MLE12 cells. These findings demonstrate that metabolic reprogramming observed in *Rnf20+/-* cells is mediated through HIF1α activation and enhanced glucose uptake. Highlighting the RNF20- HIF1α axis as a key regulatory pathway in tumor associated metabolic alterations.

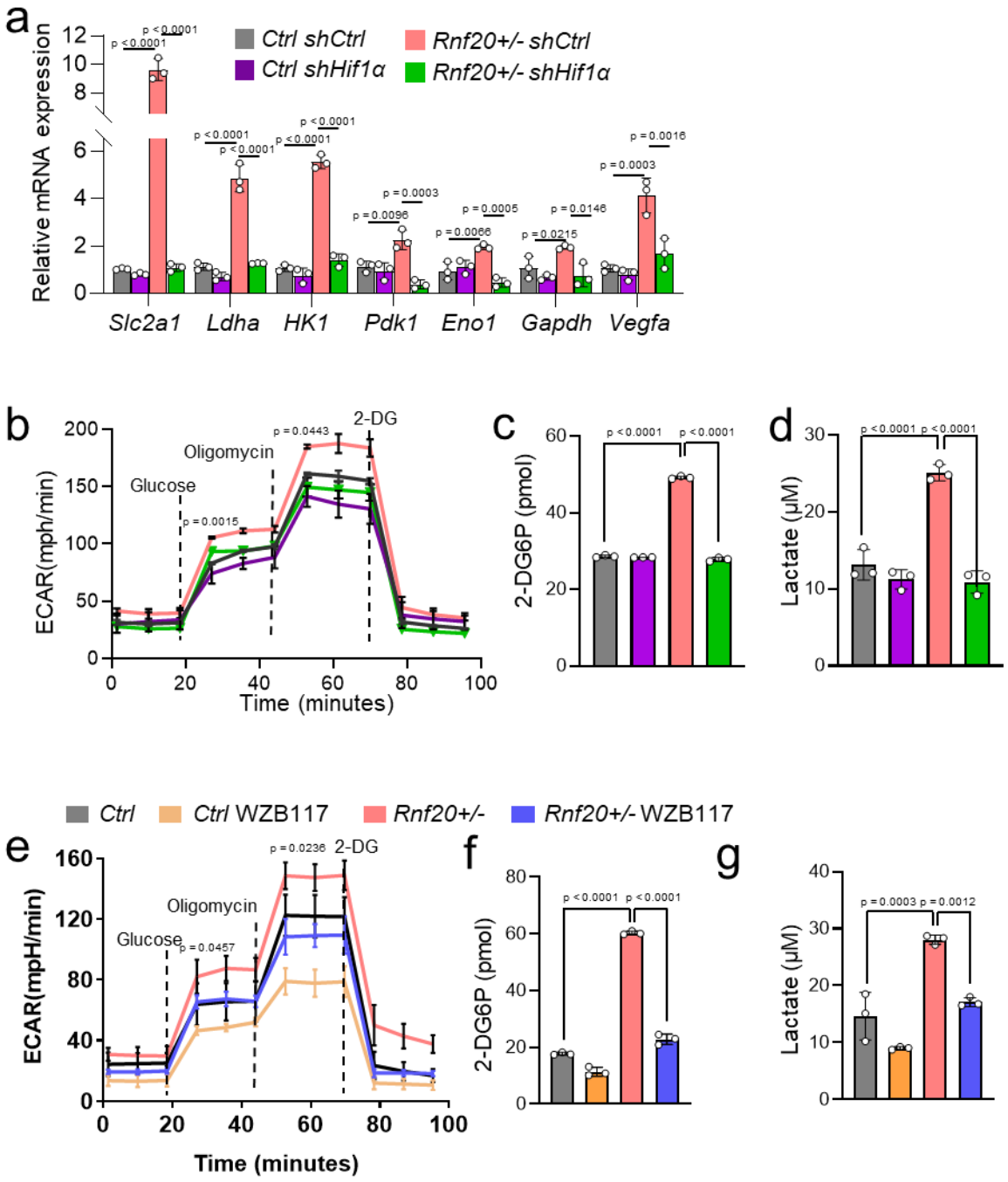

Figure 20. **HIF1α activation upon *Rnf20* loss results in metabolic rewiring.** (a) qPCR analysis was conducted to examine the expression of genes involved in glycolysis and the hypoxic response in control and *Rnf20+/-* MLE12 cells, which were stably transfected with either control shRNA or shRNA targeting *Hif1α* (n=3). (b) shows the ECAR (n=3), (c) shows the 2-DG uptake, and (d) shows the lactate secretion in control and *Rnf20+/-* MLE12 cells stably expressing either control shRNA or shRNA against *Hif1α* (n=3). The metabolic analysis of ECAR (e) (n=3), 2-DG uptake (f) (n=5), and lactate secretion (n=3) in control and *Rnf20+/-* MLE12 cells treated either DMSO or WZB117 (n=3). Multiple comparisons in (a, b, c, d, e, f, g) were performed using ANOVA. Data are shown as means ± SEM.

3.4.2 Knockdown of *Hif1α* in *Rnf20+/-* cells rescues the cell growth and cell migration.

Considering the results indicated above, I further analyzed whether the enhanced cell growth and migration observed in *Rnf20+/-* MLE12 cells could be rescued by silencing *Hif1α*. First by performing the plate colony assay, I observed a decrease of cell colonies in *Rnf20+/-* cells with silencing of *Hif1α* to control levels (Fig. 21a), suggesting that the increased proliferative capacity induced by *Rnf20* loss is mediated, at least in part, by *Hif1α*. Consistently, a soft agar colony formation assay revealed that the enhanced anchorage-independent growth capacity of *Rnf20+/-* cells was also reversed upon *Hif1α* silencing (Fig. 21c). Moreover, the migration capacity was also decreased in *Hif1α* silencing *Rnf20+/-* cells by assessing the results of the Boyden-chamber migration assay (Fig. 21b) and the wound healing assay (Fig. 21d). To determine whether these phenotypes could also be reversed through inhibition of glucose uptake, I treated cells with WZB117. Treatment significantly impaired both 3D colony formation (Fig. 21e) and migration capacity (Fig. 21f), supporting the idea that enhanced glucose metabolism plays a key role in driving the aggressive phenotype observed in *Rnf20+/-* cells. Taken together, these results demonstrate that both *Hif1α* silencing and GLUT1 inhibition can rescue the increased proliferation and migration associated with *Rnf20* loss.

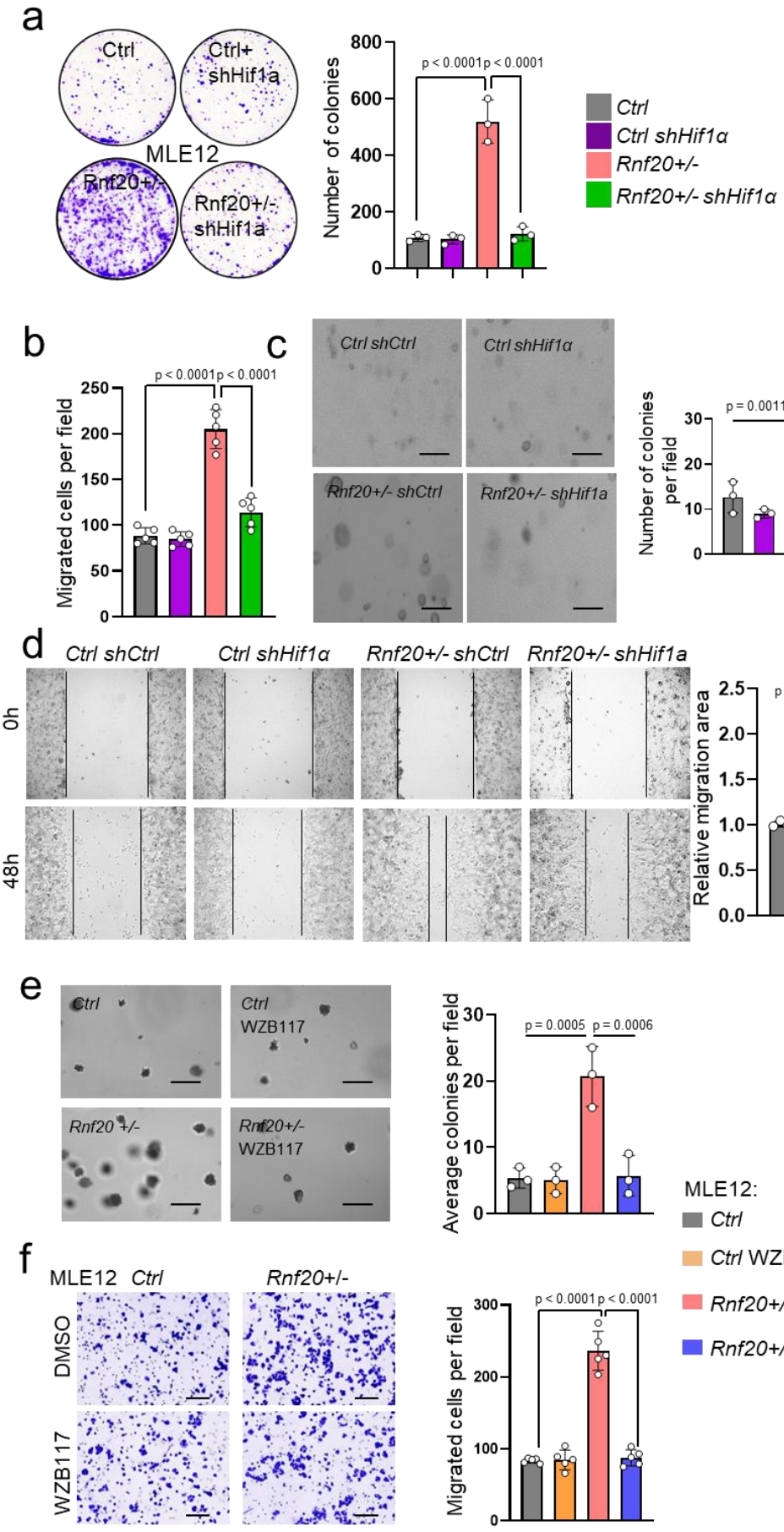
a
Ctrl
Ctrl+ shHif1a
MLE12
Rnf20+/-
Rnf20+/- shHif1a
Number of colonies
800
600
400
200
0
p < 0.0001
p < 0.0001
Ctrl
Ctrl shHif1α
Rnf20+/-
Rnf20+/- shHif1α
b
Migrated cells per field
250
200
150
100
50
0
p < 0.0001
p < 0.0001
c
Ctrl shCtrl
Ctrl shHif1α
Rnf20+/- shCtrl
Rnf20+/- shHif1a
Number of colonies per field
30
20
10
0
p = 0.0011
p = 0.0009
d
Ctrl shCtrl
Ctrl shHif1α
Rnf20+/- shCtrl
Rnf20+/- shHif1a
0h
48h
Relative migration area
2.5
2.0
1.5
1.0
0.5
0.0
p < 0.0001
p < 0.0001
e
Ctrl
Ctrl WZB117
Rnf20 +/-
Rnf20+/- WZB117
Average colonies per field
30
20
10
0
p = 0.0005
p = 0.0006
MLE12:
Ctrl
Ctrl WZB117
Rnf20+/-
Rnf20+/- WZB117
f
MLE12
Ctrl
Rnf20+/-
DMSO
WZB117
Migrated cells per field
300
200
100
0
p < 0.0001
p < 0.0001

Figure 21. **HIF1α activation upon *Rnf20* loss results in increased cell growth and migration**. (a) Plate colony assay was performed to assess proliferation levels in control and Rnf20+/- MLE12 cells treated with shRNA against control and *Hif1α* (n=3). (b) Quantification of the number of migrated cells per field performed in a Boyden-chamber migration assay of control and *Rnf20+/-* MLE12 cells expression either control shRNA or shRNA targeting *Hif1α* (n=5). (c) A soft agar assay was performed to assess the anchorage-independent growth of control and *Rnf20+/-* MLE12 cells stably expressing either control shRNA or shRNA targeting *Hif1α* (n=3). Scale bars, 200 μm. (d) Representative images of wound gap closure (left panel) and the quantification of the relative migration area (right panel) from a scratch wound healing assay using control and *Rnf20+/-* MLE12 cells expressing either control shRNA or shRNA against *Hif1α* (n=3). soft agar assay was conducted to evaluate the anchorage-independent growth (n=3) (e) and Boyden-chamber migration assay (n=5) (f) to evaluate the migration of control and *Rnf20+/-* MLE12 cells treated either DMSO or WZB117 with the specific quantification of colonies and migrated cells per field (right). Scale bar, 150 μm (f). Multiple comparisons in (a, b, c, d, e, f) were performed using ANOVA. Data are shown as means ± SEM.

3.4.3 RNF20 exhibits functional independence from RNF40

Recent study have demonstrated that the RNF20-RNF40 complex is essential for HIF-1 transcriptional activity in breast cancer, as shown through double knockdown experiments(Lyu, Yang et al. 2024). However, our results indicating that RNF20 suppresses HIF1α activity. Thus, I next investigated the role of RNF40 by silencing *Rnf40* in MLE12 cells. In contrast to RNF20 loss of function, Rnf40 silencing did not alter HIF1α protein levels (Fig. 22a), nor did it affect cell migration or clonogenic growth (Fig. 22b, 22c, 22d, 22e). But it did lead to a significant reduction in the expression of several HIF1α target genes, including *Fn1*, *Snai2*, *Vegfa*, and *Eno1* (Fig. 22f, 22g).

Moreover, we previously found out that RNF20 mRNA levels decreased in AD patients, and the lower RNF20 expression was significantly correlated with poor survival among lung AD patients. Interestingly, unlike RNF20, RNF40 mRNA levels were elevated in AD patients (Fig, 22h), and higher RNF40 expression was significantly associated with reduced survival in the KMplotter of lung AD dataset (Fig. 22i).

These results suggest that RNF20 can function independently of RNF40 in regulating cell proliferation, migration, as well as HIF1α-responsive gene expression within lung epithelial cells and lung cancer models.

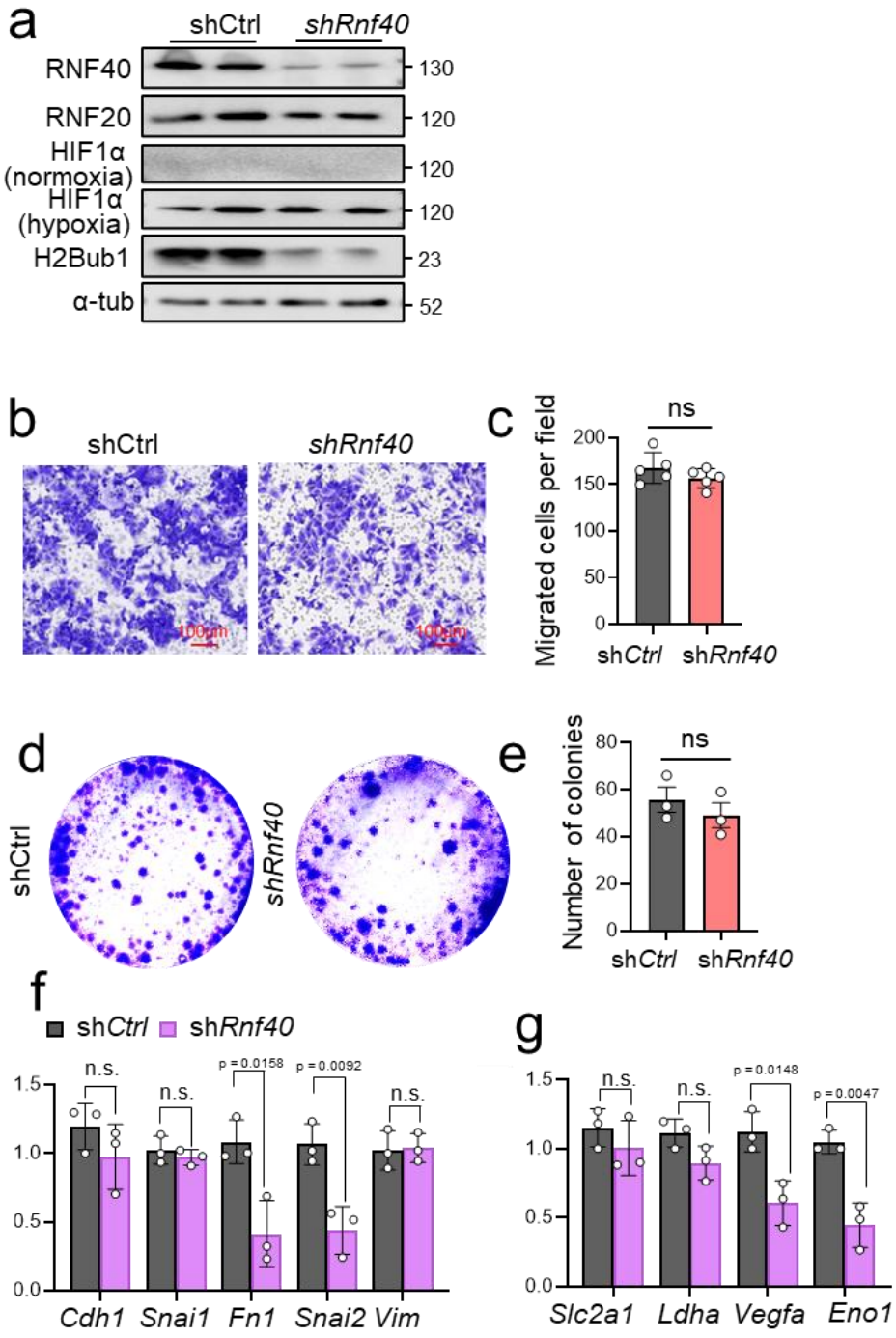
a
shCtrl
shRnf40
RNF40
RNF20
HIF1α (normoxia)
HIF1α (hypoxia)
H2Bub1
α-tub
130
120
120
120
23
52
b
shCtrl
shRnf40
100μm
100μm
c
ns
Migrated cells per field
200
150
100
50
0
shCtrl
shRnf40
d
shCtrl
shRnf40
e
ns
Number of colonies
80
60
40
20
0
shCtrl
shRnf40
f
shCtrl
shRnf40
n.s.
n.s.
p = 0.0158
p = 0.0092
n.s.
1.5
1.0
0.5
0.0
Cdh1
Snai1
Fn1
Snai2
Vim
g
n.s.
n.s.
p = 0.0148
p = 0.0047
1.5
1.0
0.5
0.0
Slc2a1
Ldha
Vegfa
Eno1

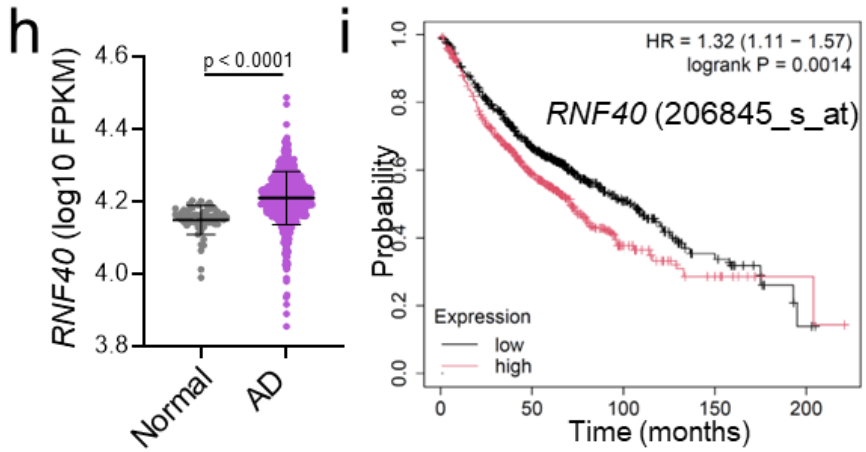

Figure 22. **RNF20 has been shown to function independently of RNF40.** (a) Western Blot analysis of RNF20, RNF40, and H2Bub1 under normoxic conditions, as well as HIF1α level under normoxic and hypoxic conditions in total cell lysates from control and *Rnf40* knockdown MLE12 cells. (b) Boyden chamber migration assay of control and *Rnf40* knockdown MLE12 cells (n=5). (c) Quantification of migrated cells per field in a Boyden chamber migration assay (n=5). (d) 2D clonogenic assay of control and *Rnf40* knockdown MLE12 cells (n=3). (e) Quantification of colony numbers in a clonogenic assay. qPCR analysis of genes involved in EMT(f) and glycolysis (g) in control and *Rnf40* knockdown MLE12 cells (n=3). (h) Normalized RNF40 expression in normal lung tissues (n=59) and lung adenocarcinoma (AD) tissues (n=515) from TCGA datasets. Expression values are shown in FPKM (fragments per kilobase of exon per million mapped reads). (i) Overall survival of lung adenocarcinoma (AD) patients based on Kaplan Meier analysis(Győrffy, Surowiak et al. 2013). Patients were stratified into high (n=580) and low (n=581), RNF40 expression groups using probe 206845_s_at. Statistical analysis in (c, e, f, g, h) was performed using a two-tailed Student's *t*-test. Data are shown as means ± SEM, ns, not significant.

3.5 RNF20 haploinsufficiency drives tumor growth and migration via HIF1α activation and metabolic rewiring

3.5.1 Loss of RNF20 promotes cell growth and migration in human adenocarcinoma cells.

To further investigate the role of RNF20 in human lung cancer progression, I ablated the *RNF20* locus using CRISPR-Cas9 gene editing in A549 cells (Fig.23a, 23b). Consistent with previous observations, homozygous deletion of *RNF20* could not be established in A549 cells. Moreover, I examined cell proliferation and migration in *RNF20+/-* A549 cells. Using a plate colony formation assay in 2D monolayer culture, I found that *RNF20+/-* cells had a marked increase in proliferative capacity compared to control A549 cells (Fig.23c), consistent with previously observed effects in MLE12 and LLC1 cells. Furthermore, Boyden chamber migration assays revealed significantly enhanced migratory ability in *RNF20+/-* A549 cells relative to controls (Fig.23d). These

findings align with our prior observations in both *Rnf20+/-* MLE12 and LLC1 cell models, supporting a conserved role for RNF20 in restraining proliferation and migration in lung epithelial and cancer cells.

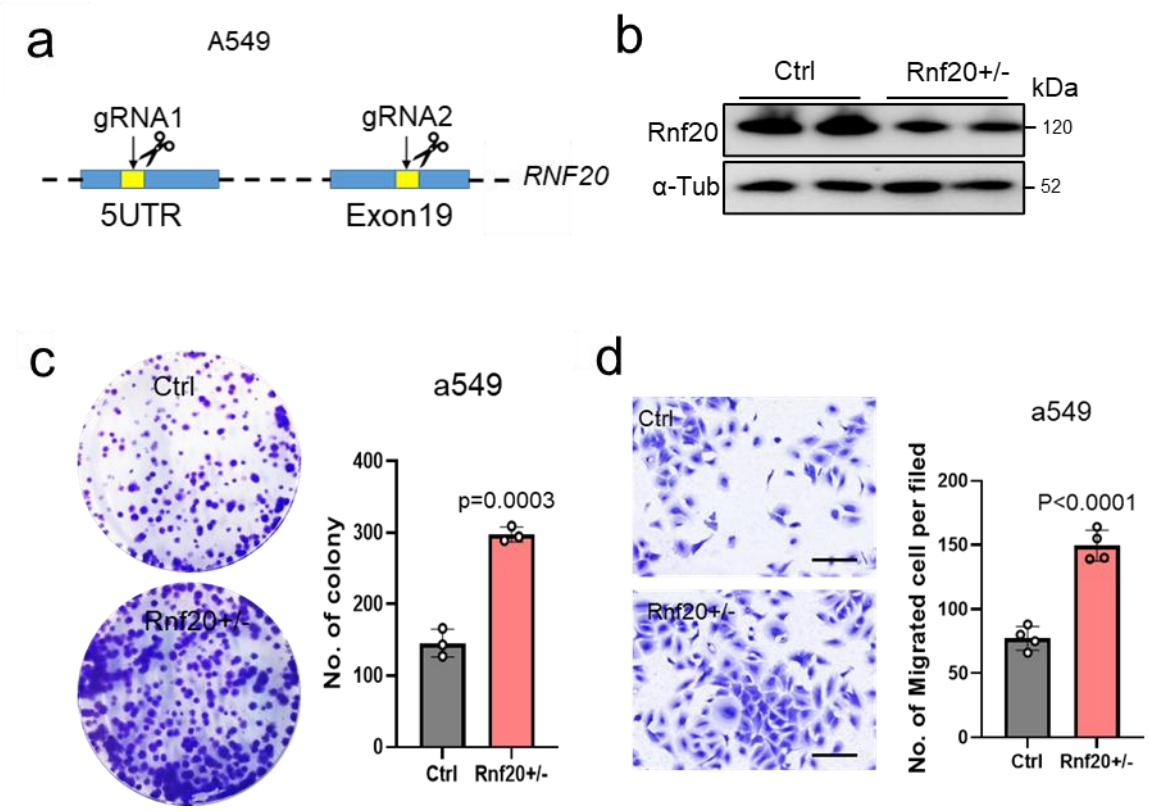

Figure 23. **Loss of *RNF20* promotes cellular growth and migration.** (a) Schematic graph of RNF20 targeting strategy. (b) Western Blot analysis of lysates from control and *RNF20+/-* A549 cells, indicating the levels of RNF20, and α-Tub serves as the control. (c) 2D-plate colony forming assay (left panel) and quantification (right panel) of control and *RNF20+/-* A549 cells (n=3). (d) Boyden chamber migration assay (left panel) and quantification (right panel) of control and *RNF20+/-* A549 cells (n=4). Scale bars, 150 μm.

3.5.2 Loss of RNF20 drives tumor cell growth and cell migration via HIF1α activation and metabolic reprogramming

3.5.2.1 Knockdown of *HIF1α* or glycolysis inhibition in A549 *RNF20+/-* cells rescues the cell growth, migration, and metabolic rewiring

Given our previous findings that HIF1α regulates cell proliferation, migration, and metabolism in mouse MLE12 cells, I next sought to determine whether silencing *HIF1α* in a human lung cancer cell line could similarly reverse the tumor promoting phenotypes associated with *RNF20* loss. To this end, I generated *HIF1α* knockdown

lines in both control and *RNF20+/-* A549 cells. I first assessed cell growth using a 2D plate colony formation assay and evaluated migratory capacity using a Boyden chamber migration assay. Consistent with results in MLE12 cells, *Hif1α* silencing effectively suppressed the enhanced clonogenic growth and migration observed in *RNF20+/-* A549 cells (Fig. 24a, 24b). Besides, Seahorse analysis revealed that the increased glycolytic capacity associated with *RNF20* loss was significantly reduced upon *HIF1α* knockdown (Fig. 24c), along with a marked decrease in the expression of key glycolytic genes (Fig. 24d).

Moreover, I further treated the control and *RNF20+/-* A549 cells with WZB117 to check the impact of glycolysis inhibition among the cells. In consistent with our findings in MLE12 cells, glucose uptake inhibition significantly attenuated the enhanced clonogenic growth and migration of *RNF20+/-* A549 cells (Fig. 24e, 24f).

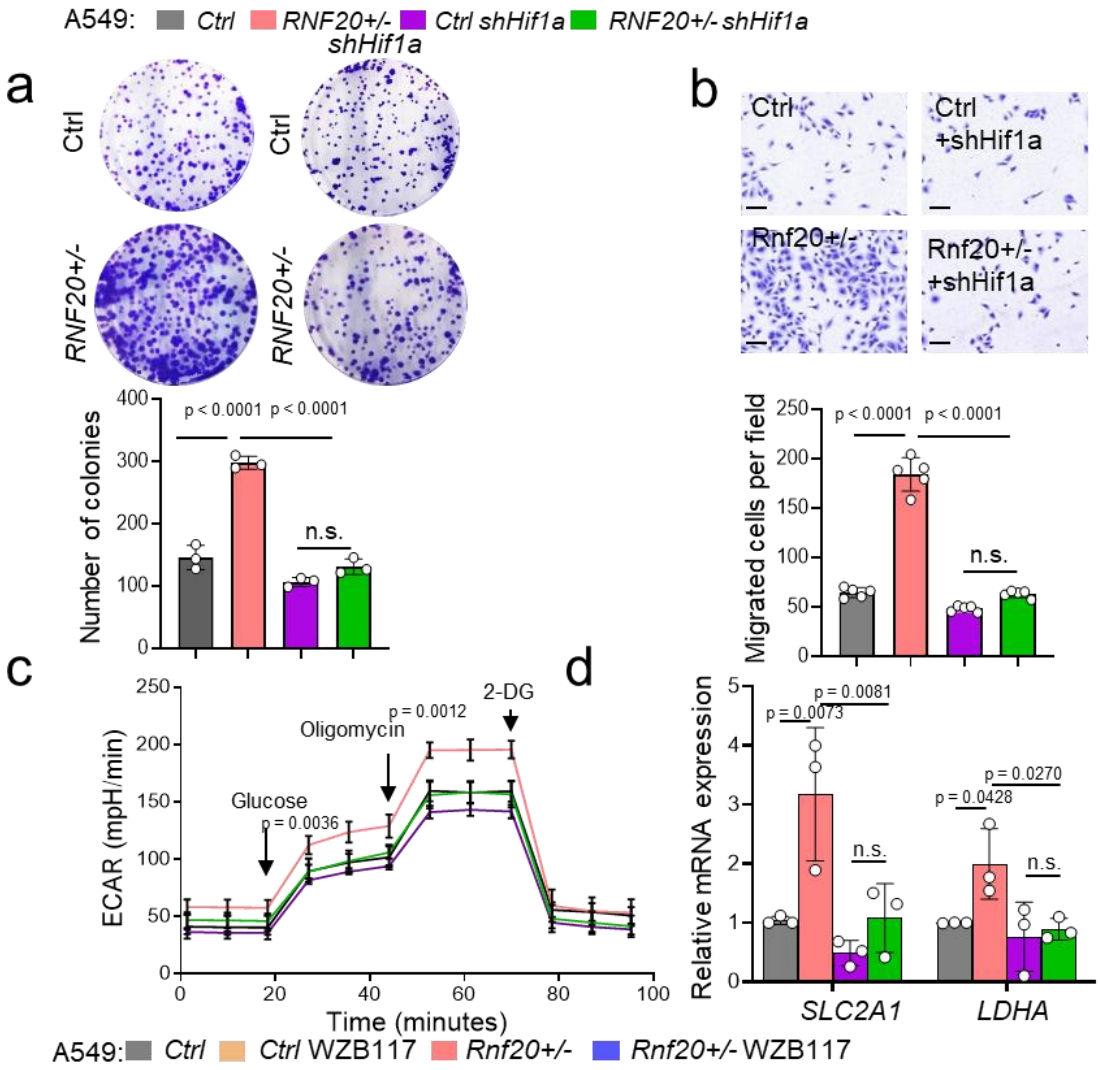
A549: Ctrl RNF20+/- Ctrl shHif1a RNF20+/- shHif1a
a
Ctrl
Ctrl
RNF20+/-
RNF20+/-
Number of colonies
p < 0.0001 p < 0.0001
n.s.
b
Ctrl
Ctrl +shHif1a
Rnf20+/-
Rnf20+/- +shHif1a
Migrated cells per field
p < 0.0001 p < 0.0001
n.s.
c
ECAR (mpH/min)
Glucose
p = 0.0036
Oligomycin
p = 0.0012
2-DG
Time (minutes)
d
Relative mRNA expression
p = 0.0081
p = 0.0073
n.s.
p = 0.0270
p = 0.0428
n.s.
SLC2A1
LDHA
A549: Ctrl Ctrl WZB117 Rnf20+/- Rnf20+/- WZB117
e
DMSO
WZB117
Ctrl
Ctrl
RNF20+/-
RNF20+/-
Number of colonies
p < 0.0001 p < 0.0001
n.s.
f
DMSO
WZB117
Ctrl
RNF20+/-
Migrated cells per field
p < 0.0001 p < 0.0001
n.s.

Figure 24. **HIF1α activation upon RNF20 loss promotes cell growth and migration in human adenocarcinoma.** (a) Clonogenic growth and Boyden chamber migration assay (b) of control and *RNF20+/-* A549 cells expressing either with control shRNA or shRNA targeting *HIF1α* with quantification (lower panels). Scale bars, 150μm. ECAR to evaluate glycolysis (c) and qPCR analysis of *Slc2a1* and *Ldha* (d) in control and *RNF20+/-* A549 cells expressing either with control shRNA or shRNA targeting *HIF1α* (n=3). Clonogenic growth (n=3) (e) and Boyden chamber migration assay (n=5) (f) of control and *RNF20+/-* A549 cells treated either with DMSO or WZB117 with quantifications (right panels). Scale bars, 150μm. Multiple comparisons in (a, b, c, d, e, f) were performed using ANOVA. Data are shown as means ± SEM.

3.5.2.2 Glycolysis inhibition in LLC1 *Rnf20+/-* cells and H82 *RNF20* KD cells rescues the cell growth and migration.

On top of that, I also treated control and *Rnf20+/-* LLC1 cells as well as H82 cells transfected with either control siRNA or siRNA targeting *Rnf20* with WZB117. Notably, I observed similar rescue phenotypes in *Rnf20* loss LLC1 and H82 cells by glycolysis inhibition. Specifically, I found out that the 3D clonogenic growth (Fig. 25a, 25b, 25e, 25f) and migration capacity (Fig. 25c, 25d) were diminished to control levels through inhibition by WZB117. Suggesting again that the knockdown of *Hif1α* in cancer *Rnf20+/-* cells rescues the cell growth and migration.

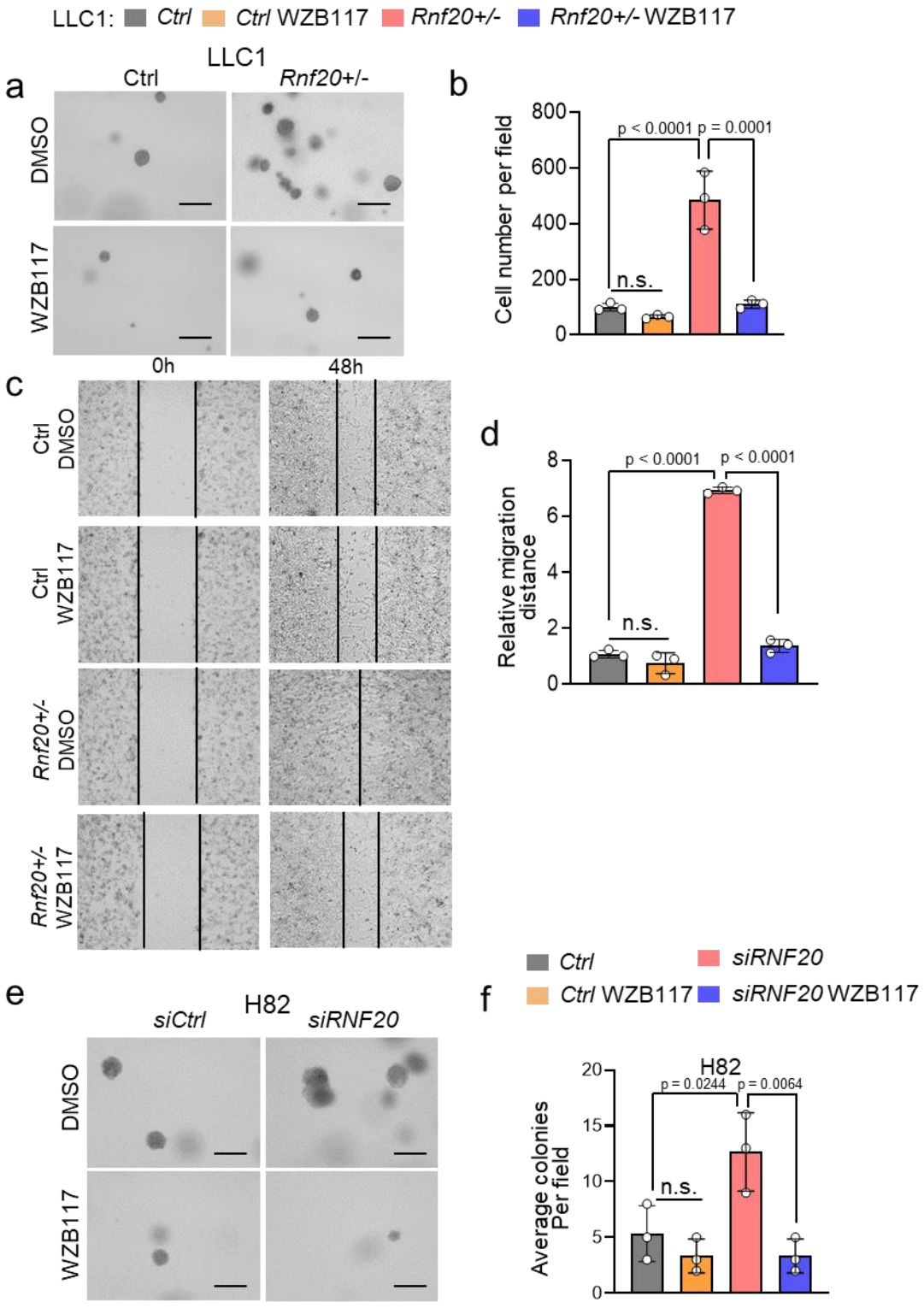

Figure 25. **Activation of glycolysis upon loss of Rnf20 is responsible for cancer cell growth and migration.** Soft agar proliferation assay (a) (b), and Wound healing assay (c) (d) of control and *Rnf20+/-* LLC1 cells treated with either DMSO or WZB117 and the quantifications (n=3). Soft agar proliferation assay (e) of H82 transfected with control siRNA and siRNA against *Rnf20* together with treatment of either DMSO and WZB117 and quantification (n=3) (f). Scale bars, 200 μm (a, e). Multiple comparisons in (b, d, f) were performed using ANOVA. Data are shown as means ± SEM. n.s no significance.

3.5.3 RNF20 loss drives tumor growth and metastasis through HIF1α activation and metabolic rewiring *in vivo*

3.5.3.1 Loss of RNF20 promotes tumor growth and metastasis

To further investigate the impact of *Rnf20* loss on tumor growth and metastasis *in vivo*, I subcutaneously injected control and *RNF20+/-* A549 cells into nude mice. 24 days after the injection, tumors derived from *RNF20+/-* A549 cells were significantly larger in volume compared to those in the control group (Fig.26a, 26b).

Consistently, I performed immunohistochemical (IHC) staining on tumors from primary and metastasis relapse mouse models. In the primary tumor model, LLC1 cells were intratracheally injected into mice. In the metastasis relapse model, LLC1 cells were injected subcutaneously, followed by surgical removal of the primary tumors 10 days later to allow for metastatic recurrence. Notably, RNF20 expression was significantly higher in primary tumors from the intratracheal injection model compared to relapsed metastatic tumors (Fig.26c, 26d).

Next, I conducted intravenous injections of control and *RNF20+/-* A549 cells in nude mice, as well as control and *Rnf20+/-* LLC1 cells in C57BL/6 mice. Consistent with *in vitro* findings, mice receiving *Rnf20+/-* cells exhibited a markedly higher number of tumor nodules and an expanded metastatic burden relative to control (Fig. 26e, 26f, 26g, 26h).

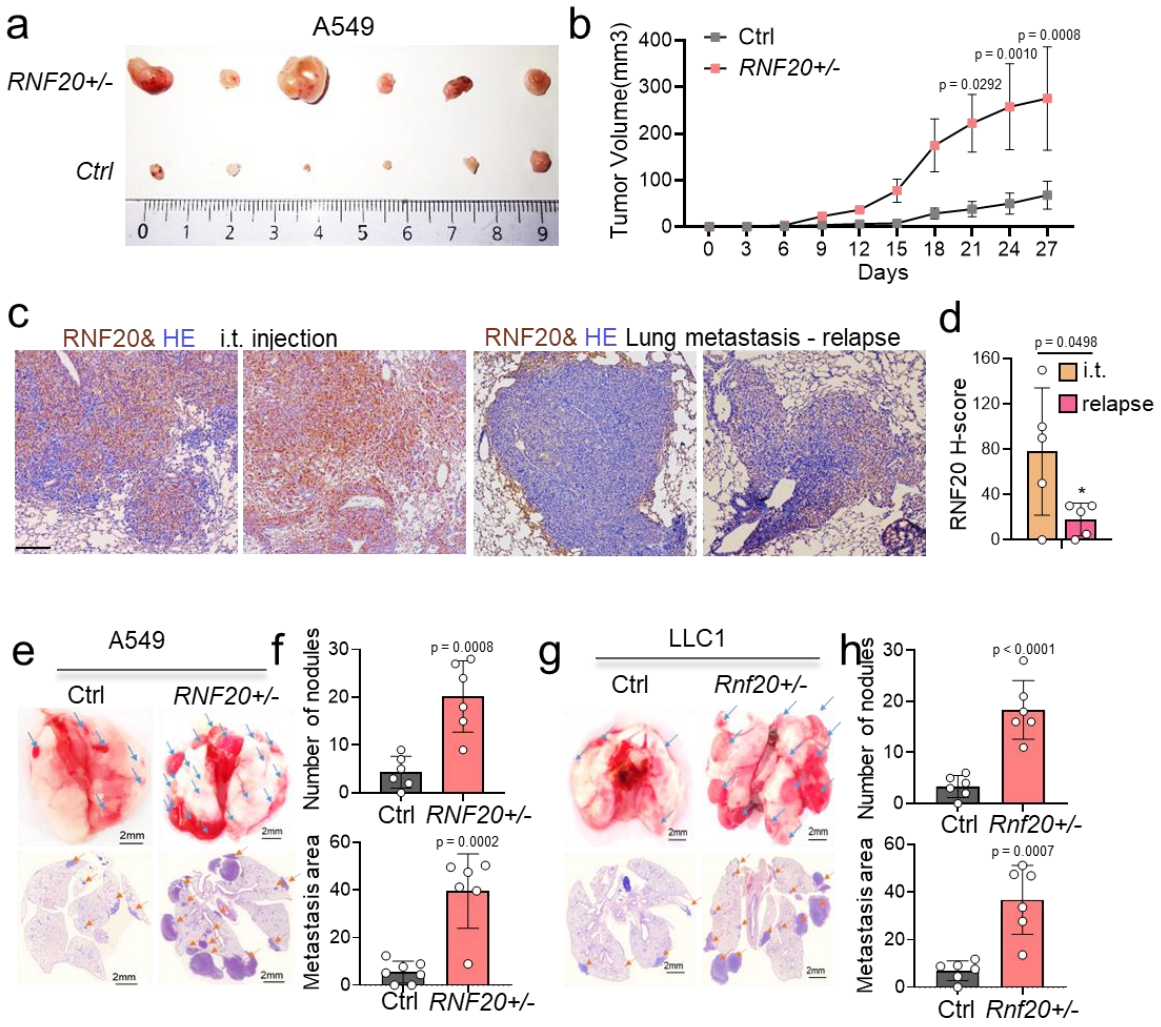

Figure 26. **Loss of *Rnf20* promotes tumor growth and metastasis.** (a) Subcutaneously injection of control and *RNF20+/-* A549 cells into the flanks of BALB/C Nude mice (n=6). Mice were sacrificed after 27 days, and the subcutaneous tumors were excised. (b) Quantification of the tumor volume was performed at various time points following injection. (c) Immunohistochemistry of lungs from the intratracheal (i.t.) injection model and the lung metastasis relapse model stained with an anti-RNF20 antibody (n=5). Scale bar, 400 μm. (d) shows the relative staining intensity (H-Score) of RNF20 in the i.t. and tumor relapse groups (n=5). (e) Control and *RNF20+/-* A549 cells were intravenously injected into the tail vein of BALB/c Nude mice (n=6). The upper panels display the macroscopic appearance of representative lungs, while the lower panels show H&E staining. Scale bars: 2 mm. (f) quantification of metastatic nodules (upper panels) and metastatic area (lower panels) in lung sections from mice injected with control and *Rnf20+/-* A549 cells. (g) control and *Rnf20+/-* LLC1 cells were intravenously injected into the tail vein of C57BL/6 mice (n=6). The upper panels show the macroscopic appearance of representative lungs, while the lower panels depict H&E staining. Scale bars: 2 mm. (h) quantification of metastatic nodules (upper panels) and metastatic area (lower panels) in lung sections from mice injected with control and *Rnf20+/-* LLC1 cells. Statistical analysis in (d, f, h) was performed using two-tailed Student's t-test. Data are shown as means ± SEM.

3.5.3.2 *HIF1α* silencing reduces tumor metastasis and metabolic rewiring in RNF20 haploinsufficiency mouse

Having established the critical role of HIF1α in regulating lung cancer cell growth and migration as well as metabolic rewiring in cell culture-based system, I next investigated its function *in vivo*. Control and *RNF20+/-* A549 cells with or without silencing of *HIF1α* were intravenously injected into nude mice. At the experimental endpoint, lungs were harvested, and both the number and size of metastatic tumor nodules were quantified. Notably, the knockdown of *HIF1α* in *RNF20+/-* A549 cells significantly reduced the number of tumor nodules and overall metastatic burden (Fig. 27a, 27b, 27c), indicating that the activation of HIF1α, driven by loss of *RNF20* contributes to lung cancer metastasis.

Simultaneously, I did the treatment either by DMSO/PBS or WZB117 for mice injected with control and *RNF20+/-* A549 cells. The inhibition of glucose uptake also impairs the role in promoting tumor metastasis upon loss of *RNF20*, evidenced by fewer tumor nodules and metastatic areas compared to the control counterpart (Fig. 27a, 27b, 27c).

To assess whether this treatment could also reverse the metabolic changes induced by *RNF20* loss, I measured levels of glycolytic metabolites in lung tissue extracts. Consistently, both *HIF1α* knockdown and WZB117 treatment significantly reduced the levels of G6P and lactate in the lungs of *Rnf20+/-* mice (Fig. 27d, 27e), confirming a rescue of the hypermetabolic phenotype *in vivo*.

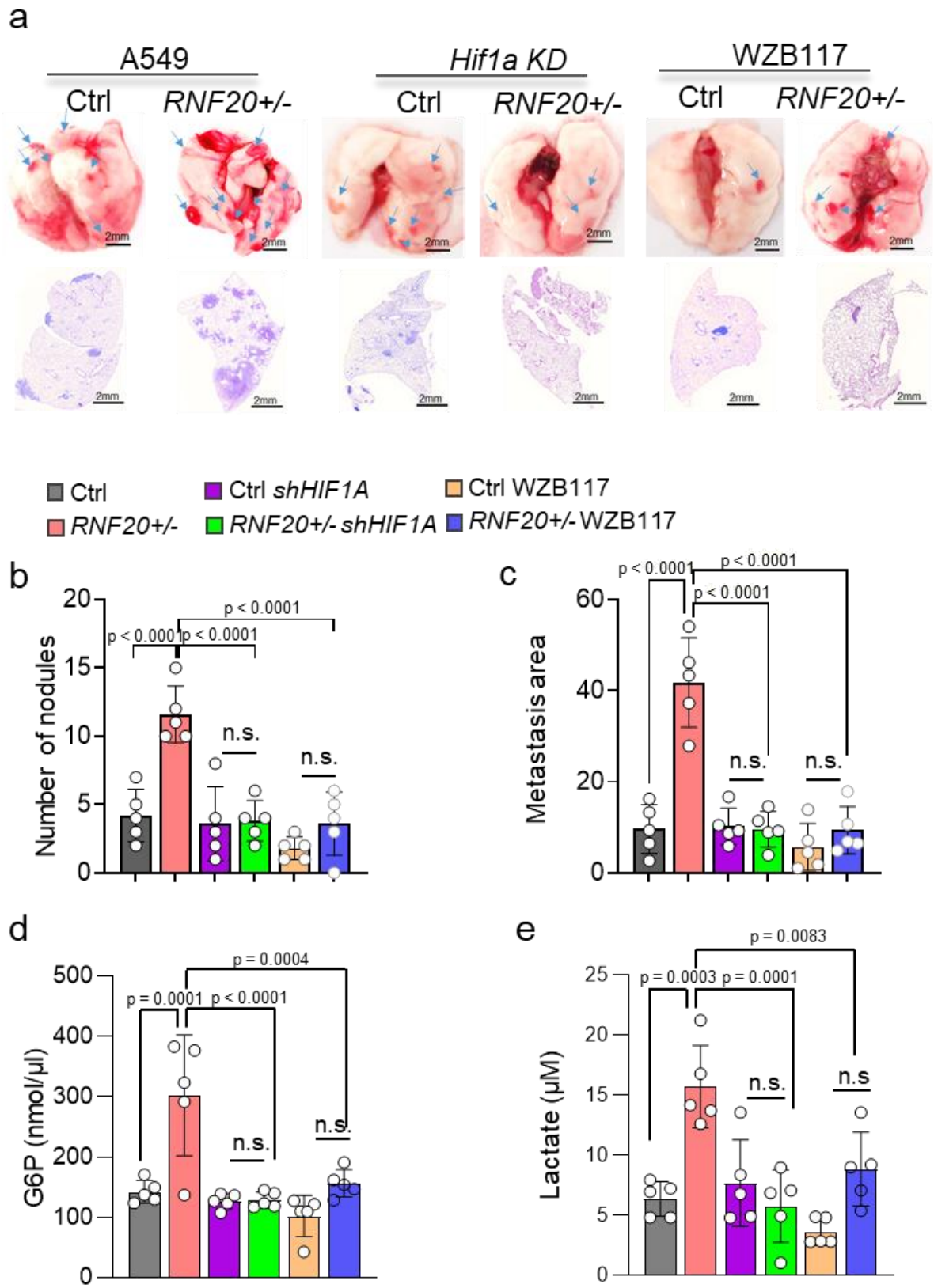

Figure 27. **Activation of glycolysis upon loss of *Rnf20* is responsible for tumor growth, metastasis.** (a) control and *RNF20+/-* A549 cells expressing control shRNA or shRNA against *HIF1α* were intravenously injected into the tail vein of BALB/C Nude mice (n=5) and injected control and

RNF20+/- A549 cells followed with treatment of either DMSO/PBS or WZB117 of the mice. Representative macroscopic appearance (upper panels) and H&E staining (lower panels) of lungs. Scale bars, 2mm. (b) Quantification of the nodules and metastatic area (c) in injected mice lungs. Measurement of glucose-6-phosphate (G6P) (d) and lactate (e) in lung homogenates in BALB/C Nude mice intravenously injected of control and *RNF20+/-* A549 cells after shRNA mediated *HIF1α* silencing or after treatment with the GLUT1 inhibitor WZB117 (n=5). Multiple comparisons in (b, c, d, e) were performed using ANOVA. Data are shown as means ± SEM. n.s. no significance.

3.5.3.3 *HIF1α* silencing and WZB117 treatment rescue the DNA damage repair deficiency in RNF20 haploinsufficiency mice

To investigate the impact of *Rnf20* loss-induced HIF1α accumulation on the DNA damage response *in vivo*, I performed IHC staining for γH2AX on lung tissue sections obtained from the intravenous injection mouse model described earlier. Notably, tumors derived from mice injected with *RNF20+/-* A549 cells exhibited significantly elevated γH2AX levels compared to those from control mice, indicating increased DNA damage (Figure 28a, 28b). Strikingly, this effect was reversed by either *HIF1α* knockdown or pharmacological inhibition of glucose uptake using WZB117 (Figure 28a, 28b), suggesting that HIF1α-mediated metabolic reprogramming contributes to impaired DNA damage response upon *Rnf20* loss.

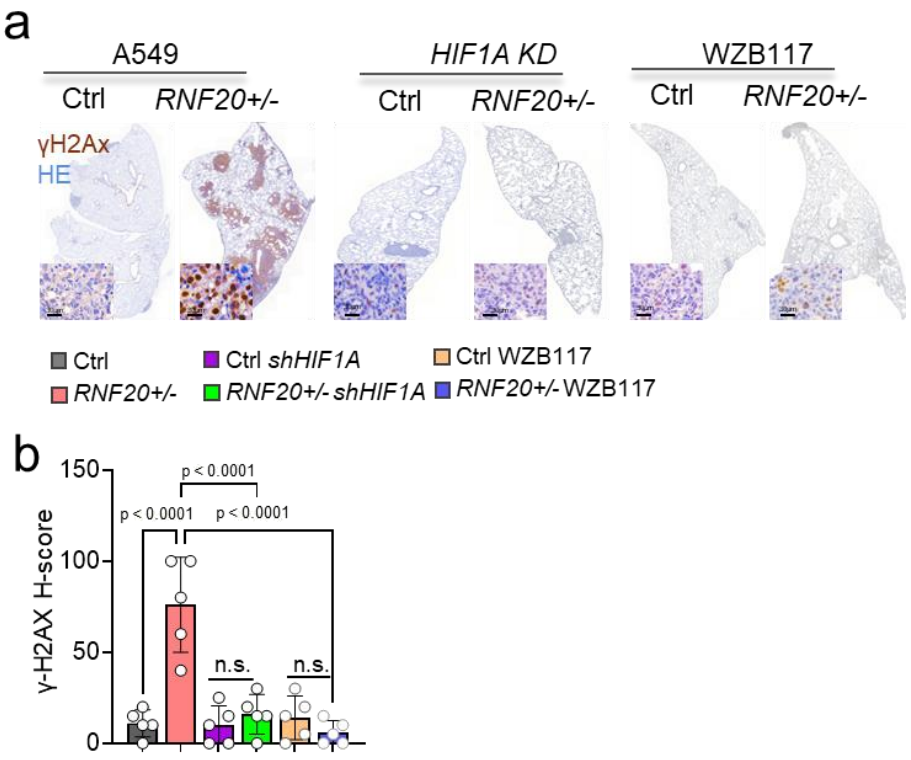

Figure 28. ***HIF1α* silencing and WZB117 treatment in *Rnf20* haploinsufficiency rescue the DNA damage repair deficiency**. (a) Immunohistochemistry staining of sections from mice injected control

and *RNF20+/-* A549 cells expressing control shRNA or shRNA against *HIF1α*, as well as control and *RNF20+/-* A549 cells followed with treatment of either DMSO/PBS or WZB117 by utilized γH2AX antibody (n=5). Scale bar, 2 mm. (b) quantification H-score of the staining. Multiple comparisons were performed using ANOVA. Data are shown as means ± SEM. n.s. no significance.

3.6 RNF20 controls RBX1 mediated HIF1α degradation

3.6.1 Genome-wide H2Bub1 levels were decreased upon loss of *Rnf20*

RNF20 is known to function as an E3 ubiquitin ligase that mediates mono-ubiquitination of histone H2B (H2Bub1), a modification associated with active transcription and chromatin remodeling. Consistent with this role, I observed a marked decrease in H2Bub1 levels following *Rnf20* loss in MLE12 cells (Fig. 29a). To further explore the underlying mechanism, I examined H2Bub1 enrichment across the genome in relation to transcriptional changes induced by *Rnf20* deficiency.

Genome-wide analysis revealed a global reduction in H2Bub1 occupancy in *Rnf20+/-* MLE12 cells compared to controls. As anticipated, genes upregulated upon *Rnf20* loss exhibited reduced H2Bub1 enrichment; however, the reduction in H2Bub1 was even more pronounced among downregulated genes (Fig. 29b). Notably, this group included critical regulators such as *p53*, components of the Notch signaling pathway, and genes involved in HIF1α degradation, including *Hes1* and *Rbx1* (Fig. 29c).

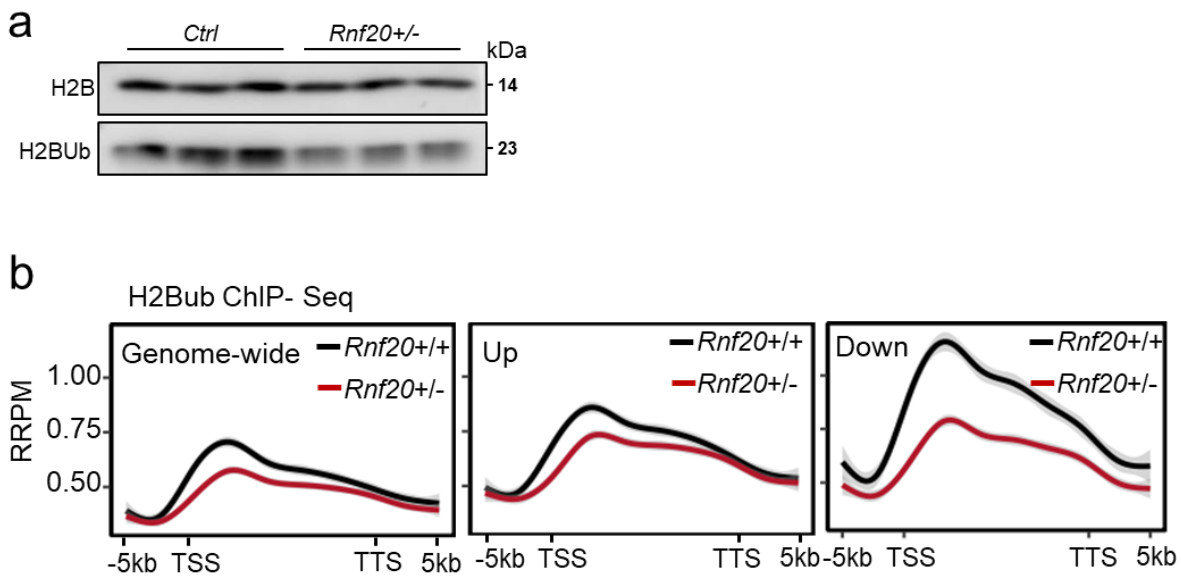

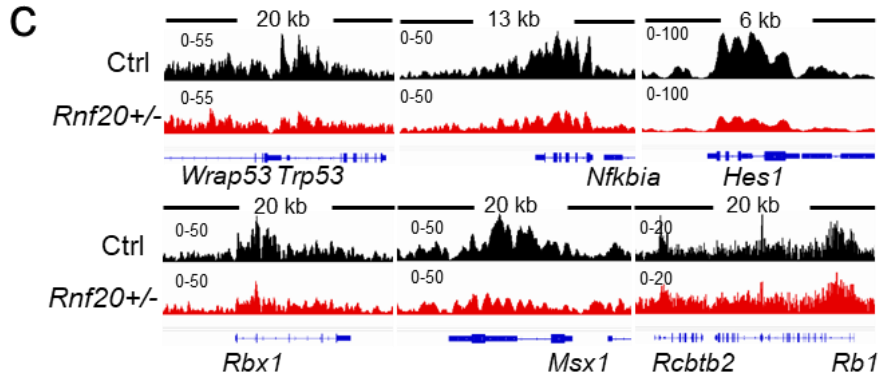

Figure 29. **H2Bub1 level decreased upon *Rnf20* loss.** (a) Representative Western Blot analysis showing H2Bub1 levels in control and *Rnf20+/-* MLE12 cells. (b) The average genome-wide H2Bub1 ChIP-seq signal, as well as the H2Bub1 ChIP-seq signal at genes upregulated and downregulated upon Rnf20 loss, was compared between control and *Rnf20+/-* MLE12 cells (n=2). (c) Genome tracks of merged H2Bub1 ChIP-seq reads in control and *Rnf20+/-* MLE12 cells at genes downregulated upon Rnf20 loss of function show a significant decrease in H2Bub1 levels at genes such as *Trp53*, *Nfkbia*, *Hes1*, *Rbx1*, and *Msx1*.

3.6.2 Overexpression of RBX1 in *Rnf20* haploinsufficiency cells impairs HIF1α accumulation

RBX1 is a key component of the Cullin-ring E3 ubiquitin ligase complex, specifically in the VHL-E3 ubiquitin ligase complex, which plays a crucial role in regulating HIF1α. Given that *Rbx1* expression was specifically downregulated upon *Rnf20* loss, I hypothesized that reduced RBX1 levels may contribute to the stabilization and accumulation of HIF1α in *Rnf20+/-* cells. To test this, I overexpressed RBX1 in *Rnf20+/-* MLE12 cells. RBX1 overexpression led to a significant reduction in HIF1α levels compared to *Rnf20+/-* cells transfected with an empty control vector (Figure 30a). This was accompanied by decreased expression of HIF1α downstream target genes (Figure 30b). Functionally, overexpression of *Rbx1* also suppressed clonogenic growth (Figure 30c) and migratory capacity (Figure 30d) in *Rnf20+/-* cells. These results suggest that RBX1 downregulation contributes to HIF1α accumulation following *Rnf20* loss and that restoring RBX1 expression can reverse both molecular and phenotypic consequences of *Rnf20* deficiency.

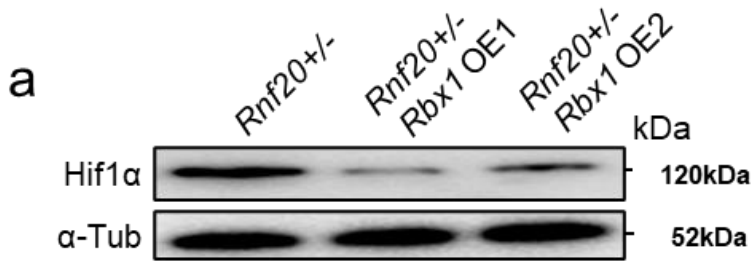
a
Rnf20+/-
Rnf20+/- Rbx1 OE1
Rnf20+/- Rbx1 OE2
kDa
Hif1α
120kDa
α-Tub
52kDa

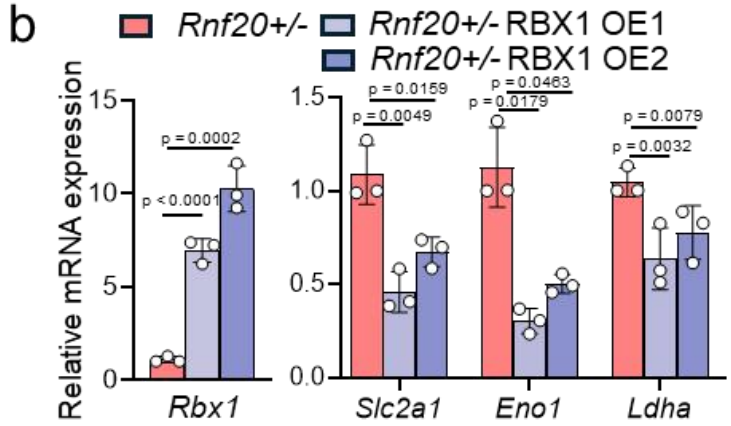
b
Rnf20+/-
Rnf20+/- RBX1 OE1
Rnf20+/- RBX1 OE2
Relative mRNA expression
p = 0.0002
p < 0.0001
p = 0.0159
p = 0.0049
p = 0.0463
p = 0.0179
p = 0.0079
p = 0.0032
Rbx1
Slc2a1
Eno1
Ldha

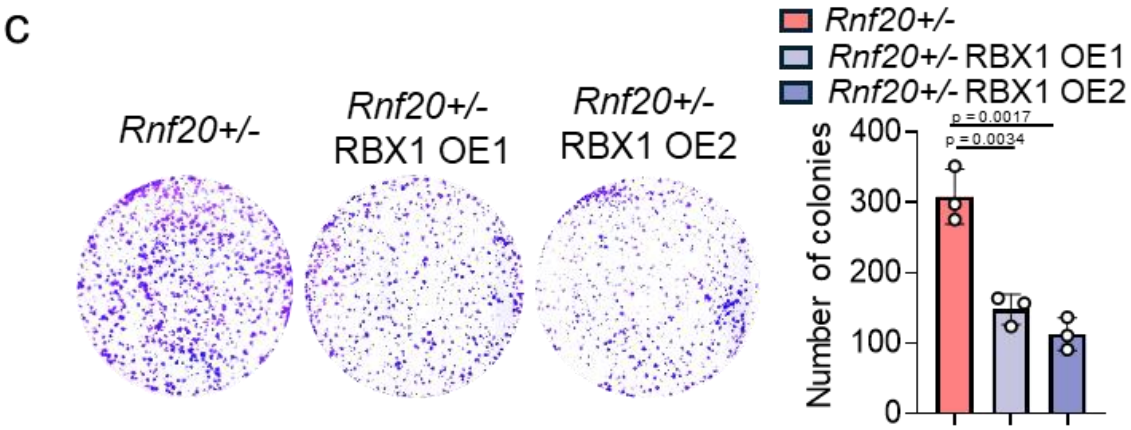
c
Rnf20+/-
Rnf20+/- RBX1 OE1
Rnf20+/- RBX1 OE2
Rnf20+/-
Rnf20+/- RBX1 OE1
Rnf20+/- RBX1 OE2
Number of colonies
p = 0.0017
p = 0.0034

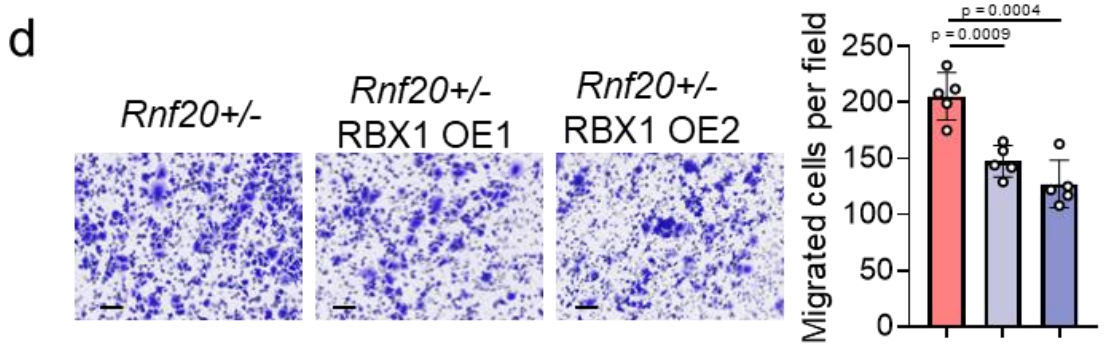
d
Rnf20+/-
Rnf20+/- RBX1 OE1
Rnf20+/- RBX1 OE2
Migrated cells per field
p = 0.0004
p = 0.0009

Figure 30. **RBX1 overexpression in *Rnf20* loss of function MLE12 cells reduced HIF1α and HIF1α involved clonogenic growth and migration.** (a) Representative Western Blot analysis showing HIF1α levels in control and *Rnf20+/-* MLE12 cells. (b) Relative mRNA expression levels of *Rbx1*, *Slc2a1*, *Eno1*, and *Ldha* in *Rnf20+/-* MLE12 cells or *Rnf20+/-* cells stably expressing RBX1 (n=3). (c) Clonogenic assay with *Rnf20+/-* MLE12 cells or *Rnf20+/-* cells stably expressing RBX1 (left panels), and quantification of the number of colonies (right panel, n=3). (d) Boyden chamber migration assay with *Rnf20+/-* MLE12 cells or *Rnf20+/-* cells stably express RBX1 (left panels), and quantification of the number of migrated cells per field (right panel, n=5). Scale bars, 150μm. Statistical analysis in (b, c, d) was performed using two-tailed Student's t-test. Data are shown as means ± SEM.

3.7 HIF1α activation upon RNF20 haploinsufficiency induces RNA polymerase II promoter-proximal pause release at metabolic genes

3.7.1 *Rnf20* loss induces the polymerase release of genes involved in HIF1α targets and EMT

RNF20 has been reported to regulate gene expression programs by modulating RNA polymerase II (Pol II) pausing, while HIF1α has also been implicated in similar transcriptional regulatory mechanisms(Shema, Kim et al. 2011, Yang, Lu et al. 2022). In light of these findings and my previous data, I investigated whether *Rnf20* loss affects Pol II pausing and transcriptional elongation. To this end, I performed total Pol II ChIP-seq in control and *Rnf20+/-* MLE12 cells. To quantify Pol II pausing, I calculated the pausing index (PI), defined as the ratio of Pol II occupancy at promoter-proximal regions versus gene body regions (Fig. 31a). Genome-wide analysis revealed that Pol II occupancy in the gene bodies of glycolytic genes, such as *Ldha*, *Pdk1*, *Eno1*, and *Pgk1* (Fig. 31b), was increased in *Rnf20+/-* cells compared to controls, indicating enhanced transcriptional elongation. Further comparison of the PI between groups revealed a significant decrease in pausing index at genes upregulated in *Rnf20+/-* cells, while genes that were unchanged or downregulated did not exhibit a notable difference in pausing index (Fig. 31c). Importantly, I identified 660 genes that were both upregulated and showed reduced PI upon *Rnf20* loss. These include metabolic and EMT-related genes such as *Eno1*, *Aldoa*, *Ldha*, *Gapdh*, *Pfkp*, *Vegfa*, *Vegfb*, and *Snai1* (Fig. 31d). Gene ontology (GO) analysis of these overlapping genes revealed enrichment in pathways related to cell cycle regulation, glycolysis, cellular metabolism, autophagy and cytoskeleton organization, most of which are regulated by HIF1α or linked to EMT (Fig. 31e). Moreover, the pausing index of HIF1α pathway and EMT genes were also decreased in *Rnf20+/-* MLE12 cells compared to control cells (Fig.

31f). Additionally, to validate these findings, I performed Pol II ChIP-qPCR on glycolytic target genes in both cultured MLE12 cells and mouse lung tissue samples. In both settings, I observed a consistent reduction in Pol II pausing upon *Rnf20* loss (Fig. 31g, 31h). These data together demonstrate that *Rnf20* loss facilitate RNA polymerase II pause release, specifically at genes associated with the HIF1α signaling pathway and EMT, thereby promoting transcriptional activation of tumor promoting gene networks.

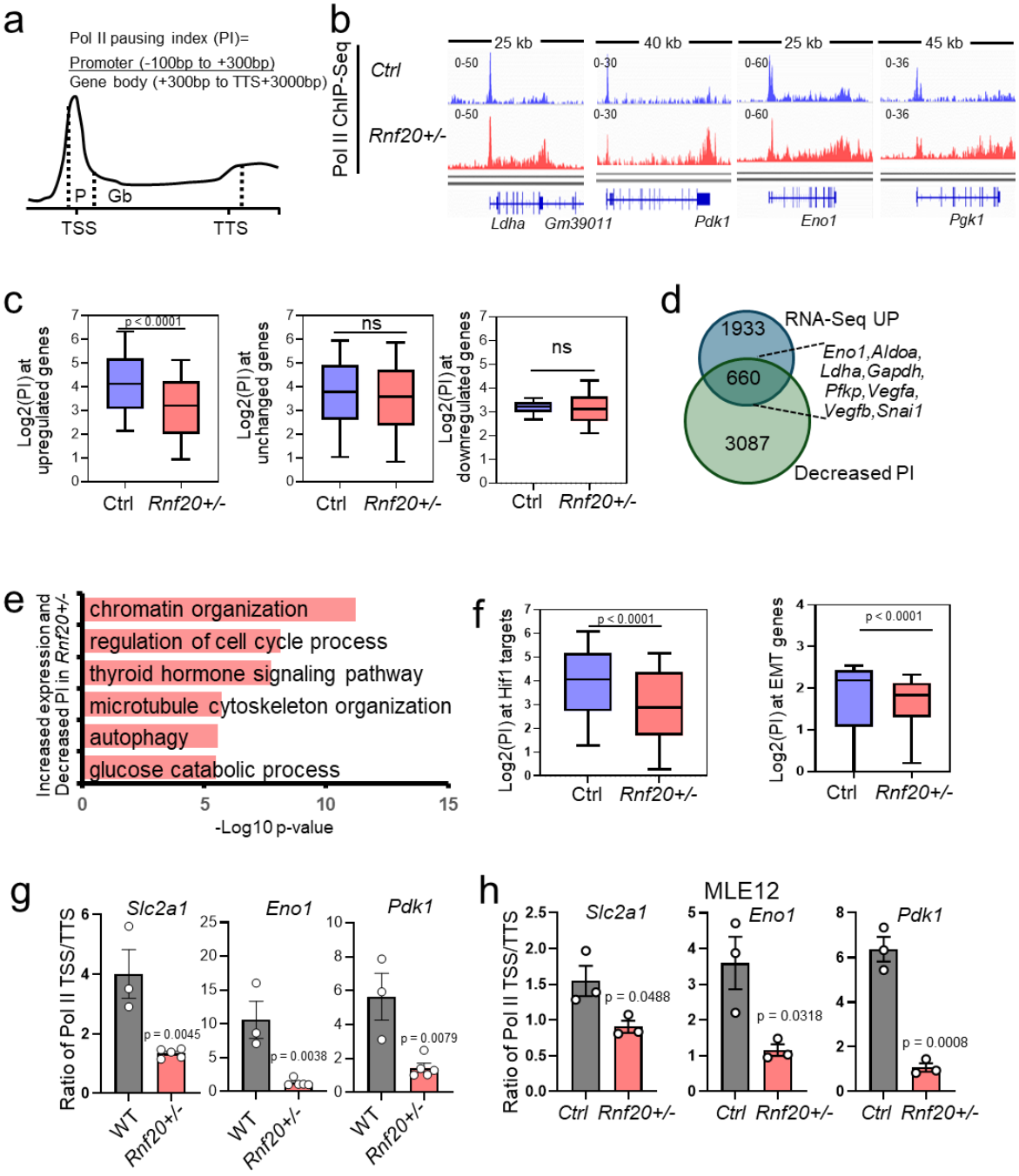

Figure 31. *Rnf20* haploinsufficiency induces RNA polymerase II promoter-proximal pause release at EMT and metabolic genes. (a) The PolI pausing index (PI) is calculated by taking the ration

of the Pol II signal density located 100 base pairs upstream and 300 base pairs downstream of the transcription start site (TSS) to the signal density within the gene body. The gene body is defined as the region extending from 300 base pairs downstream of the TSS to 3kb downstream of the transcription termination site (TTS). (b) Genome tracks showing combined RNA polymerase II RNA-seq reads from control and *Rnf20+/-* MLE12 cells at glycolysis related genes. (c) Log2 values of the Pol II pausing index (PI) at genes that are either upregulated or remain unchanged following Rnf20 loss of function (LOF) in control and *Rnf20+/-* MLE12 cells (n=3). (d) A Venn diagram illustrating the overlap of genes with decreased Pol II pausing index (PI) and upregulation in *Rnf20+/-* MLE12 cells compared to control. (e) Gene Ontology (GO) analysis of the genes that overlap in the Venn diagram. (f) Log2 values of the Pol II pausing index (PI) at HIF1α target genes (left) and EMT genes (right) in control and *Rnf20+/-* MLE12 cells (n=3). (g) The ratio of Pol II enrichment at the TSS and TTS of *Scl2a1*, *Eno1*, and *Pdk1* in control (n=3) and *Rnf20+/-* (n=5) lung samples, as determined by Pol II ChIP-qPCR. (h) The ratio of Pol II enrichment at the TSS and TTS of *Scl2a1*, *Eno1*, and *Pdk1* in control and *Rnf20+/-* MLE12 cells by Pol II ChIP-qPCR (n=3). Statistical analysis in (c, f, g, h) was performed using two-tailed Student's t-test. Data are shown as means ± SEM. n.s. no significance.

3.7.2 HIF1α mediates Pol II pause release in response to *Rnf20* haploinsufficiency

Given that HIF1α has been shown to promote RNA polymerase II (Pol II) pause release (Andrysik, Bender et al. 2021), I investigated the interplay between HIF1α activity and *Rnf20* loss in transcriptional regulation. By intersecting HIF1α-bound genes in A549 cells with genes exhibiting a decreased pausing index upon *Rnf20* depletion, I identified a subset of overlapping genes. Gene Ontology (GO) analysis of this overlapping gene set revealed significant enrichment in pathways related to glycolysis, DNA damage response, chromatin remodeling, negative regulation of apoptosis, and transcriptional repression (Fig. 32a).

To explore the mechanistic connection, I performed Pol II ChIP-seq in control, *Rnf20+/-*, and *Rnf20+/-* HIF1α knockdown MLE12 cells. Consistent with a direct role of HIF1α in facilitating Pol II pause release, HIF1α depletion in *Rnf20+/-* cells led to reduced Pol II occupancy across gene bodies of glycolytic targets such as *Ldha* and *Slc2a1* (Fig. 32b). Besides, pausing index values at HIF1α-bound genes were restored to control levels upon HIF1α knockdown in *Rnf20+/-* cells, further supporting its involvement (Fig. 32c). To further validate these findings, I conducted ChIP-qPCR to assess the distribution of initiating/paused Pol II (phosphorylated at serine 5, pSer5) and elongating Pol II (phosphorylated at serine 2, pSer2) at glycolytic target genes in control, *Rnf20+/-,* and *Rnf20+/-* HIF1α knockdown MLE12 cells. I observed increased enrichment of elongating pSer2 Pol II across the gene bodies of *Slc2a1* (Glut1), *Eno1*, and *Ldha* upon *Rnf20* loss, which was attenuated following HIF1α depletion (Fig. 32d). Concurrently,

initiating/paused pSer5 Pol II was reduced at the transcription start sites of these genes in *Rnf20+/-* MLE12 cells but was restored to control levels upon HIF1α depletion (Fig. 32e). These data indicate that HIF1α activation in response to *Rnf20* haploinsufficiency leads to the release of RNA polymerase II promoter-proximal pausing in the context of lung cancer.

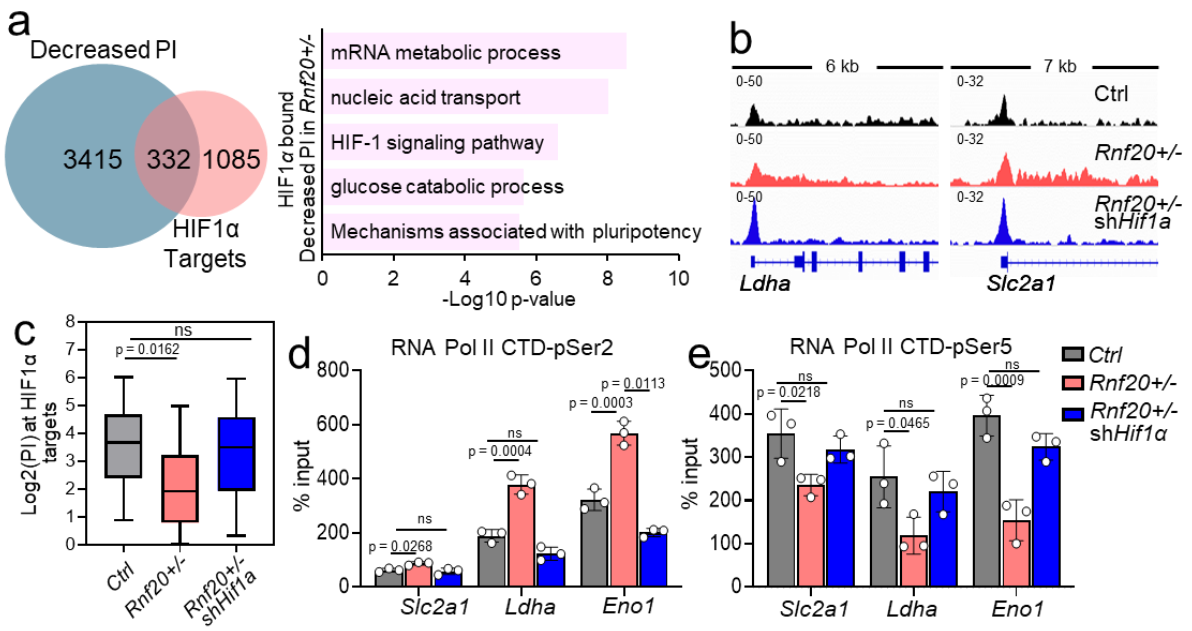

Figure 32. ***Rnf20* loss induces the polymerase release of genes through HIF1α activation.** (a) A Venn diagram (left panel) illustrating the overlap of genes with decreased Pol II pausing index (PI) in *Rnf20+/-* MLE12 cells compared to controls, and HIF1α-bound genes in A549 lung adenocarcinoma cells, as determined by ChIP-Seq(Andrysik, Bender et al. 2021), Gene Ontology (GO) analysis of genes with decreased Pol II pausing index (PI) in *Rnf20+/-* MLE12 cells compared to controls, and genes bound by HIF1α (right panel). (b) Genome tracks showing combined Pol II ChIP-Seq reads from control, *Rnf20+/-*, and *Rnf20+/-* MLE12 cells stably expressing shRNA targeting *Hif1α*. (c) Pol II pausing index (PI) of control, *Rnf20+/-*, and *Rnf20+/-* MLE12 cells stably expressing shRNA against *Hif1α* at HIF1α-bound genes in lung A549 adenocarcinoma cells (n=2). (d) ChIP-qPCR analysis for RNA Pol II CTD-pSer2 and (e) RNA Pol II CTD-pSer5 at the gene bodies of *Scl2a1*, *Ldha*, and *Eno1* in control, *Rnf20+/-*, and *Rnf20+/-* MLE12 cells, or *Rnf20+/-* MLE12 cells following shRNA-mediated *Hif1α* silencing (n=3). Multiple comparisons in (c, d, e) were performed using ANOVA. Data are shown as means ± SEM. n.s. no significance.

3.7.3 RNF20, H2Bub1, and HIF1α cooperate in transcriptional regulation through distinct mechanisms

RNF20 functions as an E3 ubiquitin ligase responsible for the monoubiquitinating of histone H2B (H2Bub1), a modification known to facilitate SET1-dependent di- and trimethylation of histone H3 at lysine 4 (H3K4me2, H3K4me3) (Soares and Buratowski 2013, Kwon, Park et al. 2020). Notably, SET1B has also been identified as a key

regulator in the activation of HIF1α-induced genes (Ortmann, Burrows et al. 2021). Suggesting potential crosstalk between RNF20, HIF1α, and histone methylation in transcriptional control. To further investigate this relationship, I examined the correlation between H2Bub1 levels and the Pol II pausing index in *Rnf20+/-* versus control MLE12 cells. Surprisingly, no significant correlation was found between changes in H2Bub1 occupancy and Pol II pausing index across both upregulated and downregulated gene sets (Fig. 33a). These results suggest that Pol II pausing, and release are regulated independently of H2Bub1.

To assess whether H3K4me3, a downstream histone mark of H2Bub1, is involved in RNF20- and HIF1α-mediated transcription regulation, I performed ChIP-seq for H3K4me3 in *Rnf20+/-* and *Rnf20+/-* HIF1α knockdown MLE12 cells. The data showed that HIF1α depletion did not alter H3K4me3 levels at HIF1α target genes or gene upregulated in *Rnf20+/-* cells. However, a notable reduction in H3K4me3 was observed at genes that were downregulated upon *Rnf20* loss (Fig. 33b). These findings indicate that the HIF1α-dependent decrease in H3k4me3 may contribute to the transcription repression of a subset of RNF20 targets genes. However, this mechanism appears to be distinct from RNF20-mediated regulation of Pol II pausing, as H3K4me3 levels do not correlate with changes in pausing at HIF1α-regulated genes.

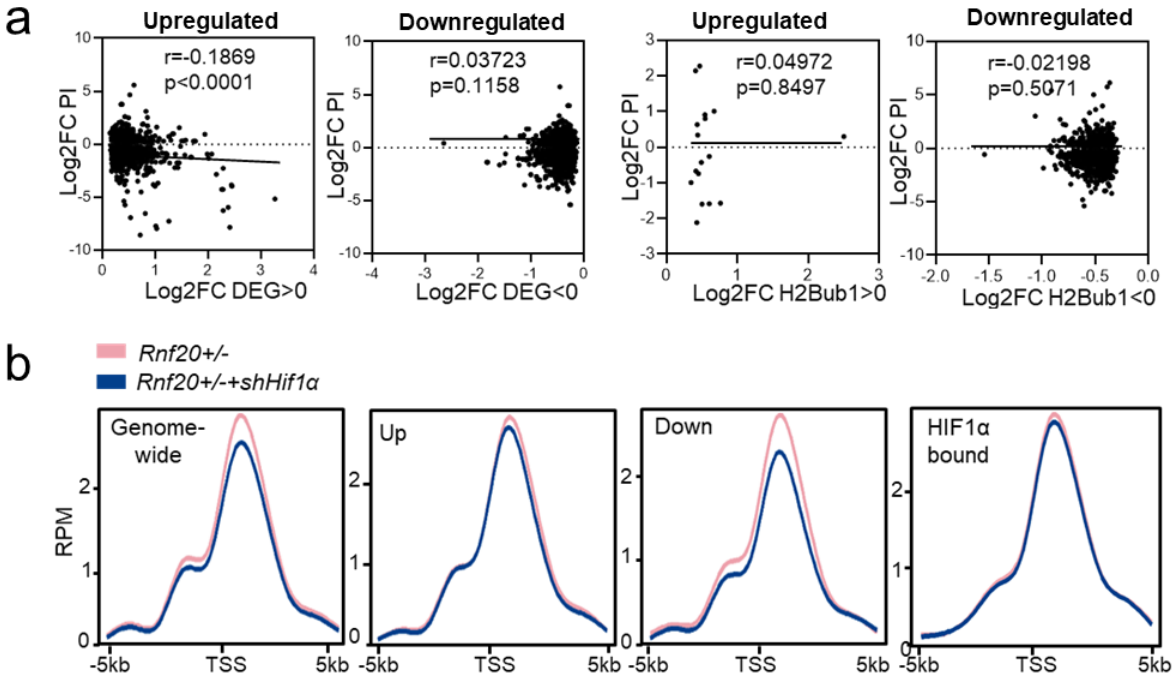

Figure 33. **RNF20 and HIF1α dependent changes in transcriptional activity.** (a) Pearson correlation (r) between the Log2 fold change (FC) of Pol II pausing index (PI) and the Log2 FC of upregulated (left) or downregulated (left) genes as well as Pearson correlation (r) between Log2 FC of PI and Log2 FC of genes showing increased (right) or decreased (right) H2Bub1 levels in Rnf20+/- versus control MLE12 cells. (b) The average genome-wide H3K4me3 ChIP-seq signal, along with the H3K4me3 ChIP-seq signal at genes upregulated or downregulated following RNF20 loss, HIF1α-bound genes in A549 lung adenocarcinoma cells in *Rnf20+/-* MLE12 cells or *Rnf20+/-* MLE12 cells after shRNA-mediated *Hif1α* silencing.

3.8 HIF1α and HIF1α-target expression correlate with RNF20 levels in lung cancer patients

3.8.1 RNF20 expression negatively correlates with HIF1α and its metabolic targets in lung cancer patients

Our study identifies a key role for *Rnf20* loss in promoting lung cancer progression through the activation of HIF1α signaling. To further substantiate this mechanistic link, I investigated the relationship between RNF20 expression and the levels of HIF1α and its downstream metabolic targets in lung cancer patient samples.

I first conducted IHC staining on a lung cancer tissue microarray using antibodies against HIF1α, ENO1, and LDHA, and quantified protein expression using H-scores. The results revealed that HIF1α, ENO1, and LDHA protein levels were significantly elevated in tumor tissues compared to normal lung tissues (Fig. 34a). Notably, in high-grade adenocarcinoma (ADs) and small cell lung cancer (SCLC) patient samples, the expression levels of HIF1α, ENO1, and LDHA were inversely correlated with RNF20 protein expression (Fig. 34b). To complement these findings, I performed correlation analysis using publicly available GEO datasets, which revealed a negative correlation between Rnf20 expression and the mRNA levels of several HIF1α-regulated genes, including *Slc2a1*, *Eno1*, *Ldha*, and *Vegfa* (Fig. 34c). Additionally, these HIF1α target genes were found to be upregulated in lung ADs patients compare to normal lung tissues (Fig. 34d). Suggesting that HIF1α and HIF1α targets were negative correlated with *Rnf20* expression in lung cancer patients.

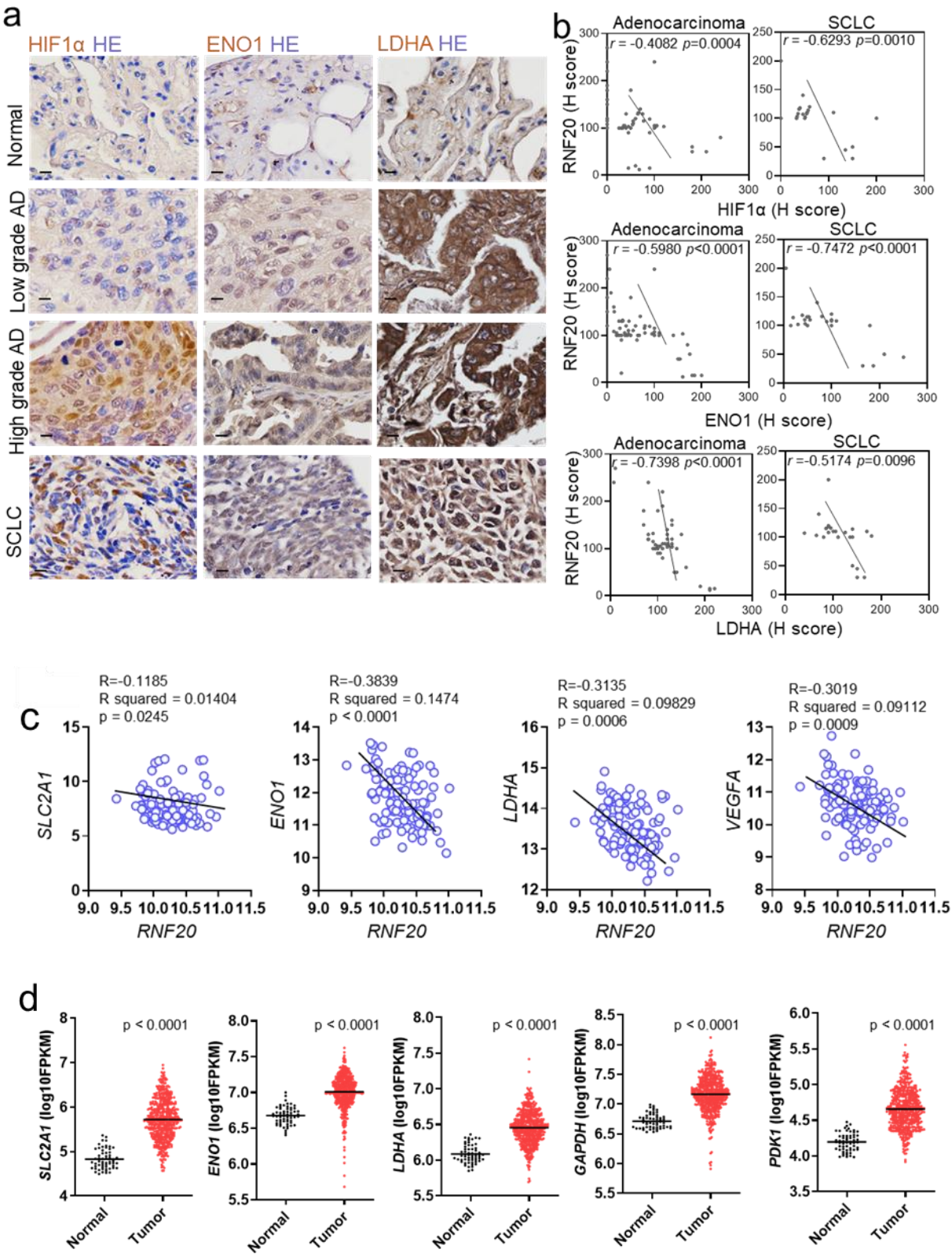

Figure 34. **Decreased RNF20 levels correlate with increased levels of HIF1α and glycolytic targets.** (a) Immunohistochemistry of representative tissue samples from various types and grades of lung tumors on a tissue microarray, stained with HIF1α, ENO1, and LDHA antibodies. Scale bars, 100 μm. (b) Pearson correlation (r) of the relative staining intensity (H-Score) for RNF20 and HIF1α (top panels), RNF20 and ENO1 (middle panels), and RNF20 and LDHA (bottom panels) in adenocarcinoma (AD) and

small cell lung cancer (SCLC) patients. n=70 for AD; n=22 for SCLC. (c) Pearson correlation (r) between the mRNA expression levels of *Rnf20* and genes involved in glycolysis (*Slc2a1*, *Eno1*, *Ldha*) or the hypoxic response (*Vegfa*) in lung adenocarcinoma (AD) cancer datasets (GSE19188, GSE27262). (d) Normalized expression levels of the metabolic enzymes SLC2A1, ENO1, LDHA, GAPDH, and PDK1 in normal lung (n=59) and adenocarcinoma (n=532) tissues from the TCGA datasets. Statistical analysis in (d) was performed using a two-tailed Student's t-test. Data are shown as means ± SEM.

3.8.2 HIF1α-dependent gene expression correlates with poor prognosis in lung adenocarcinoma patients

Building upon my previous findings, I next performed a survival analysis focusing on genes involved in the glycolysis pathway. In line with my earlier observations, where lower *RNF20* mRNA expression was associated with reduced overall survival in ADs patients but not in squamous cell carcinoma (SCC) patients, I found a similar trend among glycolytic genes. Specifically, high expression levels of *Slc2a1*, *Eno1*, *Ldha*, and *Vegfa* were significantly associated with poor prognosis in ADs patients (Fig. 35a), whereas no such correlation was observed in SCC patients (Fig. 35b).

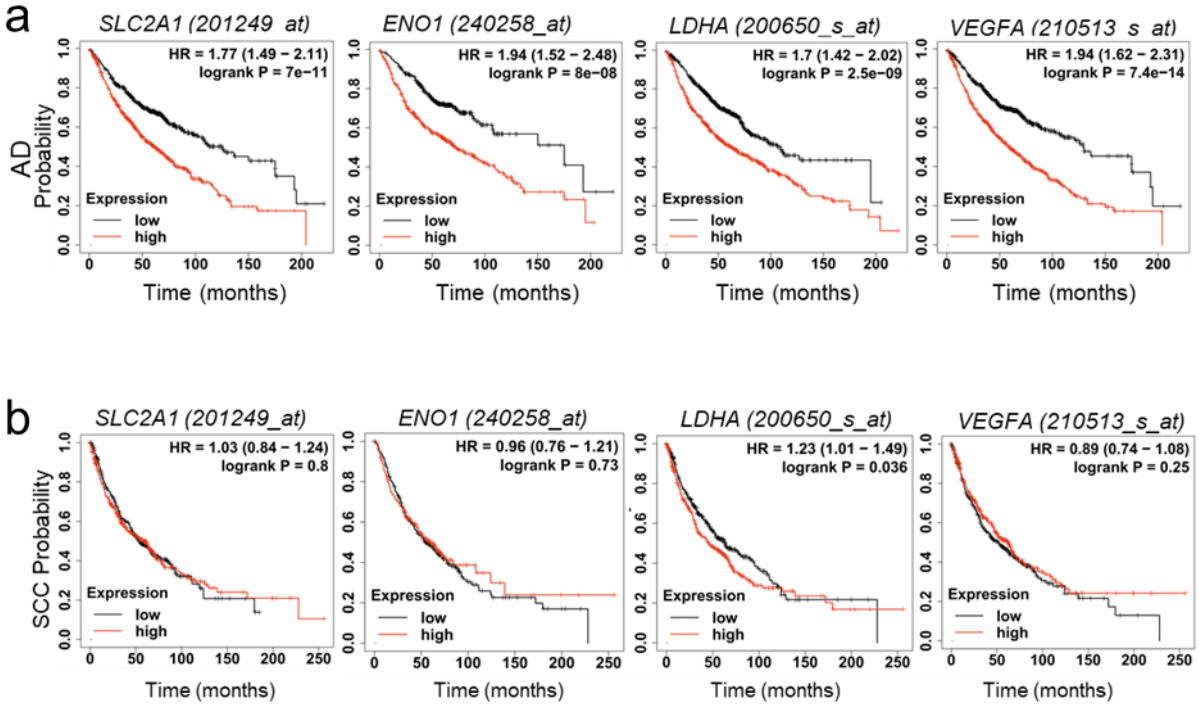

Figure 35. **glycolytic enzymes negatively correlated with ADs patients' survival.** (a) Overall survival (Kaplan-Meier plot) of lung adenocarcinoma patients expressing high versus low levels of RNF20/HIF1α-dependent target genes. (b) Overall survival (Kaplan-Meier plot) of lung squamous cell carcinoma (SCC) patients with high versus low expression levels of *SLC2A1*, *ENO1*, *LDHA*, and *VEGFA* (Győrffy, Surowiak et al. 2013).

4 DISCUSSION

4.1 Loss of *Rnf20* plays a key role in lung cancer progression

Lung cancer remains one of the leading causes of cancer deaths worldwide (Tao 2019), It is characterized by uncontrolled proliferation of abnormal cells in the lung, often driven by a combination of genetic mutations, environmental exposures, and lifestyle factors, with which tobacco smoking being the most significant risk factor (Prabavathy, Swarnalatha et al. 2018). Lung cancer is broadly classified into non-small cell lung cancer (NSCLC) and small cell lung cancer (SCLC), with NSCLC being more prevalent and further categorized into adenocarcinoma, squamous cell carcinoma, and large cell carcinoma (Adams, Stone et al. 2023).

Environmental factors consist of those in tobacco smoker or air pollution, generate carcinogens like reactive oxygen species (ROS) that damage DNA (Zhao, Ye et al. 2023). Given the lung's direct exposure to these agents, they are particularly susceptible to genotoxic insults, leading to mutations, chromosomal instability, and dysfunction of DNA repair pathways, all of which are key hallmarks of lung cancer. DNA damage is a central event in lung cancer initiation, particularly when it affected by tumor suppressor genes like *p53* (Spitz, Wei et al. 2003). The *p53* mutations are present in over 50% of NSCLC cases, especially in smokers, which impair *p53*'s ability to regulate cell cycle arrest, DNA repair, or apoptosis in response to damage (Mogi and Kuwano 2011, Gibbons, Byers et al. 2014). Moreover, *Rb1*, another tumor suppressor frequently inactivated in lung cancer, particularly in SCLC, regulates the G1/S cell cycle checkpoint by inhibiting E2F transcription factors. The simultaneous loss of *p53* and *Rb1* has been shown to induce SCLC-like tumors in mouse models (DuPage, Dooley et al. 2009). Suggesting their importance in preventing growth and transformation of cells.

RNF20 is a known E3 ubiquitin ligase that catalyze H2B monoubiquitylation, a histone modification essential for regulating transcription, chromatin remodeling, as well as DNA double-strand break (DSB) repair, including both non-homologous end joining (NHEJ) and homologous recombination (HRR) (So, Ramachandran et al. 2019, Tan, Sun et al. 2023). Disruption of H2Bub1 signaling compromises the efficiency of DNA

repair and leads to the accumulation of oncogenic mutations. In my study, I observed increased DNA damage and a markedly elevated incidence of lung tumors in RNF20 haploinsufficiency (*Rnf20+/-*) mice, highlighting the importance of RNF20 in maintaining genomic integrity. This was consistent with our previous data which showed that *p53* and *Rb1* expression were decreased upon *Rnf20* loss both *in vivo* and *in vitro*, suggesting that RNF20 loss contributes to DNA damage repair deficiency and impairs tumor suppressor pathways. Furthermore, I detected significantly lower RNF20 expression in both SCLC and ADs patient samples, which correlated with poor prognosis. Consistently, loss of RNF20 also significantly promoted cell proliferation, migration, and epithelial-mesenchymal transition (EMT), supporting the RNF20 loss plays role as a driver of lung tumor progression.

Despite RNF20's tumor suppressive role in lung cancer, its function appears to be context dependent. For example, RNF20 acts as a tumor suppressor in breast cancer (Duan, Huo et al. 2016) and colorectal cancer(Kosinsky, Zerche et al. 2021), yet has been reported to function as an oncogene in ovarian (Hooda, Novak et al. 2019) and prostate cancer(Jääskeläinen, Makkonen et al. 2012). These divergent roles may stem from tissue-specific expression, differences in chromatin context, or distinct interacting partners involved in gene regulation, DNA repair, or transcriptional control. In the context of lung cancer, our findings suggest that RNF20 loss promotes tumor cell growth and migration by impairing DNA repair and downregulating key tumor suppressors, such as *p53* and *Rb1*, indicating a lung tissue-specific tumor suppressive mechanism.

Interestingly, while RNF20 and RNF40 function together as a ubiquitin ligase complex (Foglizzo, Middleton et al. 2016), our data show a striking difference in their expression profiles in lung adenocarcinoma patients. RNF20 was significantly downregulated, whereas RNF40 expression was elevated, and high RNF40 expression was associated with poor prognosis. However, depletion of RNF40 had minimal impact on cell proliferation and migration, suggesting that RNF20 and RNF40 may have distinct and potentially independent functions in lung cancer. This functional divergence could reflect a compensatory mechanism, where increased RNF40 partially stabilizes the complex or acts in an RNF20-independent manner. Nonetheless, RNF20 is recognized as the catalytic core of the RNF20-RNF40 complex, while RNF40 primarily serves as a cofactor that enhances RNF20 activity and complex stability(Foglizzo, Middleton et

al. 2016). Therefore, RNF20 loss likely has a more profound impact on H2Bub1 and downstream tumor-suppressive pathways than RNF40 alterations. Another possible explanation lies in domain specificity. Although RNF20 and RNF40 both contain C-terminal RING domains required for E3 ligase activity, subtle difference exists in this highly conserved catalytic region(Foglizzo, Middleton et al. 2016). Given the critical role of the RING domain in recruiting E2 ubiquitin conjugates and promoting ubiquitin transfer, even minors in this region can substantially impair enzymatic efficiency, thereby affecting downstream transcriptional regulation.

4.2 HIF1α accumulation upon *Rnf20* loss involved in metabolic reprogramming

In this study, I found that the HIF1 pathway was enriched in KEGG analysis of genes upregulated upon Rnf20 loss. Although HIF1α protein levels increased following RNF20 depletion, HIF1α mRNA levels remained unchanged, suggesting that the stabilization of HIF1α may occur post-translationally. This observation led us to hypothesize that HIF1α degradation is impaired upon loss of RNF20. Normally, under normoxic conditions, HIF1α is tightly regulated through rapid degradation via the ubiquitin-proteasome pathway, primarily mediated by prolyl hydroxylase domain enzymes (PHDs). These enzymes hydroxylate specific proline residues on HIF1α, facilitating its recognition by the von Hippel-Lindau (VHL) complex, which then recruits an E3 ubiquitin ligase complex to mark HIF1α for proteasomal degradation(Herman, Latif et al. 1994). However, this degradation process is sensitive to environmental and intracellular stress. For example, hypoxia or dysregulation of PHD activity can lead to HIF1α stabilization and accumulation, promoting hypoxia-inducible gene expression. Another factor known to impair HIF1α degradation is reactive oxygen species (ROS). ROS can inhibit PHD enzymatic activity by oxidizing the iron center of their catalytic domain, thereby impairing their ability to hydroxylate HIF1α. Since DNA damage resulting from the loss of RNF20 may accompanied with the generation ROS, I initially speculated that the accumulation of HIF1α is a consequence of ROS. However, in my study, I did not observe elevated ROS levels in RNF20 haploinsufficiency cells, either in mitochondria or total cellular ROS, suggesting that HIF1α stabilization is not ROS-dependent in this context. Interestingly, I discovered a significant downregulation of RBX1 in *Rnf20+/-* cells. RBX1 is an essential component of the Cullin-RING E3 ligase (CRL) complex, which works with VHL to ubiquitinate HIF1α (Rowbotham, Enfield et

al.). During normoxia, the VHL complex, in association with CRL components like RBX1, mediates HIF1α ubiquitination and degradation. The suppression of RBX1 disrupts this degradation pathway, leading to inappropriate HIF1α stabilization and contributing to tumor progression. Consistent with this, my results showed that, RBX1 overexpression in *Rnf20+/-* MLE12 cells led to decreased HIF1α levels and significantly impaired cellular proliferation and migration, indicating that RBX1 mediates the degradation of HIF1α in an RNF20-dependent manner.

A major consequence of HIF1α activation in cancer is metabolic reprogramming, particularly the shift from oxidative phosphorylation (OXPHOS) to aerobic glycolysis, known as the Warburg effect. This adaptation allows tumor cells to rapidly produce ATP and biosynthetic intermediates to support their high proliferative demands, even in the presence of oxygen. In my model, RNF20 loss promoted glycolytic metabolism, with increased glycolytic flux and elevated levels of tricarboxylic acid (TCA) cycle intermediates. Additionally, I found that HIF1α transcriptionally activated multiple glycolytic enzymes, including SLC2A1, HK2, and LDHA, in *Rnf20* deficient cells. Notably, these metabolic changes were reversed upon HIF1α depletion, suggesting that HIF1α activation is required for the metabolic phenotype observed in *Rnf20+/-* cells. Suppression of HIF1α or inhibition of glycolysis reversed the enhanced proliferation and migratory capacity *in vitro* as well as tumor growth and metastasis *in vivo*, further supporting a direct link between RNF20 loss, HIF1α activity, and metabolic reprogramming.

Taken together, the increased DNA damage and activation of HIF1α, combined with insufficient p53 and Rb1 function, may help in explain the high incidence of cancerous lesions observed following Rnf20 loss. Interestingly, DNA damage in *Rnf20+/-* cells and tumors derived from these cells was significantly reduced when HIF1α was downregulated. During hypoxia, increased γH2AX levels contribute to the stability and nuclear accumulation of HIF1α, thereby promoting the activation of HIF1α/hypoxia signaling (Rezaeian, Li et al. 2017). This suggests a feedback mechanism between the loss of *Rnf20*, HIF1α activation, and the accumulation of γH2AX.

4.3 *Rnf20* loss induces RNA polymerase pause release at HIF1α-target genes and genes involved in EMT

Precise control of gene expression is essential for maintaining normal cellular growth, differentiation, and appropriate responses to environmental signals (Yonezawa, Higashi et al. 2011). Among the many regulatory layers, mRNA transcription plays a central role, directly influencing protein synthesis. This process comprises three main stages: initiation, elongation, and termination. Transcription begins when RNA polymerase II (Pol II) binds to the promoter region with the assistance of general transcription factors. Pol II then unwinds a small section of the DNA double helix, exposing the template strand. As it reads the DNA sequence in the 3' to 5' direction, Pol II synthesizes a complementary RNA strand until it passes a termination signal, after which the nascent mRNA is cleaved and released.

Beyond genetic mutations, transcriptional dysregulation is a key contributor to gene expression abnormalities and cancer progression (Hager, McNally et al. 2009). Pol II is the primary enzyme responsible for transcribing protein-coding genes in eukaryotic cells. A critical regulatory step in this process is Pol II pausing and release, which ensures that transcription proceeds only under the appropriate conditions. Pol II typically pauses shortly after initiation between 20 and 60 nucleotides downstream of the transcription start site, which representing a rate-limiting step for a large subset of genes, including approximately 30% of those in human embryonic stem cells (Lis 2007, Adelman and Lis 2012). RNF20, an E3 ubiquitin ligase, facilitates monoubiquitination of histone H2B (H2Bub1), which plays a key role in chromatin dynamics during transcription. H2Bub1 contributes to chromatin compaction, reinforcing Pol II pausing and preventing premature elongation (Liu, Kraus et al. 2015). Furthermore, H2Bub1 is essential for nucleosome reassembly during elongation (Osley, Fleming et al. 2006). The recruitment of the RNF20/RNF40 complex to Pol II is mediated by WAC, which directs H2B ubiquitination at actively transcribed genes (Zhang and Yu 2011). In my study, I observed a significant increase in Pol II release at upregulated genes in *Rnf20+/-* MLE12 cells, with minimal changes in downregulated or unchanged genes. Calculation of the pausing index (PI) further confirmed this finding, showing that genes with decreased PI upon RNF20 loss were significantly associated with glycolysis, cell cycle regulation, metabolism, and cytoskeleton organization. Moreover, I conducted

Pol II ChIP-qPCR targeting glycolytic genes *Slc2a1*, *Ldha*, and *Eno1* in both cultured cells and lung tissues. The data confirmed that loss of RNF20 leads to decreased Pol II pausing in both *in vitro* and *in vivo* models. Recent years, HIF1α is also believed to regulate genes via modulation of Pol II dynamics. It has been shown to recruit the CDK8-mediator complex to promote Pol II elongation (Galbraith, Allen et al. 2013). For example, a study in breast cancer is reported that Hif1α and TRIM28 cooperatively recruit DNA-PK, which phosphorylates TRIM28 at serine 824 (Yang, Lu et al. 2022), facilitating CDK9 recruitment. CDK9 then phosphorylates ser2 on the CTD of Pol II, promoting transcriptional elongation (Egloff 2021). Meanwhile, CDK9 also phosphorylates the negative elongation factor (NELF), enabling Pol II pause release (Laitem, Zaborowska et al. 2015). Consistent with these findings, the accumulation of HIF1α upon *Rnf20* loss accounts for the altered distribution of Pol II at a specific set of genes.

To further investigate the mechanism, I performed Pol II ChIP-seq in control, *Rnf20+/-*, and *Rnf20+/-* HIF1α knockdown MLE12 cells. I found that HIF1α depletion restored PI levels to those of control cells at HIF1α-bound genes, indicating that HIF1α is required for the enhanced Pol II pause release induced by RNF20 loss. Pol II CTD-phosphorylation provides additional insight into transcriptional dynamics. Phosphorylation at serine 5 (ser5), typically catalyzed by CDK7, marks transcription initiation and early elongation stages (Chlamydas, Holz et al. 2016). In contrast, serine2 phosphorylation (ser2) by CDK9 signifies active elongation and facilitates recruitment of elongation factors (Liu, Kraus et al. 2015, Ebmeier, Erickson et al. 2017). To confirm the roles of ser5 and ser2 phosphorylation in my model, I performed ChIP-qPCR using antibodies against Pol II ser2 and ser5. Upon loss of RNF20, I observed an increased Pol II ser2 occupancy across the gene bodies of *Slc2a1*, *Ldha*, and *Eno1*, consistent with increased transcriptional elongation. Conversely, Pol II ser5 enrichment at transcription start sites was reduced in *Rnf20+/-* cells, but both ser2 and ser5 levels were restored to baseline following *Hif1α* knockdown.

Together, these findings support a model in which RNF20 loss enhances Pol II pause release and elongation, particularly at glycolysis-related and HIF1α targets genes, through HIF1α-dependent activation of transcriptional machinery. These changes reflect a broader transcriptional reprogramming that may contribute to the metabolic shift and cancer progression observed in *Rnf20* deficient lung cancer cells.

4.4 H2Bub1 and H3K4me3 cross talk

H3K4 methylation is a well-established marker of active transcription, mediated by a group of histone methyltransferases (HMTs), most notably the SET1/COMPASS complex (Shilatifard 2012). Parallel to this, histone H2B monoubiquitination (H2Bub1) has been strongly linked to transcriptional activity (Marsh, Ma et al. 2020). Beyond its involvement in Pol II pause release, H2Bub1 is also known to promote post-transcriptional chromatin remodeling by loosening nucleosome structure, thereby increasing the accessibility of histone tails to modifying enzymes (Meas and Mao 2015). In fact, Previous studies in yeast have demonstrated that H2Bub1 is a prerequisite for H3K4 trimethylation, catalyzed by Set1 and Dot1 (Dover, Schneider et al. 2002). A mutation at lysine 123 on H2B, the conserved ubiquitination site, significantly suppresses H3K4 methylation demonstrating a functional link between these two modifications (Sun and Allis 2002). While the exact mechanisms by which H2Bub1 promotes H3K4 methylation remain incompletely understood, *in vitro* studies suggest that H2Bub1 influences nucleosome configuration, inhibiting chromatin compaction and enhancing the exposure of the H3 tail for methyltransferase activity (Fierz, Chatterjee et al. 2011). Moreover, the N-terminal region of the SET domain is essential for binding to Spp1, facilitating H2Bub1-dependent H3K4 methylation (Kim, Kim et al. 2013). Interestingly, in mammalian systems, Set1B has been shown to accumulate on chromatin under hypoxic conditions, where it is recruited by the HIF1α complex to the promoters of HIF1 target genes (Ortmann, Burrows et al. 2021). Suggesting that H3K4 methylation is upregulated during hypoxia to facilitate transcriptional activation of HIF1-responsive genes. These findings connect the HIF1α and H2Bub1-dependent H3K4 methylation together in transcription regulation.

In my study, I firstly observed increased expression of HIF1α target genes upon RNF20 loss, which was largely driven by enhanced Pol II pause release. However, whether this transcriptional upregulation also involves H2Bub1-regulated H3K4me3 remains unclear. To investigate this, I performed H3K4me3 ChIP-seq in *Rnf20+/-* and *Rnf20+/-Hif1α* knockdown MLE12 cells. Interestingly, *Hif1α* knockdown led to a global reduction in H3K4me3 levels, consistent with previous reports that link HIF1 signaling to H3K4 methylation. However, I did not observe significant changes in H3K4me3 enrichment at HIF1α-bound genes that were upregulated upon RNF20 loss. These results indicate

that H3K4me3 is not required for the increased transcription of these genes under *Rnf20* deficient conditions, indicating that, although H2Bub1 and H3K4me3 are functionally connected in many contexts, they can act independently, depending on gene-specific regulatory requirements. Supporting this notion, studies in *Schizosaccharomyces pombe* (fission yeast) have demonstrated that ubiquitination of H2B and methylation of H3 exhibit considerable functional divergence (Tanny, Erdjument-Bromage et al. 2007). To date, there is no evidence that RNF20 itself directly catalyzes histone methylation. Instead, RNF20 exerts indirect control over histone modification. My findings support this view and further suggest that the activation of HIF1α targets upon RNF20 loss is primarily mediated by Pol II dynamics, rather than H3K4me3-dependent chromatin remodeling.

5 SUMMARY

During my PhD research, I investigated the role of RNF20 loss in the progression of lung cancer. Previous study showed *Rnf20* haploinsufficiency in mice led to a marked increase in tumor incidence, which was accompanied by elevated DNA damage and a reduction in the tumor suppressors *p53* and *Rb1*. These findings were further corroborated *in vitro* using control and *Rnf20+/-* lung epithelial cells, where transcriptomic analysis revealed significant upregulation of genes involved in cell migration, extracellular matrix organization, metabolic pathways, and the HIF-1 signaling pathway following RNF20 loss.

To explore the impact of RNF20 on cellular metabolism, I conducted metabolomic assays, which showed that *Rnf20* deficiency enhances glycolytic capacity and increases TCA cycle metabolite levels. Integrating RNA-seq with metabolomic profiling, I found that the genes upregulated in *Rnf20+/-* cells were closely associated with glycolytic metabolism. Importantly, through *Hif1α* knockdown and glycolysis inhibition, I demonstrated that HIF1α mediates both metabolic reprogramming and tumor-promoting effects in the context of RNF20 loss. Mechanistically, Pol II ChIP-seq revealed that RNF20 loss promotes RNA polymerase release at HIF1α target genes and genes involved in EMT, contributing to transcriptional activation. In contrast, ChIP-seq for H2Bub1 and H3K4me3 showed that genes downregulated upon RNF20 loss were more closely associated with loss of histone ubiquitination rather than changes in Pol II dynamics, suggesting distinct regulatory mechanisms. Further analysis uncovered that the accumulation of HIF1α upon RNF20 loss is likely due to the downregulation of RBX1, a key component of the E3 ubiquitin ligase complex responsible for HIF1α degradation. Additionally, I observed functional divergence between RNF20 and RNF40, despite their role in the same ubiquitin ligase complex, indicating distinct roles in lung cancer progression.

In summary, my study demonstrated that RNF20 acts as a tumor suppressor in lung cancer, and its expression is significantly reduced in patient samples, correlating with poor clinical outcomes. RNF20 loss drives lung tumor progression through epigenetic deregulation of metabolic genes, particularly via HIF1α-mediated transcriptional and metabolic reprogramming.

Despite these findings, limitations remain that warrant further investigation. First, the precise upstream mechanisms leading to RNF20 downregulation in lung cancer remain undefined. While environmental carcinogens are hypothesized contributors, direct mechanistic evidence is lacking. Second, although glycolysis and parts of the TCA cycle were examined, other metabolic pathways such as lipid metabolism or amino acid biosynthesis were not addressed and may also contribute to tumor progression following RNF20 depletion. Third, the role of RBX1 in mediating HIF1α accumulation upon RNF20 loss remains incompletely understood, particularly regarding whether its downregulation is a direct epigenetic effect or part of broader disruption of the VHL complex. Last, while the functional divergence between RNF20 and RNF40 was observed, the mechanistic basis for their differential roles remains to be elucidated.

Addressing these limitations in future work will be essential to fully define RNF20’s role in lung cancer and to harness this knowledge for therapeutic benefits.

6 REFERENCES

Adams, S. J., Stone, E., Baldwin, D. R., Vliegenthart, R., Lee, P., & Fintelmann, F. J. (2023). Lung cancer screening. *The Lancet, 401*(10374), 390-408.

Adelman, K., & Lis, J. T. (2012). Promoter-proximal pausing of RNA polymerase II: emerging roles in metazoans. *Nature Reviews Genetics, 13*(10), 720-731.

Aggarwal, C. (2014). Targeted therapy for lung cancer: present and future. *Ann Palliat Med, 3*(3), 229-235.

Aiello, N. M., Brabletz, T., Kang, Y., Nieto, M. A., Weinberg, R. A., & Stanger, B. Z. (2017). Upholding a role for EMT in pancreatic cancer metastasis. *Nature, 547*(7661), E7-E8.

Aird, K. M., & Zhang, R. J. C. l. (2015). Nucleotide metabolism, oncogene-induced senescence and cancer. *Cancer letters, 356*(2), 204-210.

Anderson, N. M., Mucka, P., Kern, J. G., & Feng, H. (2018). The emerging role and targetability of the TCA cycle in cancer metabolism. *Protein & cell, 9*(2), 216-237.

Andrysik, Z., Bender, H., Galbraith, M. D., & Espinosa, J. M. (2021). Multi-omics analysis reveals contextual tumor suppressive and oncogenic gene modules within the acute hypoxic response. *Nature Communications, 12*(1), 1375.

Andrysik, Z., Bender, H., Galbraith, M. D., & Espinosa, J. M. J. N. c. (2021). Multi-omics analysis reveals contextual tumor suppressive and oncogenic gene modules within the acute hypoxic response. *Nature communications, 12*(1), 1375.

Appella, E., & Anderson, C. W. (2001). Post‐translational modifications and activation of p53 by genotoxic stresses. *European journal of biochemistry, 268*(10), 2764-2772.

Baba, Y., Nosho, K., Shima, K., Irahara, N., Chan, A. T., Meyerhardt, J. A., . . . Ogino, S. J. T. A. j. o. p. (2010). HIF1A overexpression is associated with poor prognosis in a cohort of 731 colorectal cancers. *The American journal of pathology, 176*(5), 2292-2301.

Babicki, S., Arndt, D., Marcu, A., Liang, Y., Grant, J. R., Maciejewski, A., & Wishart, D. S. (2016). Heatmapper: web-enabled heat mapping for all. *Nucleic Acids Res, 44*(W1), W147-153. doi:10.1093/nar/gkw419

Bachman, K. E., Herman, J. G., Corn, P. G., Merlo, A., Costello, J. F., Cavenee, W. K., . . . Graff, J. R. (1999). Methylation-associated silencing of the tissue inhibitor of metalloproteinase-3 gene suggests a suppressor role in kidney, brain, and other human cancers. *Cancer research, 59*(4), 798-802.

Bade, B. C., & Cruz, C. S. D. (2020). Lung cancer 2020: epidemiology, etiology, and prevention. *Clinics in chest medicine, 41*(1), 1-24.

Barber, T. D., McManus, K., Yuen, K. W., Reis, M., Parmigiani, G., Shen, D., . . . Markowitz, S. (2008). Chromatid cohesion defects may underlie chromosome instability in human colorectal cancers. *Proceedings of the National Academy of Sciences, 105*(9), 3443-3448.

Barnett, D. W., Garrison, E. K., Quinlan, A. R., Stromberg, M. P., & Marth, G. T. (2011). BamTools: a C++ API and toolkit for analyzing and managing BAM files. *Bioinformatics, 27*(12), 1691-1692.

Belaidi, E., Morand, J., Gras, E., Pépin, J. L., & Godin-Ribuot, D. (2016). Targeting the ROS-HIF-1-endothelin axis as a therapeutic approach for the treatment of obstructive sleep apnea-related cardiovascular complications. *Pharmacology & Therapeutics,* 168, 1-11.

Benayoun, B. A., Pollina, E. A., Ucar, D., Mahmoudi, S., Karra, K., Wong, E. D., . . . Mancini, E. (2014). H3K4me3 breadth is linked to cell identity and transcriptional consistency. *Cell, 158*(3), 673-688.

Berasain, C., Castillo, J., Perugorria, M., Latasa, M., Prieto, J., & Avila, M. (2009). Inflammation and liver cancer: new molecular links. *Annals of the New York Academy of Sciences, 1155*(1), 206-221.

Bin, P., Wang, C., Zhang, H., Yan, Y., & Ren, W. (2024). Targeting methionine metabolism in cancer: opportunities and challenges. *Trends in Pharmacological Sciences,* 45(5), 395-405.

Blank, M., Tang, Y., Yamashita, M., Burkett, S. S., Cheng, S. Y., & Zhang, Y. E. (2012). A tumor suppressor function of Smurf2 associated with controlling chromatin landscape and genome stability through RNF20. *Nature medicine, 18*(2), 227-234.

Bogenrieder, T., & Herlyn, M. (2003). Axis of evil: molecular mechanisms of cancer metastasis. *Oncogene, 22*(42), 6524-6536.

Bolger, A. M., Lohse, M., & Usadel, B. (2014). Trimmomatic: a flexible trimmer for Illumina sequence data. *Bioinformatics, 30*(15), 2114-2120. doi:10.1093/bioinformatics/btu170

Brabletz, T., Kalluri, R., Nieto, M. A., & Weinberg, R. A. (2018). EMT in cancer. *Nature Reviews Cancer, 18*(2), 128-134.

Büchel, G., Carstensen, A., Mak, K.-Y., Roeschert, I., Leen, E., Sumara, O., . . . Baluapuri, A. (2017). Association with Aurora-A controls N-MYC-dependent promoter escape and pause release of RNA polymerase II during the cell cycle. *Cell reports, 21*(12), 3483-3497.

Byles, V., Zhu, L., Lovaas, J., Chmilewski, L., Wang, J., Faller, D., & Dai, Y. (2012). SIRT1 induces EMT by cooperating with EMT transcription factors and enhances prostate cancer cell migration and metastasis. *Oncogene, 31*(43), 4619-4629.

Cairns, R. A. (2015). Drivers of the Warburg phenotype. *The Cancer Journal, 21*(2), 56-61.

Castellano, B. M., Thelen, A. M., Moldavski, O., Feltes, M., Van Der Welle, R. E., Mydock-McGrane, L., . . . Louie, S. M. (2017). Lysosomal cholesterol activates mTORC1 via an SLC38A9–Niemann-Pick C1 signaling complex. *Science, 355*(6331), 1306-1311.

Cenigaonandia-Campillo, A., Serna-Blasco, R., Gómez-Ocabo, L., Solanes-Casado, S., Baños-Herraiz, N., Del Puerto-Nevado, L., . . . Aguilera, Ó. (2021). Vitamin C activates pyruvate dehydrogenase (PDH) targeting the mitochondrial tricarboxylic acid (TCA) cycle in hypoxic KRAS mutant colon cancer. *Theranostics, 11*(8), 3595.

Chang, T.-C., Wentzel, E. A., Kent, O. A., Ramachandran, K., Mullendore, M., Lee, K. H., . . . Lowenstein, C. J. (2007). Transactivation of miR-34a by p53 broadly influences gene expression and promotes apoptosis. *Molecular cell, 26*(5), 745-752.

Chao, Y., & Wells, A. (2010). E-cadherin re-expression affects the growth and survival of breast cancer cells in metastatic colonization of the liver. *Cancer research, 70*(8_Supplement), 2336-2336.

Chen, J. (2016). The cell-cycle arrest and apoptotic functions of p53 in tumor initiation and progression. *Cold Spring Harbor perspectives in medicine, 6*(3), a026104.

Chen, Y.-C., Sosnoski, D. M., & Mastro, A. M. (2010). Breast cancer metastasis to the bone: mechanisms of bone loss. *Breast cancer research, 12*, 1-11.

Cheng, J., Yan, J., Liu, Y., Shi, J., Wang, H., Zhou, H., ... & Jiang, P. (2023). Cancer-cell-derived fumarate suppresses the anti-tumor capacity of CD8+ T cells in the tumor microenvironment. *Cell metabolism,* 35(6), 961-978.

Cheung, P., & Lau, P. (2005). Epigenetic regulation by histone methylation and histone variants. *Molecular endocrinology, 19*(3), 563-573.

Chlamydas, S., Holz, H., Samata, M., Chelmicki, T., Georgiev, P., Pelechano, V., . . . Cadete, F. T. (2016). Functional interplay between MSL1 and CDK7 controls RNA polymerase II Ser5 phosphorylation. *Nature structural & molecular biology, 23*(6), 580-589.

Chushi, L., Wei, W., Kangkang, X., Yongzeng, F., Ning, X., & Xiaolei, C. (2016). HMGCR is up-regulated in gastric cancer and promotes the growth and migration of the cancer cells. *Gene, 587*(1), 42-47.

Cifuentes, M., García, M. A., Arrabal, P. M., Martínez, F., Yañez, M. J., Jara, N., ... & Nualart, F. (2011). Insulin regulates GLUT1‐mediated glucose transport in MG‐63 human osteosarcoma cells. *Journal of Cellular Physiology,* 226(6), 1425-1432.

Cimprich, K. A., & Cortez, D. (2008). ATR: an essential regulator of genome integrity. *Nature reviews Molecular cell biology, 9*(8), 616-627.

Clair, S. S., Giono, L., Varmeh-Ziaie, S., Resnick-Silverman, L., Liu, W.-j., Padi, A., . . . Manfredi, J. J. (2004). DNA damage-induced downregulation of Cdc25C is mediated by p53 via two independent

mechanisms: one involves direct binding to the cdc25C promoter. *Molecular cell, 16*(5), 725-736.
Cohen, G. M. (1997). Caspases: the executioners of apoptosis. *Biochemical Journal, 326*(1), 1-16.
Cole, A. J., Dickson, K.-A., Clifton-Bligh, R., & Marsh, D. J. (2018). Targeting the E3 ubiquitin ligase RNF20 in ovarian cancer. *Cancer research, 78*(13_Supplement), 3538-3538.
Cooper, S., & Spiro, S. G. (2006). Small cell lung cancer: treatment review. *Respirology, 11*(3), 241-248.
Coussens, L. M., & Werb, Z. (2002). Inflammation and cancer. *Nature, 420*(6917), 860-867.
da Cunha Santos, G., Shepherd, F. A., & Tsao, M. S. (2011). EGFR mutations and lung cancer. *Annual Review of Pathology: Mechanisms of Disease, 6*(1), 49-69.
Dang, C. V., Le, A., & Gao, P. (2009). MYC-induced cancer cell energy metabolism and therapeutic opportunities. *Clinical cancer research, 15*(21), 6479-6483.
Davalos, V., & Esteller, M. J. C. a. c. j. f. c. (2023). Cancer epigenetics in clinical practice. *CA: a cancer journal for clinicians, 73*(4), 376-424.
Davidson, S. M., Papagiannakopoulos, T., Olenchock, B. A., Heyman, J. E., Keibler, M. A., Luengo, A., . . . Pierce, K. A. (2016). Environment impacts the metabolic dependencies of Ras-driven non-small cell lung cancer. *Cell metabolism, 23*(3), 517-528.
de Sá Junior, P. L., Câmara, D. A. D., Porcacchia, A. S., Fonseca, P. M. M., Jorge, S. D., Araldi, R. P., . . . longevity, c. (2017). The roles of ROS in cancer heterogeneity and therapy. *Oxidative medicine and cellular longevity, 2017*(1), 2467940.
de Souza, C. R. T., Leal, M. F., Calcagno, D. Q., Costa Sozinho, E. K., Borges, B. d. N., Montenegro, R. C., . . . Assumpção, P. P. J. P. o. (2013). MYC deregulation in gastric cancer and its clinicopathological implications. *PloS one*, *8*(5), e64420.
Debernardi, C., Libera, L., Berrino, E., Sahnane, N., Chiaravalli, A. M., Laudi, C., . . . Venesio, T. J. C. E. (2021). Evaluation of global and intragenic hypomethylation in colorectal adenomas improves patient stratification and colorectal cancer risk prediction. *Clinical Epigenetics, 13*(1), 154.
Deng, Z., Ai, H., Sun, M., Tong, Z., Du, Y., Qu, Q., . . . Shi, Q. (2023). Mechanistic insights into nucleosomal H2B monoubiquitylation mediated by yeast Bre1-Rad6 and its human homolog RNF20/RNF40-hRAD6A. *Molecular cell, 83*(17), 3080-3094. e3014.
Denko, N. C. J. N. R. C. (2008). Hypoxia, HIF1 and glucose metabolism in the solid tumour. *Nature Reviews Cancer, 8*(9), 705-713.
Dobin, A., Davis, C. A., Schlesinger, F., Drenkow, J., Zaleski, C., Jha, S., . . . Gingeras, T. R. (2013). STAR: ultrafast universal RNA-seq aligner. *Bioinformatics, 29*(1), 15-21. doi:10.1093/bioinformatics/bts635
Donato, E., Croci, O., Sabo, A., Muller, H., Morelli, M., Pelizzola, M., & Campaner, S. (2017). Compensatory RNA polymerase 2 loading determines the efficacy and transcriptional selectivity of JQ1 in Myc-driven tumors. *Leukemia, 31*(2), 479-490.
Donehower, L. A., Harvey, M., Slagle, B. L., McArthur, M. J., Montgomery Jr, C. A., Butel, J. S., & Bradley, A. (1992). Mice deficient for p53 are developmentally normal but susceptible to spontaneous tumours. *Nature, 356*(6366), 215-221.
Dover, J., Schneider, J., Tawiah-Boateng, M. A., Wood, A., Dean, K., Johnston, M., & Shilatifard, A. J. J. o. B. C. (2002). Methylation of histone H3 by COMPASS requires ubiquitination of histone H2B by Rad6. *Journal of Biological Chemistry, 277*(32), 28368-28371.
Duan, Y., Huo, D., Gao, J., Wu, H., Ye, Z., Liu, Z., . . . Wang, Y. (2016). Ubiquitin ligase RNF20/40 facilitates spindle assembly and promotes breast carcinogenesis through stabilizing motor protein Eg5. *Nature Communications, 7*(1), 12648.
DuPage, M., Dooley, A. L., & Jacks, T. (2009). Conditional mouse lung cancer models using adenoviral or lentiviral delivery of Cre recombinase. *Nature protocols, 4*(7), 1064-1072.
Ebmeier, C. C., Erickson, B., Allen, B. L., Allen, M. A., Kim, H., Fong, N., . . . Dowell, R. D. (2017). Human TFIIH kinase CDK7 regulates transcription-associated chromatin modifications. *Cell reports, 20*(5), 1173-1186.

Ebright, R. Y., Zachariah, M. A., Micalizzi, D. S., Wittner, B. S., Niederhoffer, K. L., Nieman, L. T., . . . Shaw, B. J. N. c. (2020). HIF1A signaling selectively supports proliferation of breast cancer in the brain. *Nature communications*, *11*(1), 6311.

Egloff, S. (2021). CDK9 keeps RNA polymerase II on track. *Cellular and Molecular Life Sciences, 78*(14), 5543-5567.

Engeland, K. (2022). Cell cycle regulation: p53-p21-RB signaling. *Cell Death & Differentiation, 29*(5), 946-960.

Ewels, P., Magnusson, M., Lundin, S., & Kaller, M. (2016). MultiQC: summarize analysis results for multiple tools and samples in a single report. *Bioinformatics, 32*(19), 3047-3048. doi:10.1093/bioinformatics/btw354

Falck, J., Mailand, N., Syljuåsen, R. G., Bartek, J., & Lukas, J. (2001). The ATM–Chk2–Cdc25A checkpoint pathway guards against radioresistant DNA synthesis. *Nature, 410*(6830), 842-847.

Fatma, H., Maurya, S. K., & Siddique, H. R. (2022). *Epigenetic modifications of c-MYC: Role in cancer cell reprogramming, progression and chemoresistance. Seminars in cancer biology* (Vol. 83, pp. 166-176).

Faubert, B., Boily, G., Izreig, S., Griss, T., Samborska, B., Dong, Z., . . . Viollet, B. J. C. m. (2013). AMPK is a negative regulator of the Warburg effect and suppresses tumor growth in vivo. *Cell metabolism*, *17*(1), 113-124.

Fazzari, M. J., & Greally, J. M. (2004). Epigenomics: beyond CpG islands. *Nature Reviews Genetics, 5*(6), 446-455.

Ferone, G., Lee, M. C., Sage, J., & Berns, A. (2020). Cells of origin of lung cancers: lessons from mouse studies. *Genes & development, 34*(15-16), 1017-1032.

Ferrer, I., Zugazagoitia, J., Herbertz, S., John, W., Paz-Ares, L., & Schmid-Bindert, G. (2018). KRAS-Mutant non-small cell lung cancer: From biology to therapy. *Lung cancer, 124*, 53-64.

Ferrigno, D., Buccheri, G., & Giordano, C. (2003). Neuron-specific enolase is an effective tumour marker in non-small cell lung cancer (NSCLC). *Lung cancer, 41*(3), 311-320.

Fidler, I. J., & Poste, G. (2008). The “seed and soil” hypothesis revisited. *The lancet oncology, 9*(8), 808.

Fierz, B., Chatterjee, C., McGinty, R. K., Bar-Dagan, M., Raleigh, D. P., & Muir, T. W. J. N. c. b. (2011). Histone H2B ubiquitylation disrupts local and higher-order chromatin compaction. *Nature chemical biology,7*(2), 113-119.

Foglizzo, M., Middleton, A. J., & Day, C. L. (2016). Structure and function of the RING domains of RNF20 and RNF40, dimeric E3 ligases that monoubiquitylate histone H2B. *Journal of molecular biology, 428*(20), 4073-4086.

Fujinaga, K., Irwin, D., Huang, Y., Taube, R., Kurosu, T., & Peterlin, B. M. (2004). Dynamics of human immunodeficiency virus transcription: P-TEFb phosphorylates RD and dissociates negative effectors from the transactivation response element. *Molecular and cellular biology, 24*(2), 787-795.

Fulda, S., & Debatin, K.-M. (2006). Extrinsic versus intrinsic apoptosis pathways in anticancer chemotherapy. *Oncogene, 25*(34), 4798-4811.

Gadgeel, S. M., Ramalingam, S. S., & Kalemkerian, G. P. (2012). Treatment of lung cancer. *Radiologic Clinics, 50*(5), 961-974.

Galbraith, M. D., Allen, M. A., Bensard, C. L., Wang, X., Schwinn, M. K., Qin, B., . . . Dowell, R. D. (2013). HIF1A employs CDK8-mediator to stimulate RNAPII elongation in response to hypoxia. *Cell, 153*(6), 1327-1339.

García-Carpizo, V., Sarmentero, J., Han, B., Graña, O., Ruiz-Llorente, S., Pisano, D. G., . . . Barrero, M. J. J. S. R. (2016). NSD2 contributes to oncogenic RAS-driven transcription in lung cancer cells through long-range epigenetic activation. *Scientific reports, 6*(1), 32952.

Gibbons, D. L., Byers, L. A., & Kurie, J. M. (2014). Smoking, p53 mutation, and lung cancer. *Molecular cancer research, 12*(1), 3-13.

Gottschling, S., Jauch, A., Kuner, R., Herpel, E., Mueller-Decker, K., Schnabel, P. A., . . . Bender, C. (2012). Establishment and comparative characterization of novel squamous cell non-small cell lung cancer cell lines and their corresponding tumor tissue. *Lung cancer, 75*(1), 45-57.

Greer, E. L., & Shi, Y. (2012). Histone methylation: a dynamic mark in health, disease and inheritance. *Nature Reviews Genetics, 13*(5), 343-357.

Grote, H. J., Schmiemann, V., Geddert, H., Bocking, A., Kappes, R., Gabbert, H. E., & Sarbia, M. (2006). Methylation of RAS association domain family protein 1A as a biomarker of lung cancer. *Cancer Cytopathology: Interdisciplinary International Journal of the American Cancer Society, 108*(2), 129-134.

Grunnet, M., & Sorensen, J. (2012). Carcinoembryonic antigen (CEA) as tumor marker in lung cancer. *Lung cancer, 76*(2), 138-143.

Guo, L., Liang, J., Dai, W., Li, J., Si, Y., Ren, W., . . . Chen, D. (2022). PD-1/L1 with or without CTLA-4 inhibitors versus chemotherapy in advanced non-small cell lung cancer. *Cancer control, 29*, 10732748221107590.

Győrffy, B., Surowiak, P., Budczies, J., & Lánczky, A. (2013). Online survival analysis software to assess the prognostic value of biomarkers using transcriptomic data in non-small-cell lung cancer. *PloS one, 8*(12), e82241.

Győrffy, B., Surowiak, P., Budczies, J., & Lánczky, A. J. P. o. (2013). Online survival analysis software to assess the prognostic value of biomarkers using transcriptomic data in non-small-cell lung cancer. *PloS one*, *8*(12), e82241.

Hager, G. L., McNally, J. G., & Misteli, T. (2009). Transcription dynamics. *Molecular cell, 35*(6), 741-753.

Hainaut, P., & Pfeifer, G. P. (2001). Patterns of p53 G⟶ T transversions in lung cancers reflect the primary mutagenic signature of DNA-damage by tobacco smoke. *Carcinogenesis, 22*(3), 367-374.

Hanahan, D., & Weinberg, R. A. (2011). Hallmarks of cancer: the next generation. *Cell, 144*(5), 646-674. doi:10.1016/j.cell.2011.02.013

Hansen, K. H., Bracken, A. P., Pasini, D., Dietrich, N., Gehani, S. S., Monrad, A., . . . Helin, K. (2008). A model for transmission of the H3K27me3 epigenetic mark. *Nature cell biology, 10*(11), 1291-1300.

Harami-Papp, H., Pongor, L. S., Munkácsy, G., Horváth, G., Nagy, Á. M., Ambrus, A., . . . Győrffy, B. J. O. (2016). TP53 mutation hits energy metabolism and increases glycolysis in breast cancer. *Oncotarget*, *7*(41), 67183.

Harris, C. (1996). The 1995 Walter Hubert Lecture--molecular epidemiology of human cancer: insights from the mutational analysis of the p53 tumour-suppressor gene. *British journal of cancer, 73*(3), 261.

Heinz, S., Benner, C., Spann, N., Bertolino, E., Lin, Y. C., Laslo, P., . . . Glass, C. K. (2010). Simple combinations of lineage-determining transcription factors prime cis-regulatory elements required for macrophage and B cell identities. *Molecular cell, 38*(4), 576-589. doi:10.1016/j.molcel.2010.05.004

Herman, J. G., Latif, F., Weng, Y., Lerman, M. I., Zbar, B., Liu, S., . . . Linehan, W. M. (1994). Silencing of the VHL tumor-suppressor gene by DNA methylation in renal carcinoma. *Proceedings of the National Academy of Sciences, 91*(21), 9700-9704.

Hirschhaeuser, F., Sattler, U. G., & Mueller-Klieser, W. J. C. r. (2011). Lactate: a metabolic key player in cancer. *Cancer research, 71*(22), 6921-6925.

Hooda, J., Novak, M., Salomon, M. P., Matsuba, C., Ramos, R. I., MacDuffie, E., . . . Parkash, V. (2019). Early loss of histone H2B monoubiquitylation alters chromatin accessibility and activates key immune pathways that facilitate progression of ovarian cancer. *Cancer research, 79*(4), 760-772.

Hoshino, A., Costa-Silva, B., Shen, T.-L., Rodrigues, G., Hashimoto, A., Tesic Mark, M., . . . Ceder, S. (2015). Tumour exosome integrins determine organotropic metastasis. *Nature, 527*(7578), 329-335.

Hu, M., Chen, X., Ma, L., Ma, Y., Li, Y., Song, H., . . . Jiang, Y. J. J. o. C. (2019). AMPK inhibition suppresses the malignant phenotype of pancreatic cancer cells in part by attenuating aerobic glycolysis. *Journal of Cancer*, *10*(8), 1870.

Hu, Z., Wei, F., Su, Y., Wang, Y., Shen, Y., Fang, Y., . . . therapy, t. (2023). Histone deacetylase inhibitors promote breast cancer metastasis by elevating NEDD9 expression. *Signal transduction and targeted therapy*, *8*(1), 11.

Huang, B., Eberstadt, M., Olejniczak, E. T., Meadows, R. P., & Fesik, S. W. (1996). NMR structure and mutagenesis of the Fas (APO-1/CD95) death domain. *Nature, 384*(6610), 638-641.

Huang da, W., Sherman, B. T., & Lempicki, R. A. (2009). Systematic and integrative analysis of large gene lists using DAVID bioinformatics resources. *Nat Protoc, 4*(1), 44-57. doi:10.1038/nprot.2008.211

Igolkina, A. A., Zinkevich, A., Karandasheva, K. O., Popov, A. A., Selifanova, M. V., Nikolaeva, D., . . . Buzdin, A. (2019). H3K4me3, H3K9ac, H3K27ac, H3K27me3 and H3K9me3 histone tags suggest distinct regulatory evolution of open and condensed chromatin landmarks. *Cells, 8*(9), 1034.

Jääskeläinen, T., Makkonen, H., Visakorpi, T., Kim, J., Roeder, R. G., & Palvimo, J. J. (2012). Histone H2B ubiquitin ligases RNF20 and RNF40 in androgen signaling and prostate cancer cell growth. *Molecular and Cellular Endocrinology, 350*(1), 87-98.

Jang, M. K., Mochizuki, K., Zhou, M., Jeong, H.-S., Brady, J. N., & Ozato, K. (2005). The bromodomain protein Brd4 is a positive regulatory component of P-TEFb and stimulates RNA polymerase II-dependent transcription. *Molecular cell, 19*(4), 523-534.

Jaroenlapnopparat, A., Bhatia, K., & Coban, S. (2022). Inflammation and gastric cancer. *Diseases, 10*(3), 35.

Jaspers, J. E., Khan, J. F., Godfrey, W. D., Lopez, A. V., Ciampricotti, M., Rudin, C. M., & Brentjens, R. J. (2023). IL-18–secreting CAR T cells targeting DLL3 are highly effective in small cell lung cancer models. *The Journal of Clinical Investigation, 133*(9).

Jeon, Y. G., Lee, J. H., Ji, Y., Sohn, J. H., Lee, D., Kim, D. W., . . . Seong, J. K. (2020). RNF20 functions as a transcriptional coactivator for PPARγ by promoting NCoR1 degradation in adipocytes. *Diabetes, 69*(1), 20-34.

Jeon, Y. G., Nahmgoong, H., Oh, J., Lee, D., Kim, D. W., Kim, J. E., . . . Kim, S. M. (2024). Ubiquitin ligase RNF20 coordinates sequential adipose thermogenesis with brown and beige fat-specific substrates. *Nature Communications, 15*(1), 940.

Jeong, S.-Y., & Seol, D.-W. (2008). The role of mitochondria in apoptosis. *BMB reports, 41*(1), 11-22.

Kargbo, R. B. (2019). Inhibition of ACSS2 for treatment of cancer and neuropsychiatric diseases. *ACS Medicinal Chemistry Letters,* 10(8), 1100-1101.

Kasper, D., Fauci, A., Hauser, S., Longo, D., Jameson, J., & Loscalzo, J. (2015). *Harrison's principles of internal medicine, 19e* (Vol. 1): Mcgraw-hill New York, NY, USA:.

Keerthana, C. K., Rayginia, T. P., Shifana, S. C., Anto, N. P., Kalimuthu, K., Isakov, N., & Anto, R. J. J. F. i. i. (2023). The role of AMPK in cancer metabolism and its impact on the immunomodulation of the tumor microenvironment. *Frontiers in immunology, 14*, 1114582.

Kim, J., Kim, J.-A., McGinty, R. K., Nguyen, U. T., Muir, T. W., Allis, C. D., & Roeder, R. G. J. M. c. (2013). The n-SET domain of Set1 regulates H2B ubiquitylation-dependent H3K4 methylation. *Molecular cell, 49*(6), 1121-1133.

Kim, J. H., Kim, H. S., Kim, B. J., Han, B., Choi, D. R., & Kwon, J. H. (2018). Prognostic impact of TTF-1 expression in non-squamous non-small-cell lung cancer: a meta-analysis. *Journal of Cancer, 9*(22), 4279.

Kim, L. C., & Simon, M. C. (2022). Hypoxia-Inducible Factors in Cancer. *Cancer Res, 82*(2), 195-196. doi:10.1158/0008-5472.CAN-21-3780

Klebe, S., Leigh, J., Henderson, D. W., & Nurminen, M. (2020). Asbestos, smoking and lung cancer: an update. *International Journal of Environmental Research and Public Health, 17*(1), 258.

Kosinsky, R. L., Chua, R. L., Qui, M., Saul, D., Mehlich, D., Ströbel, P., . . . Johnsen, S. A. (2019). Loss of RNF40 decreases NF-κB activity in colorectal cancer cells and reduces colitis burden in mice. *Journal of Crohn's and Colitis, 13*(3), 362-373.

Kosinsky, R. L., Zerche, M., Kutschat, A. P., Nair, A., Ye, Z., Saul, D., . . . Paglilla, N. (2021). RNF20 and RNF40 regulate vitamin D receptor-dependent signaling in inflammatory bowel disease. *Cell Death & Differentiation, 28*(11), 3161-3175.

Kostaki, M., Manona, A. D., Stavraka, I., Korkolopoulou, P., Levidou, G., Trigka, E. A., . . . Katsambas, A. J. E. d. (2014). High‐frequency p16 INK 4A promoter methylation is associated with histone methyltransferase SETDB 1 expression in sporadic cutaneous melanoma. *Experimental dermatology, 23*(5), 332-338.

Kouzarides, T. (2002). Histone methylation in transcriptional control. *Current opinion in genetics & development, 12*(2), 198-209.

Krysztofiak, A., Szymonowicz, K., Hlouschek, J., Xiang, K., Waterkamp, C., Larafa, S., . . . Matschke, V. (2021). Metabolism of cancer cells commonly responds to irradiation by a transient early mitochondrial shutdown. *IScience, 24*(11).

Kumar, S., Basu, M., & Ghosh, M. K. (2024). E3 ubiquitin ligases and deubiquitinases in colorectal cancer: Emerging molecular insights and therapeutic opportunities. *Biochimica et Biophysica Acta (BBA)-Molecular Cell Research*, 119827.

Kuzu, O. F., Noory, M. A., & Robertson, G. P. (2016). The role of cholesterol in cancer. *Cancer research, 76*(8), 2063-2070.

Kwon, M., Park, K., Hyun, K., Lee, J.-H., Zhou, L., Cho, Y.-W., . . . Kim, J. (2020). H2B ubiquitylation enhances H3K4 methylation activities of human KMT2 family complexes. *Nucleic acids research, 48*(10), 5442-5456.

Lahiri, A., Maji, A., Potdar, P. D., Singh, N., Parikh, P., Bisht, B., . . . Paul, M. K. (2023). Lung cancer immunotherapy: progress, pitfalls, and promises. *Molecular cancer, 22*(1), 40.

Laitem, C., Zaborowska, J., Isa, N. F., Kufs, J., Dienstbier, M., & Murphy, S. (2015). CDK9 inhibitors define elongation checkpoints at both ends of RNA polymerase II–transcribed genes. *Nature structural & molecular biology, 22*(5), 396-403.

Lambert, A. W., & Weinberg, R. A. (2021). Linking EMT programmes to normal and neoplastic epithelial stem cells. *Nat Rev Cancer, 21*(5), 325-338. doi:10.1038/s41568-021-00332-6

Lamouille, S., Xu, J., & Derynck, R. (2014). Molecular mechanisms of epithelial–mesenchymal transition. *Nature reviews Molecular cell biology, 15*(3), 178-196.

Langmead, B., & Salzberg, S. L. (2012). Fast gapped-read alignment with Bowtie 2. *Nat Methods, 9*(4), 357-359. doi:10.1038/nmeth.1923

Lavrik, I., & Krammer, P. (2012). Regulation of CD95/Fas signaling at the DISC. *Cell Death & Differentiation, 19*(1), 36-41.

Lawrence, M., Gentleman, R., & Carey, V. (2009). rtracklayer: an R package for interfacing with genome browsers. *Bioinformatics, 25*(14), 1841-1842. doi:10.1093/bioinformatics/btp328

Lee, M., Hwang, J.-T., Yun, H., Kim, E. J., Kim, M.-J., Kim, S.-S., & Ha, J. J. B. p. (2006). Critical roles of AMP-activated protein kinase in the carcinogenic metal-induced expression of VEGF and HIF-1 proteins in DU145 prostate carcinoma. *Biochemical pharmacology, 72*(1), 91-103.

Li, C., Liu, W., Liu, Y., Wang, W., & Deng, W. (2024). Role of ATP citrate lyase and its complementary partner on fatty acid synthesis in gastric cancer. *Scientific Reports, 14*(1), 1-18.

Li, H., Handsaker, B., Wysoker, A., Fennell, T., Ruan, J., Homer, N., . . . Genome Project Data Processing, S. (2009). The Sequence Alignment/Map format and SAMtools. *Bioinformatics, 25*(16), 2078-2079. doi:10.1093/bioinformatics/btp352

Liang, W., Cai, K., Chen, C., Chen, H., Fang, W., Fu, J., . . . Huang, Y. (2019). Society for Translational Medicine consensus on postoperative management of EGFR-mutant lung cancer (2019 edition). *Translational lung cancer research, 8*(6), 1163.

Liang, X., Tao, C., Pan, J., Zhang, L., Liu, L., Zhao, Y., . . . Zhang, J. (2021). Rnf20 deficiency in adipocyte impairs adipose tissue development and thermogenesis. *Protein & Cell, 12*(6), 475-492.

Lin, Q., Zhou, C.-R., Bai, M.-J., Zhu, D., Chen, J.-W., Wang, H.-F., . . . Huang, M.-S. (2020). Exosome-mediated miRNA delivery promotes liver cancer EMT and metastasis. *American journal of translational research, 12*(3), 1080.

Lin, Y.-T., & Wu, K.-J. (2020). Epigenetic regulation of epithelial-mesenchymal transition: focusing on hypoxia and TGF-β signaling. *Journal of biomedical science, 27*(1), 39.

Lis, J. T. (2007). Imaging Drosophila gene activation and polymerase pausing in vivo. *Nature, 450*(7167), 198-202.

Liu, B., Hu, X., Feng, K., Gao, R., Xue, Z., Zhang, S., . . . Han, W. (2022). Temporal single-cell tracing reveals clonal revival and expansion of precursor exhausted T cells during anti-PD-1 therapy in lung cancer. *Nature Cancer, 3*(1), 108-121.

Liu, B., Xue, Q., Tang, Y., Cao, J., Guengerich, F. P., & Zhang, H. (2016). Mechanisms of mutagenesis: DNA replication in the presence of DNA damage. *Mutation Research/Reviews in Mutation Research, 768*, 53-67.

Liu, J., Zhi, Q., Liu, Y., Wang, Y., Chen, L., Ke, Y., . . . Guleng, B. J. E. C. R. (2021). Insulin promotes hepatocarcinoma tumorigenesis by up-regulating PKM2 expression. Exp Cell Res, *408*(2), 112872.

Liu, X., Kraus, W. L., & Bai, X. (2015). Ready, pause, go: regulation of RNA polymerase II pausing and release by cellular signaling pathways. *Trends in biochemical sciences, 40*(9), 516-525.

Liu, X., Liu, T., Hu, L., Jiang, T., Liu, H., Wang, Y., . . . Bu, Y. (2020). Identification and characterization of the promoter of cancer-related gene LOXL2. *Experimental Cell Research, 387*(2), 111786.

Liu, Y. L., Yang, Y. M., Xu, H., & Dong, X. S. (2010). Increased expression of ubiquitin‐specific protease 22 can promote cancer progression and predict therapy failure in human colorectal cancer. *Journal of gastroenterology and hepatology, 25*(11), 1800-1805.

Liu, Z., Oh, S.-M., Okada, M., Liu, X., Cheng, D., Peng, J., . . . Gu, W. (2009). Human BRE1 is an E3 ubiquitin ligase for Ebp1 tumor suppressor. *Molecular Biology of the Cell, 20*(3), 757-768.

Love, M. I., Huber, W., & Anders, S. (2014). Moderated estimation of fold change and dispersion for RNA-seq data with DESeq2. *Genome Biol, 15*(12), 550. doi:10.1186/s13059-014-0550-8

Luker, K. E., & Luker, G. D. (2006). Functions of CXCL12 and CXCR4 in breast cancer. *Cancer letters, 238*(1), 30-41.

Lunt, S. Y., & Vander Heiden, M. G. (2011). Aerobic glycolysis: meeting the metabolic requirements of cell proliferation. *Annual review of cell and developmental biology, 27*, 441-464.

Luo, Z., Saha, A. K., Xiang, X., & Ruderman, N. B. J. T. i. p. s. (2005). AMPK, the metabolic syndrome and cancer. *Trends in pharmacological sciences*, *26*(2), 69-76.

Lv, X., Chen, Q., Zhang, S., Gao, F., & Liu, Q. (2022). CGRP: a new endogenous cell stemness maintenance molecule. *Oxidative Medicine and Cellular Longevity, 2022*(1), 4107433.

Lyssiotis, C. A., Son, J., Cantley, L. C., & Kimmelman, A. C. (2013). Pancreatic cancers rely on a novel glutamine metabolism pathway to maintain redox balance. *Cell cycle, 12*(13), 1987-1988.

Lyu, Y., Yang, Y., Talwar, V., Lu, H., Chen, C., Salman, S., . . . Wang, Y. (2024). Hypoxia-inducible factor 1 recruits FACT and RNF20/40 to mediate histone ubiquitination and transcriptional activation of target genes. *Cell Reports, 43*(4).

Ma, X., & Bai, Y. J. M. m. r. (2012). IGF-1 activates the P13K/AKT signaling pathway via upregulation of secretory clusterin. *Molecular medicine reports, 6*(6), 1433-1437.

Magdinier, F., Ribieras, S., Lenoir, G. M., Frappart, L., & Dante, R. J. O. (1998). Down-regulation of BRCA1 in human sporadic breast cancer; analysis of DNA methylation patterns of the putative promoter region. *Oncogene*, *17*(24), 3169-3176.

Maishi, N., & Hida, K. (2017). Tumor endothelial cells accelerate tumor metastasis. *Cancer science, 108*(10), 1921-1926.

Mallick, R., Bhowmik, P., & Duttaroy, A. K. (2023). Targeting fatty acid uptake and metabolism in cancer cells: A promising strategy for cancer treatment. *Biomedicine & Pharmacotherapy, 167*, 115591.

Manfredi, S., Lepage, C., Hatem, C., Coatmeur, O., Faivre, J., & Bouvier, A.-M. (2006). Epidemiology and management of liver metastases from colorectal cancer. *Annals of surgery, 244*(2), 254-259.

Marin-Valencia, I., Yang, C., Mashimo, T., Cho, S., Baek, H., Yang, X.-L., . . . Zhao, Z. (2012). Analysis of tumor metabolism reveals mitochondrial glucose oxidation in genetically diverse human glioblastomas in the mouse brain in vivo. *Cell metabolism, 15*(6), 827-837.

Markouli, M., Strepkos, D., Basdra, E. K., Papavassiliou, A. G., & Piperi, C. (2021). Prominent role of histone modifications in the regulation of tumor metastasis. *International Journal of Molecular Sciences, 22*(5), 2778.

Marsh, D. J., Ma, Y., & Dickson, K.-A. (2020). Histone monoubiquitination in chromatin remodelling: focus on the histone H2B interactome and cancer. *Cancers, 12*(11), 3462.

Marte, B. (2004). Cell division and cancer. *Nature, 432*(7015), 293-294.

Martín-Caballero, J., Flores, J. M., García-Palencia, P., & Serrano, M. (2001). Tumor susceptibility of p21 Waf1/Cip1-deficient mice. *Cancer research, 61*(16), 6234-6238.

Martin-Gisbert, L., Ruano-Ravina, A., Varela-Lema, L., Penabad, M., Giraldo-Osorio, A., Candal-Pedreira, C., . . . Pérez-Ríos, M. (2023). Lung cancer mortality attributable to residential radon: a systematic scoping review. *Journal of Exposure Science & Environmental Epidemiology, 33*(3), 368-376.

Matthews, H. K., Bertoli, C., & de Bruin, R. A. (2022). Cell cycle control in cancer. *Nature Reviews Molecular Cell Biology, 23*(1), 74-88.

Mattson, M. P. (2000). Apoptosis in neurodegenerative disorders. *Nature reviews Molecular cell biology, 1*(2), 120-130.

Mayekar, M. K., & Bivona, T. G. (2017). Current landscape of targeted therapy in lung cancer. *Clinical Pharmacology & Therapeutics, 102*(5), 757-764.

McClellan, B., Pham, T., Harlow, B., Lee, G., Quach, D., Jolly, C., . . . Research, C. (2022). Modulation of Breast Cancer Cell FASN Expression by Obesity-Related Systemic Factors. *Breast Cancer: Basic and Clinical Research*, *16*, 11782234221111374.

Meas, R., & Mao, P. (2015). Histone ubiquitylation and its roles in transcription and DNA damage response. *DNA repair, 36*, 36-42.

Medeiros, B., & Allan, A. L. (2019). Molecular mechanisms of breast cancer metastasis to the lung: clinical and experimental perspectives. *International journal of molecular sciences, 20*(9), 2272.

Meijer, T. W., Kaanders, J. H., Span, P. N., & Bussink, J. J. C. c. r. (2012). Targeting hypoxia, HIF-1, and tumor glucose metabolism to improve radiotherapy efficacy. *Clinical cancer research, 18*(20), 5585-5594.

Messier, T. L., Gordon, J. A., Boyd, J. R., Tye, C. E., Browne, G., Stein, J. L., . . . Stein, G. S. (2016). Histone H3 lysine 4 acetylation and methylation dynamics define breast cancer subtypes. *Oncotarget, 7*(5), 5094.

Metallo, C. M., Gameiro, P. A., Bell, E. L., Mattaini, K. R., Yang, J., Hiller, K., . . . Guarente, L. (2012). Reductive glutamine metabolism by IDH1 mediates lipogenesis under hypoxia. *Nature, 481*(7381), 380-384.

Metro, G., & Crinò, L. (2012). Advances on EGFR mutation for lung cancer. *Translational lung cancer research, 1*(1), 5.

Miziak, P., Baran, M., Borkiewicz, L., Trombik, T., & Stepulak, A. (2024). Acetylation of Histone H3 in Cancer Progression and Prognosis. *International Journal of Molecular Sciences, 25*(20), 10982.

Mogi, A., & Kuwano, H. (2011). TP53 mutations in nonsmall cell lung cancer. *BioMed Research International, 2011*(1), 583929.

Mook, O. R., Frederiks, W. M., & Van Noorden, C. J. (2004). The role of gelatinases in colorectal cancer progression and metastasis. *Biochimica et Biophysica Acta (BBA)-Reviews on Cancer, 1705*(2), 69-89.

Moore, L. D., Le, T., & Fan, G. J. N. (2013). DNA methylation and its basic function. *Neuropsychopharmacology*, *38*(1), 23-38.

Morris IV, J. P., Yashinskie, J. J., Koche, R., Chandwani, R., Tian, S., Chen, C.-C., . . . Leach, S. D. (2019). α-Ketoglutarate links p53 to cell fate during tumour suppression. *Nature, 573*(7775), 595-599.

Moyal, L., Lerenthal, Y., Gana-Weisz, M., Mass, G., So, S., Wang, S.-Y., . . . Shema, E. (2011). Requirement of ATM-dependent monoubiquitylation of histone H2B for timely repair of DNA double-strand breaks. *Molecular cell, 41*(5), 529-542.

Muir, A., Danai, L. V., & Vander Heiden, M. G. (2018). Microenvironmental regulation of cancer cell metabolism: implications for experimental design and translational studies. *Disease models & mechanisms, 11*(8), dmm035758.

Muller, P. A., & Vousden, K. H. (2013). p53 mutations in cancer. *Nature cell biology, 15*(1), 2-8.

Nair, A., & Sarma, S. J. (2021). The impact of carbon and nitrogen catabolite repression in microorganisms. *Microbiological Research, 251*, 126831.

Nakamura, H., & Takada, K. (2021). Reactive oxygen species in cancer: Current findings and future directions. *Cancer science, 112*(10), 3945-3952.

Nakamura, K., Kato, A., Kobayashi, J., Yanagihara, H., Sakamoto, S., Oliveira, D. V., . . . Tashiro, S. (2011). Regulation of homologous recombination by RNF20-dependent H2B ubiquitination. *Molecular cell, 41*(5), 515-528.

Ng, K., Ng, K., Chu, K., Kung, B., & Yong, T. (2023). Diagnostic accuracy of 18F-fluorodeoxyglucose positron emission tomography/computed tomography in preoperative mediastinal/extramediastinal nodal staging of non–small-cell lung carcinoma. *Radiol, 26*, 6-13.

Nicholson, A. G., Tsao, M. S., Beasley, M. B., Borczuk, A. C., Brambilla, E., Cooper, W. A., . . . Lantuejoul, S. (2022). The 2021 WHO classification of lung tumors: impact of advances since 2015. *Journal of Thoracic Oncology, 17*(3), 362-387.

Nishigaki, M., Aoyagi, K., Danjoh, I., Fukaya, M., Yanagihara, K., Sakamoto, H., . . . Sasaki, H. J. C. r. (2005). Discovery of aberrant expression of R-RAS by cancer-linked DNA hypomethylation in gastric cancer using microarrays. *Cancer research, 65*(6), 2115-2124.

Oda, A., Inoue, S., Kaneko, R., Narita, Y., Shiono, S., Kaneko, T., . . . Ohtani-Kaneko, R. J. S. R. (2022). Involvement of IGF-1R-PI3K-AKT-mTOR pathway in increased number of GnRH3 neurons during androgen-induced sex reversal of the brain in female tilapia. *Scientific Reports, 12*(1), 2450.

Ogrunc, M., Di Micco, R., Liontos, M., Bombardelli, L., Mione, M., Fumagalli, M., . . . Differentiation. (2014). Oncogene-induced reactive oxygen species fuel hyperproliferation and DNA damage response activation. *Cell Death & Differentiation*, *21*(6), 998-1012.

Ojelabi, O. A., Lloyd, K. P., Simon, A. H., De Zutter, J. K., & Carruthers, A. (2016). WZB117 (2-Fluoro-6-(m-hydroxybenzoyloxy) Phenyl m-Hydroxybenzoate) inhibits GLUT1-mediated sugar transport by binding reversibly at the exofacial sugar binding site. *Journal of Biological Chemistry, 291*(52), 26762-26772.

Okamura, K., Takayama, K., Izumi, M., Harada, T., Furuyama, K., & Nakanishi, Y. (2013). Diagnostic value of CEA and CYFRA 21-1 tumor markers in primary lung cancer. *Lung cancer, 80*(1), 45-49.

Ooi, A. T., & Gomperts, B. N. J. C. C. R. (2015). Molecular pathways: targeting cellular energy metabolism in cancer via inhibition of SLC2A1 and LDHA. *Clinical Cancer Research, 21*(11), 2440-2444.

Ortmann, B. M., Burrows, N., Lobb, I. T., Arnaiz, E., Wit, N., Bailey, P. S., . . . McCaffrey, J. (2021a). The HIF complex recruits the histone methyltransferase SET1B to activate specific hypoxia-inducible genes. *Nature genetics, 53*(7), 1022-1035.

Ortmann, B. M., Burrows, N., Lobb, I. T., Arnaiz, E., Wit, N., Bailey, P. S., . . . McCaffrey, J. J. N. g. (2021b). The HIF complex recruits the histone methyltransferase SET1B to activate specific hypoxia-inducible genes. *Nature genetics*, *53*(7), 1022-1035.

Osellame, L. D., Blacker, T. S., Duchen, M. R. J. B. p., endocrinology, r. C., & metabolism. (2012). Cellular and molecular mechanisms of mitochondrial function. *Best Pract Res Clin Endocrinol Metab, 26*(6), 711-723.

Osley, M. A., Fleming, A. B., & Kao, C.-F. (2006). Histone ubiquitylation and the regulation of transcription. *Chromatin dynamics in cellular function*, 47-75.

Palmieri, D., Smith, Q. R., Lockman, P. R., Bronder, J., Gril, B., Chambers, A. F., . . . Steeg, P. S. (2007). Brain metastases of breast cancer. *Breast disease, 26*(1), 139-147.

Pan, S. Y., Johnson, K. C., Ugnat, A.-M., Wen, S. W., & Mao, Y. (2004). Association of obesity and cancer risk in Canada. *American journal of epidemiology, 159*(3), 259-268.

Panatta, E., Butera, A., Mammarella, E., Pitolli, C., Mauriello, A., Leist, M., . . . Amelio, I. (2022). Metabolic regulation by p53 prevents R-loop-associated genomic instability. *Cell reports, 41*(5).

Park, M., Kim, M., Suh, Y., Kim, R., Kim, H., Lim, E., . . . Differentiation. (2014). Novel signaling axis for ROS generation during K-Ras-induced cellular transformation. *Cell Death & Differentiation, 21*(8), 1185-1197.

Peinado, H., Zhang, H., Matei, I. R., Costa-Silva, B., Hoshino, A., Rodrigues, G., . . . Kang, Y. (2017). Pre-metastatic niches: organ-specific homes for metastases. *Nature Reviews Cancer, 17*(5), 302-317.

Pemberton, J. M., Nguyen, D., Osterlund, E. J., Schormann, W., Pogmore, J. P., Hirmiz, N., . . . Andrews, D. W. (2023). The carboxyl-terminal sequence of PUMA binds to both anti-apoptotic proteins and membranes. *Elife, 12*, e88329.

Peterson, E. J., Bögler, O., & Taylor, S. M. (2003). p53-mediated repression of DNA methyltransferase 1 expression by specific DNA binding. *Cancer research, 63*(20), 6579-6582.

Pierre, T. H., Liu, Y., Bethea, M. M., Coutinho, K., & Hunter, C. (2024). 9366 The Rnf20 Histone Modifier Is A Crucial Mediator Of Pancreatic Beta Cell Identity And Function. *Journal of the Endocrine Society, 8*(Supplement_1), bvae163. 969.

Prabavathy, D., Swarnalatha, Y., & Ramadoss, N. (2018). Lung cancer stem cells—origin, characteristics and therapy. *Stem cell investigation, 5*, 6.

Prenzel, T., Begus-Nahrmann, Y., Kramer, F., Hennion, M., Hsu, C., Gorsler, T., . . . Simons, M. (2011). Estrogen-dependent gene transcription in human breast cancer cells relies upon proteasome-dependent monoubiquitination of histone H2B. *Cancer research, 71*(17), 5739-5753.

Quinlan, A. R., & Hall, I. M. (2010). BEDTools: a flexible suite of utilities for comparing genomic features. *Bioinformatics, 26*(6), 841-842. doi:10.1093/bioinformatics/btq033

Radi, E., Formichi, P., Battisti, C., & Federico, A. (2014). Apoptosis and oxidative stress in neurodegenerative diseases. *Journal of Alzheimer's disease, 42*(s3), S125-S152.

Ramirez, F., Ryan, D. P., Gruning, B., Bhardwaj, V., Kilpert, F., Richter, A. S., . . . Manke, T. (2016). deepTools2: a next generation web server for deep-sequencing data analysis. *Nucleic Acids Res, 44*(W1), W160-165. doi:10.1093/nar/gkw257

Rankin, E. B., & Giaccia, A. J. (2016). Hypoxic control of metastasis. *Science, 352*(6282), 175-180.

Rattner, A., Williams, J., & Nathans, J. J. T. J. o. c. i. (2019). Roles of HIFs and VEGF in angiogenesis in the retina and brain. *Journal of clinical investigation, 129*(9), 3807-3820.

Rezaeian, A.-H., Li, C.-F., Wu, C.-Y., Zhang, X., Delacerda, J., You, M. J., . . . Jin, G. J. N. c. b. (2017). A hypoxia-responsive TRAF6–ATM–H2AX signalling axis promotes HIF1α activation, tumorigenesis and metastasis. *Nature cell biology*, *19*(1), 38-51.

Riely, G. J., Marks, J., & Pao, W. (2009). KRAS mutations in non–small cell lung cancer. *Proceedings of the American Thoracic Society, 6*(2), 201-205.

Robles, A. I., Linke, S. P., & Harris, C. C. (2002). The p53 network in lung carcinogenesis. *Oncogene, 21*(45), 6898-6907.

Ropero, S., & Esteller, M. (2007). The role of histone deacetylases (HDACs) in human cancer. *Molecular oncology, 1*(1), 19-25.

Ross-Innes, C. S., Stark, R., Teschendorff, A. E., Holmes, K. A., Ali, H. R., Dunning, M. J., . . . Carroll, J. S. (2012). Differential oestrogen receptor binding is associated with clinical outcome in breast cancer. *Nature, 481*(7381), 389-U177. doi:10.1038/nature10730

Rowbotham, D. A., Enfield, K. S., Martinez, V. D., Thu, K. L., Vucic, E. A., Stewart, G. L., . . . Lam, W. L. Research Article Multiple Components of the VHL Tumor Suppressor Complex Are Frequently

Affected by DNA Copy Number Loss in Pheochromocytoma. *International journal of endocrinology*, *2014*(1), 546347.

Rudin, C. M., Brambilla, E., Faivre-Finn, C., & Sage, J. (2021). Small-cell lung cancer. *Nature Reviews Disease Primers, 7*(1), 3.

Ruscito, I., Dimitrova, D., Vasconcelos, I., Gellhaus, K., Schwachula, T., Bellati, F., . . . Mahner, S. J. E. j. o. c. (2014). BRCA1 gene promoter methylation status in high-grade serous ovarian cancer patients–a study of the tumour Bank ovarian cancer (TOC) and ovarian cancer diagnosis consortium (OVCAD). *European journal of cancer*, *50*(12), 2090-2098.

Sainz de Aja, J., Dost, A., & Kim, C. (2021). Alveolar progenitor cells and the origin of lung cancer. *Journal of internal medicine, 289*(5), 629-635.

Saitoh, M. (2018). Involvement of partial EMT in cancer progression. *The Journal of Biochemistry, 164*(4), 257-264.

Santivasi, W. L., & Xia, F. (2014). Ionizing radiation-induced DNA damage, response, and repair. *Antioxidants & redox signaling, 21*(2), 251-259.

Sasidharan Nair, V., El Salhat, H., Taha, R. Z., John, A., Ali, B. R., & Elkord, E. (2018). DNA methylation and repressive H3K9 and H3K27 trimethylation in the promoter regions of PD-1, CTLA-4, TIM-3, LAG-3, TIGIT, and PD-L1 genes in human primary breast cancer. *Clinical epigenetics, 10*, 1-12.

Sasidharan Nair, V., Toor, S. M., Taha, R. Z., Shaath, H., & Elkord, E. (2018). DNA methylation and repressive histones in the promoters of PD-1, CTLA-4, TIM-3, LAG-3, TIGIT, PD-L1, and galectin-9 genes in human colorectal cancer. *Clinical epigenetics, 10*, 1-9.

Schabath, M. B., & Cote, M. L. (2019). Cancer progress and priorities: lung cancer. *Cancer epidemiology, biomarkers & prevention, 28*(10), 1563-1579.

Schmall, A., Al-Tamari, H. M., Herold, S., Kampschulte, M., Weigert, A., Wietelmann, A., . . . medicine, c. c. (2015). Macrophage and cancer cell cross-talk via CCR2 and CX3CR1 is a fundamental mechanism driving lung cancer. *American journal of respiratory and critical care medicine*, *191*(4), 437-447.

Schmitt, M., & Greten, F. R. (2021). The inflammatory pathogenesis of colorectal cancer. *Nature Reviews Immunology, 21*(10), 653-667.

Schneider, J. (2006). Tumor markers in detection of lung cancer. *Advances in clinical chemistry, 42*, 1-41.

Schofield, C. J., & Ratcliffe, P. J. (2004). Oxygen sensing by HIF hydroxylases. *Nature reviews Molecular cell biology, 5*(5), 343-354.

Sciacovelli, M., Frezza, C. J. C. D., & Differentiation. (2017). Fumarate drives EMT in renal cancer. *Cell Death & Differentiation, 24*(1), 1.

Scorrano, L., Oakes, S. A., Opferman, J. T., Cheng, E. H., Sorcinelli, M. D., Pozzan, T., & Korsmeyer, S. J. (2003). BAX and BAK regulation of endoplasmic reticulum Ca2+: a control point for apoptosis. *Science, 300*(5616), 135-139.

Selzner, M., Morse, M. A., Vredenburgh, J. J., Meyers, W. C., & Clavien, P.-A. (2000). Liver metastases from breast cancer: long-term survival after curative resection. *Surgery, 127*(4), 383-389.

Sena, L. A., & Chandel, N. S. J. M. c. (2012). Physiological roles of mitochondrial reactive oxygen species. *Molecular cell*, *48*(2), 158-167.

Sethi, G., Shanmugam, M. K., Arfuso, F., & Kumar, A. P. (2018). Role of RNF20 in cancer development and progression–a comprehensive review. *Bioscience Reports, 38*(4), BSR20171287.

Sethi, G., Shanmugam, M. K., & Kumar, A. P. (2017). SREBP-1c as a molecular bridge between lipogenesis and cell cycle progression of clear cell renal carcinoma. *Bioscience Reports, 37*(6), BSR20171270.

Shaw, A. T., & Engelman, J. A. (2013). ALK in lung cancer: past, present, and future. *Journal of clinical oncology, 31*(8), 1105-1111.

Shema, E., Kim, J., Roeder, R. G., & Oren, M. (2011). RNF20 inhibits TFIIS-facilitated transcriptional elongation to suppress pro-oncogenic gene expression. *Molecular cell, 42*(4), 477-488.

Shema, E., Kim, J., Roeder, R. G., & Oren, M. J. M. c. (2011). RNF20 inhibits TFIIS-facilitated transcriptional elongation to suppress pro-oncogenic gene expression. *Molecular cell*, *42*(4), 477-488.

Shen, L., Fang, J., Qiu, D., Zhang, T., Yang, J., Chen, S., & Xiao, S. (1998). Correlation between DNA methylation and pathological changes in human hepatocellular carcinoma. *Hepato-gastroenterology, 45*(23), 1753-1759.

Shen, L., Shao, N., Liu, X., & Nestler, E. (2014). ngs.plot: Quick mining and visualization of next-generation sequencing data by integrating genomic databases. *BMC Genomics, 15*, 284. doi:10.1186/1471-2164-15-284

Sherr, C. J., & McCormick, F. (2002). The RB and p53 pathways in cancer. *Cancer cell, 2*(2), 103-112.

Shi, Y., Nikulenkov, F., Zawacka-Pankau, J., Li, H., Gabdoulline, R., Xu, J., . . . Differentiation. (2014). ROS-dependent activation of JNK converts p53 into an efficient inhibitor of oncogenes leading to robust apoptosis. *Cell Death & Differentiation*, *21*(4), 612-623.

Shilatifard, A. (2012). The COMPASS family of histone H3K4 methylases: mechanisms of regulation in development and disease pathogenesis. *Annual review of biochemistry, 81*(1), 65-95.

Shiloh, Y., Shema, E., Moyal, L., & Oren, M. (2011). RNF20–RNF40: A ubiquitin-driven link between gene expression and the DNA damage response. *FEBS letters, 585*(18), 2795-2802.

Shivji, M. K., Renaudin, X., Williams, Ç. H., & Venkitaraman, A. R. (2018). BRCA2 regulates transcription elongation by RNA polymerase II to prevent R-loop accumulation. *Cell reports, 22*(4), 1031-1039.

Silke, J., & Meier, P. (2013). Inhibitor of apoptosis (IAP) proteins–modulators of cell death and inflammation. *Cold Spring Harbor perspectives in biology, 5*(2), a008730.

Singh, P., & Lim, B. J. C. o. r. (2022). Targeting apoptosis in cancer. *Current oncology reports, 24*(3), 273-284.

Sinha, R. P., & Häder, D.-P. (2002). UV-induced DNA damage and repair: a review. *Photochemical & Photobiological Sciences, 1*(4), 225-236.

Skoulidis, F., Li, B. T., Dy, G. K., Price, T. J., Falchook, G. S., Wolf, J., . . . Barlesi, F. (2021). Sotorasib for lung cancers with KRAS p. G12C mutation. *New England Journal of Medicine, 384*(25), 2371-2381.

Smith, A. H., Ercumen, A., Yuan, Y., & Steinmaus, C. M. (2009). Increased lung cancer risks are similar whether arsenic is ingested or inhaled. *Journal of exposure science & environmental epidemiology, 19*(4), 343-348.

So, C. C., Ramachandran, S., & Martin, A. (2019a). E3 ubiquitin ligases RNF20 and RNF40 are required for double-stranded break (DSB) repair: evidence for monoubiquitination of histone H2B lysine 120 as a novel axis of DSB signaling and repair. *Molecular and cellular biology*.

So, C. C., Ramachandran, S., & Martin, A. (2019b). E3 ubiquitin ligases RNF20 and RNF40 are required for double-stranded break (DSB) repair: evidence for monoubiquitination of histone H2B lysine 120 as a novel axis of DSB signaling and repair. *Molecular and cellular biology, 39*(8), e00488-00418.

Soares, L. M., & Buratowski, S. (2013). Histone crosstalk: H2Bub and H3K4 methylation. *Molecular cell, 49*(6), 1019-1020.

Song, L., Coppola, D., Livingston, S., Cress, W. D., & Haura, E. B. (2005). Mcl-1 regulates survival and sensitivity to diverse apoptotic stimuli in human non-small cell lung cancer cells. *Cancer biology & therapy, 4*(3), 267-276.

Song, Y., Wu, F., Wu, J. J. J. o. h., & oncology. (2016). Targeting histone methylation for cancer therapy: enzymes, inhibitors, biological activity and perspectives. *Journal of hematology & oncology, 9*, 1-21.

Spitz, M. R., Wei, Q., Dong, Q., Amos, C. I., & Wu, X. (2003). Genetic susceptibility to lung cancer: the role of DNA damage and repair. *Cancer Epidemiology Biomarkers & Prevention, 12*(8), 689-698.

Srinivas, U. S., Tan, B. W., Vellayappan, B. A., & Jeyasekharan, A. D. (2019). ROS and the DNA damage response in cancer. *Redox biology, 25*, 101084.

Srinivas, U. S., Tan, B. W., Vellayappan, B. A., & Jeyasekharan, A. D. J. R. b. (2019). ROS and the DNA damage response in cancer. *Redox biology*, *25*, 101084.

Sun, Z.-W., & Allis, C. D. J. N. (2002). Ubiquitination of histone H2B regulates H3 methylation and gene silencing in yeast. *Nature, 418*(6893), 104-108.

Sutherland, K. D., & Berns, A. (2010). Cell of origin of lung cancer. *Molecular oncology, 4*(5), 397-403.

Tan, J., Sun, X., Zhao, H., Guan, H., Gao, S., & Zhou, P. K. (2023). Double‐strand DNA break repair: molecular mechanisms and therapeutic targets. *MedComm, 4*(5), e388.

Tanny, J. C., Erdjument-Bromage, H., Tempst, P., Allis, C. D. J. G., & development. (2007). Ubiquitylation of histone H2B controls RNA polymerase II transcription elongation independently of histone H3 methylation. *Genes & development*, *21*(7), 835-847.

Tao, M.-H. (2019). Epidemiology of lung cancer. *Lung Cancer and Imaging*, 4-1-4-15.

Tao, Y., Liu, S., Briones, V., Geiman, T. M., & Muegge, K. (2011). Treatment of breast cancer cells with DNA demethylating agents leads to a release of Pol II stalling at genes with DNA-hypermethylated regions upstream of TSS. *Nucleic acids research, 39*(22), 9508-9520.

Tarcic, O., Granit, R. Z., Pateras, I. S., Masury, H., Maly, B., Zwang, Y., . . . Ben-Porath, I. (2017). RNF20 and histone H2B ubiquitylation exert opposing effects in Basal-Like versus luminal breast cancer. *Cell Death & Differentiation, 24*(4), 694-704.

Tarcic, O., Pateras, I. S., Cooks, T., Shema, E., Kanterman, J., Ashkenazi, H., . . . Baniyash, M. (2016). RNF20 links histone H2B ubiquitylation with inflammation and inflammation-associated cancer. *Cell Reports, 14*(6), 1462-1476.

Tardito, S., Oudin, A., Ahmed, S. U., Fack, F., Keunen, O., Zheng, L., . . . Wagner, A. (2015). Glutamine synthetase activity fuels nucleotide biosynthesis and supports growth of glutamine-restricted glioblastoma. *Nature cell biology, 17*(12), 1556-1568.

Thomadaki, H., & Scorilas, A. (2006). BCL2 family of apoptosis-related genes: functions and clinical implications in cancer. *Critical reviews in clinical laboratory sciences, 43*(1), 1-67.

Timoféeff-Ressovsky, N. W., Zimmer, K. G., & Delbruck, M. (2011). On the nature of gene mutation and gene structure. *Creating a Physical Biology: The Three-Man Paper and Early Molecular Biology; Sloan, PR, Fogel, B., Eds*.

Topalian, S. L., Taube, J. M., & Pardoll, D. M. (2020). Neoadjuvant checkpoint blockade for cancer immunotherapy. *Science, 367*(6477), eaax0182.

Tran, T. A., Kappelhoff, J., Jüstel, T., Anderson, R. R., & Purschke, M. (2022). UV emitting nanoparticles enhance the effect of ionizing radiation in 3D lung cancer spheroids. *International Journal of Radiation Biology, 98*(9), 1484-1494.

Tripathi, K., Goel, A., Singhai, A., & Garg, M. J. M. B. R. (2021). Promoter hypomethylation as potential confounder of Ras gene overexpression and their clinical significance in subsets of urothelial carcinoma of bladder. *Mol Biol Rep, 48*(3), 2183-2199.

Turner, B. M., Cagle, P. T., Sainz, I. M., Fukuoka, J., Shen, S. S., & Jagirdar, J. (2012). Napsin A, a new marker for lung adenocarcinoma, is complementary and more sensitive and specific than thyroid transcription factor 1 in the differential diagnosis of primary pulmonary carcinoma: evaluation of 1674 cases by tissue microarray. *Archives of pathology & laboratory medicine, 136*(2), 163-171.

Unterlass, J. E., & Curtin, N. J. J. E. R. i. M. M. (2019). Warburg and Krebs and related effects in cancer. *Expert Reviews in Molecular Medicine*, *21*, e4.

Vaddavalli, P. L., & Schumacher, B. (2022). The p53 network: Cellular and systemic DNA damage responses in cancer and aging. *Trends in Genetics, 38*(6), 598-612.

Vazquez, A., Bond, E. E., Levine, A. J., & Bond, G. L. J. N. r. D. d. (2008). The genetics of the p53 pathway, apoptosis and cancer therapy. *Nature reviews Drug discovery, 7*(12), 979-987.

Vihervaara, A., Mahat, D. B., Himanen, S. V., Blom, M. A., Lis, J. T., & Sistonen, L. (2021). Stress-induced transcriptional memory accelerates promoter-proximal pause release and decelerates termination over mitotic divisions. *Molecular cell, 81*(8), 1715-1731. e1716.

Vyas, S., Zaganjor, E., & Haigis, M. C. (2016). Mitochondria and cancer. *Cell, 166*(3), 555-566.

Wallace, D. C. (2012). Mitochondria and cancer. *Nature Reviews Cancer, 12*(10), 685-698.
Wallace, D. C. J. N. R. C. (2012). Mitochondria and cancer. *Nature Reviews Cancer, 12*(10), 685-698.
Walser, T., Cui, X., Yanagawa, J., Lee, J. M., Heinrich, E., Lee, G., . . . Dubinett, S. M. (2008). Smoking and lung cancer: the role of inflammation. *Proceedings of the American Thoracic Society, 5*(8), 811-815.
Wang, J. Q., Yan, F. Q., Wang, L. H., Yin, W. J., Chang, T. Y., Liu, J. P., & Wu, K. J. (2020). Identification of new hypoxia-regulated epithelial-mesenchymal transition marker genes labeled by H3K4 acetylation. *Genes, Chromosomes and Cancer, 59*(2), 73-83.
Wang, L., Xu, Z., Wang, L., Liu, C., Wei, H., Zhang, R., . . . Xiao, S. (2021). Histone H2B ubiquitination mediated chromatin relaxation is essential for the induction of somatic cell reprogramming. *Cell Proliferation, 54*(8), e13080.
Wang, X., Liu, R., Zhu, W., Chu, H., Yu, H., Wei, P., . . . Liang, J. (2019). UDP-glucose accelerates SNAI1 mRNA decay and impairs lung cancer metastasis. *Nature, 571*(7763), 127-131.
Wang, Y., & Patti, G. J. (2023). The Warburg effect: a signature of mitochondrial overload. *Trends in Cell Biology*.
Wang, Z., Himanen, S. V., Haikala, H. M., Friedel, C. C., Vihervaara, A., & Barborič, M. (2023). Inhibition of CDK12 elevates cancer cell dependence on P-TEFb by stimulation of RNA polymerase II pause release. *Nucleic acids research, 51*(20), 10970-10991.
Warburg, O. (1956). On the origin of cancer cells. *Science, 123*(3191), 309-314.
Weidemann, A., & Johnson, R. S. (2008). Biology of HIF-1α. *Cell Death & Differentiation, 15*(4), 621-627. doi:10.1038/cdd.2008.12
Weinberg, R. L., Veprintsev, D. B., Bycroft, M., & Fersht, A. R. (2005). Comparative binding of p53 to its promoter and DNA recognition elements. *Journal of molecular biology, 348*(3), 589-596.
Widschwendter, M., Jiang, G., Woods, C., Müller, H. M., Fiegl, H., Goebel, G., . . . Laird, P. W. (2004). DNA hypomethylation and ovarian cancer biology. *Cancer research, 64*(13), 4472-4480.
Wong, E. M., Southey, M. C., & Terry, M. B. J. B. j. o. c. (2020). Integrating DNA methylation measures to improve clinical risk assessment: are we there yet? The case of BRCA1 methylation marks to improve clinical risk assessment of breast cancer. *British journal of cancer, 122*(8), 1133-1140.
Wong, S. K., Mohamad, N.-V., Giaze, T. R., Chin, K.-Y., Mohamed, N., & Ima-Nirwana, S. (2019). Prostate cancer and bone metastases: the underlying mechanisms. *International journal of molecular sciences, 20*(10), 2587.
Wu, B.-K., & Brenner, C. J. C. r. (2014). Suppression of TET1-dependent DNA demethylation is essential for KRAS-mediated transformation. *Cell reports, 9*(5), 1827-1840.
Wu, C., Cui, Y., Liu, X., Zhang, F., Lu, L.-Y., & Yu, X. (2020). The RNF20/40 complex regulates p53-dependent gene transcription and mRNA splicing. *Journal of molecular cell biology, 12*(2), 113-124.
Wu, K., House, L., Liu, W., & Cho, W. C. (2012). Personalized targeted therapy for lung cancer. *International Journal of Molecular Sciences, 13*(9), 11471-11496.
Xiang, Y., Stine, Z. E., Xia, J., Lu, Y., O'Connor, R. S., Altman, B. J., . . . Gao, P. (2015). Targeted inhibition of tumor-specific glutaminase diminishes cell-autonomous tumorigenesis. *The Journal of clinical investigation, 125*(6), 2293-2306.
Xiao, G.-Y., Tan, X., Rodriguez, B. L., Gibbons, D. L., Wang, S., Wu, C., . . . Tran, H. T. (2023). EMT activates exocytotic Rabs to coordinate invasion and immunosuppression in lung cancer. *Proceedings of the National Academy of Sciences, 120*(28), e2220276120.
Xiong, X., Wen, Y.-A., Fairchild, R., Zaytseva, Y. Y., Weiss, H. L., Evers, B. M., & Gao, T. (2020). Upregulation of CPT1A is essential for the tumor-promoting effect of adipocytes in colon cancer. *Cell death & disease, 11*(9), 736.
Xu, X., Tan, X., Tampe, B., Sanchez, E., Zeisberg, M., & Zeisberg, E. M. J. J. o. B. C. (2015). Snail is a direct target of hypoxia-inducible factor 1α (HIF1α) in hypoxia-induced endothelial to mesenchymal transition of human coronary endothelial cells. *J Biol Chem*, *290*(27), 16653-16664.

Yang, M.-H., Li, B., & Chang, K.-J. (2022). Notch pathway inhibition mediated by arsenic trioxide depletes tumor initiating cells in small cell lung cancer. *Molecular Biology Reports*, 1-9.

Yang, Y., Lu, H., Chen, C., Lyu, Y., Cole, R. N., & Semenza, G. L. J. N. c. (2022). HIF-1 Interacts with TRIM28 and DNA-PK to release paused RNA polymerase II and activate target gene transcription in response to hypoxia. *Nature communications*, *13*(1), 316.

Yasui, W., Oue, N., Ono, S., Mitani, Y., Ito, R., & Nakayama, H. (2003). Histone acetylation and gastrointestinal carcinogenesis. *Annals of the New York Academy of Sciences, 983*(1), 220-231.

Ye, X., Brabletz, T., Kang, Y., Longmore, G. D., Nieto, M. A., Stanger, B. Z., . . . Weinberg, R. A. (2017). Upholding a role for EMT in breast cancer metastasis. *Nature, 547*(7661), E1-E3.

Yen, C.-Y., Huang, H.-W., Shu, C.-W., Hou, M.-F., Yuan, S.-S. F., Wang, H.-R., . . . Chang, H.-W. (2016). DNA methylation, histone acetylation and methylation of epigenetic modifications as a therapeutic approach for cancers. *Cancer letters, 373*(2), 185-192.

Yeung, S., Pan, J., & Lee, M.-H. (2008). Roles of p53, MYC and HIF-1 in regulating glycolysis—the seventh hallmark of cancer. *Cellular and Molecular Life Sciences, 65*, 3981-3999.

Yonezawa, S., Higashi, M., Yamada, N., Yokoyama, S., Kitamoto, S., Kitajima, S., & Goto, M. (2011). Mucins in human neoplasms: clinical pathology, gene expression and diagnostic application. *Pathology international, 61*(12), 697-716.

Yousefi, M., Bahrami, T., Salmaninejad, A., Nosrati, R., Ghaffari, P., & Ghaffari, S. H. (2017). Lung cancer-associated brain metastasis: Molecular mechanisms and therapeutic options. *Cellular Oncology, 40*, 419-441.

Yu, G., Wang, L. G., & He, Q. Y. (2015). ChIPseeker: an R/Bioconductor package for ChIP peak annotation, comparison and visualization. *Bioinformatics, 31*(14), 2382-2383. doi:10.1093/bioinformatics/btv145

Yuan, H., Wu, H., Cheng, J., & Xiong, J. (2023). SIAH1 ubiquitination-modified HMGCR inhibits lung cancer progression and promotes drug sensitivity through cholesterol synthesis. *Cancer Cell International, 23*(1), 71.

Yun, J., Rago, C., Cheong, I., Pagliarini, R., Angenendt, P., Rajagopalan, H., . . . Zhou, S. (2009). Glucose deprivation contributes to the development of KRAS pathway mutations in tumor cells. *Science, 325*(5947), 1555-1559.

Zhang, F., & Yu, X. (2011). WAC, a functional partner of RNF20/40, regulates histone H2B ubiquitination and gene transcription. *Molecular cell, 41*(4), 384-397.

Zhang, H., Xie, W., Zhang, Y., Dong, X., Liu, C., Yi, J., . . . Wang, H. (2022). Oncolytic adenoviruses synergistically enhance anti-PD-L1 and anti-CTLA-4 immunotherapy by modulating the tumour microenvironment in a 4T1 orthotopic mouse model. *Cancer Gene Therapy, 29*(5), 456-465.

Zhang, Y., Liu, Z., Yang, X., Lu, W., Chen, Y., Lin, Y., . . . Yun, J.-P. J. T. (2021). H3K27 acetylation activated-COL6A1 promotes osteosarcoma lung metastasis by repressing STAT1 and activating pulmonary cancer-associated fibroblasts. *Theranostics*, *11*(3), 1473.

Zhang, Y., Yao, L., Zhang, X., Ji, H., Wang, L., Sun, S., & Pang, D. (2011). Elevated expression of USP22 in correlation with poor prognosis in patients with invasive breast cancer. *Journal of cancer research and clinical oncology, 137*, 1245-1253.

Zhao, G. (2019). Functions of metabolic enzymes in the development of non-small cell lung cancer. *Thoracic Cancer, 10*(9), 1744.

Zhao, J., Guo, Z., Wang, Q., Si, T., Pei, S., Qu, H., . . . Wang, L. (2019). HPV infection associated DNA damage correlated with cervical precancerous lesions and cancer in the highest area of cervical cancer mortality, Longnan, China. *Cancer Management and Research*, 7197-7210.

Zhao, Y., Ye, X., Xiong, Z., Ihsan, A., Ares, I., Martínez, M., . . . Wang, X. (2023). Cancer metabolism: the role of ROS in DNA damage and induction of apoptosis in cancer cells. *Metabolites, 13*(7), 796.

Zhou, S., Cai, Y., Liu, X., Jin, L., Wang, X., Ma, W., & Zhang, T. (2021). Role of H2B mono-ubiquitination in the initiation and progression of cancer. *Bulletin du Cancer, 108*(4), 385-398.

Zhou, Y., Zhou, B., Pache, L., Chang, M., Khodabakhshi, A. H., Tanaseichuk, O., . . . Chanda, S. K. J. N. c. (2019). Metascape provides a biologist-oriented resource for the analysis of systems-level datasets. *Nature communications*, *10*(1), 1523.

Zhu, L., Shu, Y., Liu, C., Zhu, Y., Xiao, Y., Ran, J., & Zhang, C. (2022). Dietary glycemic index, glycemic load intake, and risk of lung cancer: A meta-analysis of observational studies. *Nutrition, 99*, 111676.

7 CURRICULUM VITAE

Contact

Name: Hao Liu

Birthday:19/01/1991

Email: Hao.Liu@medma.uni-heidelberg.de

Address: Ludolf-Krehl-Str. 7-11 Haus B, Eben 4, Raum B 2.28, 68167 Mannheim, Germany

Education

- 2020-Present Heidelberg University Mannheim Medical Faculty, PhD
- 2015-2018 Chongqing Medical University, College of Basic Medicine, Master degree
- 2010-2015 Chongqing Medical University, College of Basic Medicine, Bachelor degree

Publications

- *Liu H, Tang Y, Singh A, et al. RNF20 links the DNA damage response and metabolic rewiring in lung cancer through HIF1α[J]. Nature Communications, 2025, 16(1): 1-22.*
- *Zhou J, Liu H, Zhang L, et al. DJ-1 promotes colorectal cancer progression through activating PLAGL2/Wnt/BMP4 axis[J]. Cell death & disease, 2018, 9(9): 865.*
- *Liu H, Liu X, Zhang C, et al. Redox imbalance in the development of colorectal cancer[J]. Journal of Cancer, 2017, 8(9): 1586.*
- *Liu X, Liu T, Hu L, Jiang T, Liu H, et al. Identification and characterization of the promoter of cancer-related gene LOXL2[J]. Experimental Cell Research, 2020, 387(2): 111786.*
- *刘浩,刘心,王义涛,等.人 ETV4 蛋白截短体的构建与其在结直肠中的功能分析[J].重庆医科大学学报, 2018, 43(9):6.DOI:10.13406/j.cnki.cyxb.001700.*
- *刘心,刘浩,王义涛,雷云龙, 卜友泉等.人 LOXL2 启动子的鉴定与初步分析[J].中国生物化学与分子生物学报,2018(05):540-547.*

8 ACKNOWLEDGEMENT

I would like to express my heartfelt appreciation to everyone who supported me throughout my doctoral research.

First and foremost, I would like to express my deepest gratitude to my supervisor, Prof. Dr. Gergana Dobreva, for her invaluable guidance, continuous support, and encouragement throughout my PhD journey. Her expertise, insight, and patience have greatly shaped both my research and personal growth, I am truly thankful for the opportunity to work under her mentorship, this dissertation would not have been possible without her.

I also wish to sincerely thank all the members of our lab and the colleagues from collaborating groups who contributed to this project. Special thanks go to Dr. Yongqin Tang for his generous assistance during the research, Dr. Yonggang Ren for his intellectual support and insightful bioinformatic suggestions, Arthur Mathes for his help in both scientific matters and daily life in Germany, and Dr. Julio Cordero for his contributions to the bioinformatic analysis. Their collaboration, support, and friendship have made this journey more fulfilling and memorable.

On a personal note, I am deeply thankful to my family. To my parents, thanks for their unconditional love and constant encouragement throughout every stage of my life. To my spouse, Xin Liu, thanks for their patience, understanding, and unwavering support during the most challenging times. I would also like to thank my son Sheldon Jinrun Liu, the joy he brings has been a continuous source of strength and motivation.

Finally, I would like to express my appreciation to all the friends who accompanied me along the way, both near and far. Your presence, humor, and encouragement have made this journey not only bearable, but joyful.

This dissertation is the culmination of the contributions, sacrifices, and support of many people, to whom I am sincerely and eternally grateful.